Universidade de Brasília-UnB
Instituto de Geociências-IG
Programa de Pós-Graduação em Geologia-PPG

Geologia, Geocronologia e Geoquímica dos Granitoides Paleoproterozoicos do Domínio Almas-Conceição do Tocantins, Norte do Orógeno Brasília: Implicações Magmáticas e Geodinâmicas

Área de Concentração: Geologia Regional

André Menezes Saboia

Tese de Doutorado nº **179**

Brasília – DF
2021

Universidade de Brasília-UnB
Instituto de Geociências-IG
Programa de Pós-Graduação em Geologia-PPG

ANDRÉ MENEZES SABOIA

Geologia, Geocronologia e Geoquímica dos Granitoides Paleoproterozoicos do Domínio Almas-Conceição do Tocantins, Norte do Orógeno Brasília: Implicações Magmáticas e Geodinâmicas

Tese apresentada ao Programa de Pós-Graduação em Geologia da Universidade de Brasília, como requisito parcial para obtenção do grau de Doutor em Geologia. Área de concentração: Geologia Regional.

Orientador: Prof. Dr. Claudinei Gouveia de Oliveira (IG/UnB)
Co-orientador: Prof. Dr. Elton Luiz Dantas (IG/UnB)

Brasília, setembro de 2021

Universidade de Brasília-UnB
Instituto de Geociências-IG
Programa de Pós-Graduação em Geologia-PPG

BANCA EXAMINADORA

PROF. DR. CLAUDINEI GOUVEIA DE OLIVEIRA
Instituto de Geociências / Universidade de Brasília - IG/UnB
Presidente da Banca

PROF. DR. CIRO ALEXANDRE ÁVILA
Departamento de Geologia e Paleontologia / Museu Nacional - Universidade Federal do Rio de Janeiro - UFRJ
Examinador Externo

PROF. DR. LUÍS ANTÔNIO ROSA SEIXAS
Departamento de Geologia / Universidade Federal de Ouro Preto – DEGEO/UFOP
Examinador Externo

PROF. DR. FEDERICO ALBERTO CUADROS JIMÉNEZ
Instituto de Geociências / Universidade de Brasília - IG/UnB
Examinador Interno

Brasília, Setembro de 2021

Universidade de Brasília-UnB
Instituto de Geociências-IG
Programa de Pós-Graduação em Geologia-PPG

FICHA CATALÓGRAFICA

MM543g

Menezes Saboia, André
Geologia, Geocronologia e Geoquímica dos Granitoides Paleoproterozoicos do Domínio Almas-Conceição do Tocantins, Norte do Orógeno Brasília: Implicações Magmáticas e Geodinâmicas / André Menezes Saboia; orientador Claudinei Gouveia de Oliveira; co-orientador Elton Luiz Dantas. -- Brasília, 2021.
126 p.

Tese (Doutorado - Doutorado em Geologia) -- Universidade de Brasília, 2021.

1. Magmatismo TTG. 2. Orógeno Brasília. 3. Geocronologia U-Pb. 4. Geoquímica de rocha total. 5. Maciço de Goiás. I. Gouveia de Oliveira, Claudinei, orient. II. Luiz Dantas, Elton, co-orient. III. Título.

CESSÃO DE DIREITOS

NOME DO AUTOR: André Menezes Saboia

TÍTULO DA TESE DE DOUTORADO: Geologia, Geocronologia e Geoquímica dos Granitoides Paleoproterozoicos do Domínio Almas-Conceição do Tocantins, Norte do Orógeno Brasília: Implicações Magmáticas e Geodinâmicas.

Autorizo a Universidade de Brasília à reprodução parcial ou total desta tese de doutorado por meio eletrônico, impressão e/ou download, para fins de pesquisa e produção científica brasileira. Com obrigatoriedade de citação da obra.

GRAU: Doutor ANO: 2021

“Bem-aventurado o homem que acha sabedoria, e o homem que adquire conhecimento”.

(Provérbios 3:13)

“A ciência é um processo social. Decorre numa escala temporal mais longa do que a vida humana. Caso eu morra, alguém ocupará o meu lugar. Se tu morreres, alguém ocupará o teu. O que realmente é importante é que alguém faça o trabalho.”

(Alfred Wegener)

DEDICATÓRIA

Dedico...

Ao meu Deus e Pai Jesus Cristo...
Aos meus ancestrais familiares que me amaram e me fizeram chegar neste mundo...

Ao meu querido filho, meu príncipe André, meu novo amor e minha fonte de motivação para ser um ser humano melhor...

À minha amada esposa, minha rainha Josiane, meu exemplo de mulher e companheira, com você sou completo...

Aos meus Pais, Dr. Saboia e Profa. Esp. Marília, meus exemplos de família, honestidade e trabalho.
Que me apoiaram e me incentivaram com um amor eterno...

A minha irmã Flávia e meus irmãos Fernando e Mário, pelo privilégio e sorte de poder desfrutar a vida com vocês...

Às minhas cunhadas, aos meus Tios e Tias, Primos e Primas, pelo amor, amizade e companheirismo...

Aos meus verdadeiros amigos e amigas, pela feliz convivência e pelos momentos inesquecíveis...

AGRADECIMENTOS

Agradeço:

Ao Meu Deus Pai, minha Esposa e Filho, meus Pais e meus Irmãos pelo amor, carinho, força e conforto durante o período desta pesquisa. Sem vocês seria impossível realizar essa conquista.

Aos meus Professores e Orientadores Drs. Claudinei Gouveia e Elton Dantas que acreditaram na minha pesquisa, ajudando com novas ideias e me guiando para finalização desta tese.

Ao Serviço Geológico do Brasil (SGB-CPRM) e ao Instituto de Geociências - IG, da Universidade de Brasília - UnB, pelo suporte técnico-científico e pela oportunidade de crescimento profissional.

Aos colegas Jaime Scandolara e Pedro Cordeiro e as colegas Joseneusa Brilhante e Isabela Moreno, coautores desta pesquisa e que possibilitaram e deram luz a esta tese.

Aos editores e revisores dos dois artigos publicados que possibilitaram e melhoraram de forma significativa as contribuições desta pesquisa.

Aos colegas Hugo Polo, Marcus Chiarini, Rhapael Teixeira, Loiane Rocha, Helena Eyben, Diogo De Sordi e Isabelle Serafim, pelos debates sobre geologia, pela amizade e pelo convívio saudável dentro da nossa empresa.

Ao saudoso, em memória, Prof. Marcel Auguste Dardenne que me introduziu no estudo geológico da região de Natividade-Almas (TO) em 2004. Graças ao seu trabalho e conhecimento transmitido pude alcançar este título. Amém.

Aos colegas Paulo Meneghini, Cléber Alves, Joffre Valmório e Gabriel Gonçalves da Sureg-GO, pela ajuda e apoio no pojeto de mapeamento da Folha Dianópolis.

Aos diversos profissionais e técnicos do SGB-CPRM e do IG, relacionados com as partes de laboratórios e infraestrutura organizacional, pela viabilização desta pesquisa.

À população acolhedora e simpática de Natividade-Pindorama-Almas-Porto Alegre do Tocantins-Dianópolis, das fazendas e dos povoados, pela enorme ajuda e disponibilidade nos momentos difíceis.

O presente trabalho foi realizado com apoio da Coordenação de Aperfeiçoamento de Pessoal de Nível Superior - Brasil (CAPES) - Código de Financiamento 001.

Enfim, a todos que contribuíram de forma direta e indireta para realização desta tese.

Meu sincero Muito Obrigado!!!

Ruína da Igreja N. Sra. do Rosário dos Pretos - Natividade-TO.

Resumo

O embasamento da porção norte do Orógeno Brasília, no Brasil Central, é constituído por grandes volumes de magmatismo TTG (trondhjemito-tonalito-granodiorito) gerado durante o início do Paleoproterozoico, e representa um bloco continental formado antes da colagem do paleocontinente São Francisco durante o Riaciano, contendo importantes informações sobre os mecanismos e produtos do crescimento e amalgamação da crosta Paleoproterozoica. Novos dados geocronológicos U-Pb em zircão foram obtidos a partir de metagranitóides e intrusões máfico-ultramáficas do Domínio Almas-Conceição do Tocantins (ACTD). Isso foi associado a dados geoquímicos dos metagranitóides para melhor caracterizar os processos de evolução da crosta continental nesta região durante o período Sideriano. Dois episódios plutônicos principais foram reconhecidos na área mapeada: (i) uma unidade mais antiga (2,47 Ga) constituída por tonalitos e trondhjemitos com biotita granitos subordinados (Complexo Ribeirão das Areias - RAC); e (ii) uma suíte mais jovem (2,30 Ga) incluindo tonalitos e trondhjemitas (Suíte Ribeirão Itaboca - RIS). A maioria das rochas TTG do RAC são caracterizadas por padrões fracionados de REE com alta razão $(La/Yb)_N$ = 15-107 e média a alta razão Sr/Y (28-257). Esses TTG incluem tipos de alto e baixo Al e grupos de alta e média pressão. A suíte TTG RIS exibe maiores conteúdos de HREE com altas razões $(La/Yb)_N$ = 65-89 e Sr/Y (59-95) e contém o tipo de alto Al e o grupo de média pressão. Apesar da grande diferença de idade entre estas associações, ambos RAC e RIS são caracterizados por rochas TTG formadas em um ambiente tectônico semelhante a uma subducção. Os biotita granitos estão relacionados a um estágio magmático após a formação das rochas TTG. As rochas máficas da Suíte Gameleira apresentam abundância de zircão interpretada como contaminação crustal, com populações dominantes de idade $^{207}Pb/^{206}Pb$ de 2,48 e 2,30 Ga, e são interpretadas como associadas a um evento magmático extensional após o período Sideriano. Correlações geotectônicas regionais com o Cráton do São Francisco, com base em dados compilados da literatura, indicam um volume significativo de geração de crosta Sideriana que não foi bem considerado nos modelos de amalgamação continental, e que a assinatura geoquímica de magmatismo TTG mais comum em rochas Paleoproterozoicas do que foi sugerido anteriormente.

Rochas com idades Riacianas predominam no embasamento da porção norte do Orógeno Neoproterozóico Brasília, e suas gêneses foram atribuídas ao evento de amalgamação orogênica que formou o paleocontinente São Francisco-Congo entre 2,18 a 2,07 Ga. No entanto, a configuração tectônica e a gênese dos blocos crustais envolvidos neste evento de colagem continental não são claros, particularmente em relação aos terrenos do Domínio Almas-Conceição do Tocantins, no Maciço de Goiás, no Brasil central. Este trabalho fornece novos dados geoquímicos de rocha total e geocronológicos (U-Pb em zircão), que indicam a geração de magmatismo ácido a intermediário em torno de 2,29 e 2,28 Ga correspondendo à Unidade Monzogranítica e à Suíte Quartzo-diorítica, respectivamente. Eventos magmáticos posteriores ocorreram em ambiente de arco continental, em torno de 2,2 Ga representados pelo magmatismo metaluminoso a peraluminoso tipo I da Suíte Granodiorítica a Tonalítica (GTS) e da Suíte Serra do Boqueirão. Por volta de 2,18 Ga ocorreu magmatismo peraluminoso tipo I que gerou a Suíte Peraluminosa (PS). Nossos dados mostram que após um evento magmático Sideriano anterior em torno de 2,45 Ga, relatado em trabalhos anteriores, o Domínio Almas Conceição do Tocantins foi afetado por eventos Riacianos adicionais com atividade magmática em torno de 2,29 Ga a 2,18 Ga. Correlações geotectônicas regionais com o Cráton do São Francisco e outros segmentos pericratônicos indicam eventos magmáticos coevos que ocorreram durante os estágios iniciais de amalgamação do Supercontinente Columbia.

Palavras-chave: Magmatismo TTG; Granitos tipo I; Orógeno Brasília; Maciço de Goiás; Geocronologia U-Pb; Geoquímica de rocha total.

Abstract

The basement of the northern Brasília Belt, in Central Brazil, is dominated by large volumes of TTG magmatism generated during the Early Paleoproterozoic, and represents a continental block formed prior to the welding of the São Francisco paleocontinent during the Rhyacian, holding important information concerning the mechanisms and products of Paleoproterozoic crustal growth and amalgamation. New U-Pb zircon geochronological data was obtained from metagranitoids and mafic-ultramafic intrusions from the Almas-Conceição do Tocantins Domain (ACTD). This was coupled with geochemical data from the metagranitoids to better constrain the processes of continental crust evolution in this region during the Siderian period. Two main plutonic episodes were recognized in the mapped area: (i) an early suite (2.47 Ga) dominated by tonalites and trondhjemites with subordinate biotite granites (Ribeirão das Areias Complex - RAC); and (ii) a later suite (2.30 Ga) including tonalites and trondhjemites (Ribeirão Itaboca Suite - RIS). Most of the RAC trondhjemite-tonalite-granodiorite (TTG) rocks are marked by fractionated REE patterns with high $(La/Yb)_N = 15 – 107$ and samples have medium to high Sr/Y ratio (28 - 257). These TTG include both high- and low-Al types and high- and medium-pressure groups. The RIS TTG suite displays higher HREE contents with high $(La/Yb)_N = 65 – 89$ and high Sr/Y ratio (59 - 95) and contains the high-Al type and the medium pressure group. In spite of the wide age gap between them, both RAC and RIS are characterized by TTG rocks formed in a subduction-like tectonic setting. The biotite granites are related to a magmatic stage after the TTG formation. Mafic rocks of the Gameleira Suite have an abundance of zircon, interpreted as crustal contamination, with dominant $^{207}Pb/^{206}Pb$ age populations of 2.48 and 2.30 Ga, and are interpreted to be associated with an extensional magmatic event following the Siderian period. Regional geotectonic correlations within the São Francisco Craton based on data compiled from the literature indicate a significant volume of Siderian crust generation that has been overlooked in continental amalgamation models and that TTG magmatism is a more common geochemical signature in Paleoproterozoic rocks than has been previously suggested.
Paleoproterozoic (Rhyacian) rocks dominate within the basement of the Neoproterozoic Brasília Belt and their genesis has been attributed to the orogenic amalgamation event that assembled the São Francisco-Congo paleocontinent from 2.18 to 2.07 Ga. However, the tectonic framework and genesis of the building blocks involved in this continent-wide amalgamation event are unclear, particularly in relation to terranes from the Almas-Conceição do Tocantins Domain, in the Goiás Massif, central Brazil. This work provides new whole-rock chemical and geochronological data, which indicate the generation of felsic to intermediate magmatism around 2.29 and 2.28 Ga corresponding to the Monzogranitic Unit and the Quartz-dioritic Suite, respectively. Later magmatic events occurred in a continental arc setting, around 2.2 Ga represented by metaluminous to peraluminous I-type magmatism of the Granodioritic to Tonalitic Suite (GTS) and the Serra do Boqueirão Suite. Around 2.18 Ga a peraluminous I-type magmatism took place and generated the Peraluminous Suite (PS). Our data show that after an earlier Siderian magmatic event around 2.45 Ga, reported in previous works, the Almas do Conceição do Tocantins Domain oversaw additional Rhyacian events of magmatic activity around 2.29 Ga to 2.18 Ga. Regional geotectonic correlations with the São Francisco Craton and other pericratonic belts indicate coeval magmatic events taking place during the early stages of the Columbia Supercontinent amalgamation.

Keywords: TTG rocks; I-type granites; Brasília Orogen; Goiás Massif; U-Pb Geochronology;

Whole-rock geochemistry.

SUMÁRIO

ÍNDICE DE FIGURAS

ÍNDICE DE TABELAS

Capítulo 1

1. INTRODUÇÃO

1.1. Contextualização Geotectônica

A geração de crosta continental durante o período Riaciano (~2.200-2.100 Ma; Cohen *et al*., 2013), representa um dos principais eventos de formação de rochas durante o Paleoproterozoico na Plataforma Sul-Americana, e no Brasil está presente tanto nos núcleos cratônicos quanto no interior dos orógenos Neoproterozoicos (Brito Neves, 2011; Seixas *et al.*, 2012; Fuck *et al.*, 2014; Teixeira *et al.*, 2015).

A transição entre as Eras Arqueana e Paleoproterozoica é marcada por uma mudança fundamental da petrogênese das rochas granitoides, bem como dos processos geodinâmicos da tectônica de placas (Laurent *et al*., 2014). Dentre esses aspectos geológicos destacam-se a considerável diminuição de associações TTGs após 2,5 Ga e a identificação de associações TTGs em conjunto com grandes volumes de rochas cálcioalcalinas em terrenos de idade Sideriana (2,5-2,3 Ga; Moyen & Martin, 2012).

Uma carência de idades no intervalo entre 2,45 e 2,2 Ga foi proposta e denominada de *global magmatic shutdown (or slowdown*) por Condie *et al*. (2009), com base na distribuição global de idades U/Pb de granitoides relacionados à subdução e de zircão detríticos. Condie *et al*. (2011) mostraram picos de idades de zircão detríticos, em associação com razões isotópicas de Hf, a partir de sedimentos de rios modernos e novamente encontraram uma lacuna de idades juvenis entre 2.400–2.200 Ma. Segundo esses autores, os picos de preservação que refletem a crosta continental juvenil e retrabalhada são preservados seletivamente durante as colisões continentais. Eriksson & Condie (2014) com base no registro sedimentar de 2,45–2,0 Ga de uma série de terrenos cratônicos (incluindo o Cráton São Francisco), interpretaram que os fatores geodinâmicos e eustático-climáticos neste período são compatíveis com o *global magmatic slowdown event* postulado por Condie *et al*. (2009).

Trabalhos recentes, com dados isotópicos de Lu-Hf aliados com robustas revisões bibliográficas, indicam que o magmatismo do Sideriano, tanto juvenil como crustal, está presente em vários continentes ao redor do mundo (Berman *et al*., 2013; Pehrsson *et al*., 2013; Partin *et al*., 2014; Diwu *et al*., 2014; Barbosa *et al*., 2019; Cutts *et al*., 2020; Martins-Ferreira *et al*., 2020; Saboia *et al*., 2020a). Nestes estudos é possível observar eventos magmáticos relacionados a múltiplas associações de rochas e configurações tectônicas, tais como granitoides de arcos

continentais e oceânicos, diques máficos intraplacas e rochas máficas-ultramáficas relacionadas à LIPs. Portanto, esses trabalhos abrem um debate sobre o *global magmatic slowdown event* com relação ao crescimento, preservação e tipo de crosta continental no banco de dados global sobre as idades U-Pb e isotópicos de Lu-Hf em zircão.

Laurent *et al*. (2014) mostraram que a diversidade dos tipos de granitoides no final do Arqueano constitui uma sequência de dois estágios de colocação destas rochas, resultando na iniciação global do "estilo moderno" da tectônica de placas. Esta sequência representa o primeiro ciclo de subducção-colisão da história da Terra e ocorreu em momentos diferentes ao redor do mundo, por exemplo, antes de ~2,95 Ga no Cráton Pilbara, depois de ~2,55 Ga nos Crátons de Dharwar e do Norte da China e cerca de 2,88 Ga no Cráton Amazônico. Portanto, a identificação destas mudanças nas composições magmáticas e nos estilos tectônicos, relacionados com a participação da cunha mantélica, em cada orógeno específico é um ponto importante para ser abordado (Cruz *et al*., 2003; Fuck *et al.*, 2014; Moreira *et al.*, 2018; Bruno *et al*., 2020; Saboia *et al*., 2020a).

As principais ocorrências de rochas Siderianas no Brasil foram exemplificadas por Brito Neves (2011), estas são: (i) Domínio Bacajá (Cráton Amazônico) rochas de baixo a alto grau metamórfico são representadas por terrenos do tipo granito-*greenstone* com idades U-Pb de 2,36-2,34 Ga e que são intrudidas por granitoides de 2,31 Ga. Adicionalmente no Cinturão Maroni-Itacaiunas (Estado do Amapá) foram descritas idades U-Pb e Pb-Pb no intervalo entre 2,4-2,3 Ga. (ii) Cráton São Francisco estas rochas estão detalhadas nos capítulos 2 e 3 desta tese. O autor destacou o Supergrupo Minas que tem parte de sua evolução no Sideriano. (iii) Cráton Rio de La Plata (Bloco Taquarembó) rochas granulíticas do Complexo Santa Maria Chico possuem idades U-Pb de núcleos de zircão de 2,35 Ga. (iv) Cráton Luiz Alves o Complexo Granulítico de Santa Catarina (principalmente ortognaisses TTG) apresenta eventos magmáticos e metamórficos entre 2,4-2,3 Ga. (v) Província Borborema, o Maciço Granja (rochas de alto grau, principalmente ortognaisses TTG) possui idades U-Pb entre 2,30 e 2,36 Ma. (vi) Maciço Rio Piranhas (Terreno Rio Grande do Norte) a Sequência Santa Luzia apresenta idades U-Pb de ~2,33 Ga. (vii) Bloco Almas-Conceição as rochas são detalhadas nesta tese. (viii) Província Mantiqueira o Complexo Quirino possui rochas de alto potássio com idades de zircão U-Pb de ~2.308 Ma. Brito Neves *et al*. (2021) mostram que o Complexo Encantadas (Cinturão Dom Feliciano, Estado do Rio Grande do Sul) possui gnaisses tonalíticos com idade de cristalização do zircão de ~2,35 Ga.

Durante o Riaciano (2,3-2,05 Ga) e o Orosiriano (2,05-1,8 Ga) são registrados globalmente sucessivos eventos de crescimento continental por orogenias acrescionárias e colisionais (Condie, 2007, 2013), que podem estar relacionadas com longos períodos de duração da subducção e caracterizando orógenos de vida longa (*long-lived orogens*). Ambientes de

subdução provavelmente representam importantes locais de geração da nova crosta continental, enquanto que os orógenos colisionais seriam preferencialmente locais de seu retrabalhamento (Moyen *et al*., 2016).

O período entre ~2,1-1,8 Ga se destaca por estar relacionado com as fases iniciais e de construção (*assembly*) do supercontinente Columbia/Atlantica/Nuna, implicando em sistemas orogênicos desenvolvidos durante este intervalo de tempo (Rogers & Santosh, 2009; Condie, 2013; Terentiev & Santosh, 2020). Dentre estes cinturões orogênicos paleoproterozoicos se ressaltam as orogenias entre ~2,2-1,9 Ga, responsáveis pela edificação do Paleocontinente São Francisco-Congo (Delgado *et al*., 2003; Brito Neves, 2011; Fuck *et al.*, 2014; Teixeira *et al.*, 2015; Alkmim & Teixeira, 2017; Cutts *et al*., 2018).

Na Porção Norte do Orógeno Brasília, no Domínio Almas-Conceição do Tocantins (DACT) que é o objeto de estudo desta Tese de Doutorado, ocorrem associações TTGs do Sideriano e um grande volume de metagranitoides do Riaciano considerados como representantes do Paleocontinente São Francisco (Cruz *et al*., 2003; Hasui *et al*., 2012; Fuck *et al*. 2014; Cordeiro & Oliveira, 2017). O DACT preserva um conjunto de segmentos e eventos orogenéticos com subducção da crosta oceânica, geração de arcos magmáticos juvenis e continentais, e posterior espessamento crustal através de processos acrescionários (Cruz & Kuyumjian, 1998; Cruz *et al*., 2003; Fuck *et al*. 2014; Sousa *et al*., 2016; Martins-Ferreira *et al*., 2020; Saboia *et al*., 2020b). Os resultados dos principais trabalhos sobre a região deste estudo mostram uma complexa estruturação geotectônica de corpos plutônicos (metagranitoides e metamáfico/ultramáficos) e sequências metavulconossedimentares com idades distintas, cujas caracterizações geológicas têm sido elucidadas e detalhadas através de estudos geológicos específicos, respaldados por geocronologia e geoquímica.

A aplicação de técnicas geocronológicas e isotópicas (U-Pb, Sm-Nd, Lu-Hf) em associação com interpretações litoquímicas, tem proporcionado um panorama mais aprofundado sobre a evolução tectono-magmática do DACT (Fuck *et al*., 2014; Sousa *et al*., 2016; Saboia & Meneghini, 2019; Martins-Ferreira *et al*., 2020; Saboia *et al*., 2020a, b). Neste contexto, a combinação de ferramentas como petrografia, geocronologia, geoquímica isotópica e litogeoquímica, aliadas a uma base cartográfica de detalhe tem permitido a interpretação petrogenética e tectônica dos diversos corpos metaplutônicos do DACT. A singularidade do magmatismo plutônico deste terreno Paleoproterozoico demonstra a importância científica dos estudos desta Tese de Doutorado. Portanto, a obtenção de novos dados (em especial geocronológicos e geoquímicos) é fundamental para uma melhor compreensão da petrogênese dos plútons, dos ambientes tectônicos e dos processos geodinâmicos que constituíram este terreno.

1.2. Objetivo

O objetivo desta Tese é a avaliação conjunta dos processos geológicos, por meio de mapeamento geológico, estudos geocronológicos (U-Pb) e litoquímicos de rocha total do embasamento Paleoproterozoico da Porção Norte do Orógeno Brasília. Volta-se para o estudo dos corpos intrusivos selecionados que ocorrem no Domínio Almas-Conceição do Tocantins na região de Natividade-Almas-Dianópolis, Estado do Tocantins. Foram utilizados produtos e amostras do trabalho de mapeamento geológico (escala 1:250.000) do Serviço Geológico do Brasil (SGB-CPRM).

Os novos dados obtidos têm ênfase nas idades U-Pb em zircão dos corpos de metagranitoides e metamáfico/ultramáficos, análises litoquímicas de rocha total dos metagranitoides, acompanhados de dados petrográficos (assembléia mineral, textura e estrutura) para distinguir, agrupar e caracterizar os diferentes corpos plutônicos. Durante a interpretação, essas informações foram comparadas com o acervo de dados já publicados para determinar a evolução tectono-magmática da área estudada e suas correlações com os segmentos orogênicos de mesma idade e/ou diacrônicos do Cráton São Francisco.

Apesar dos avanços recentes da última década, o conhecimento geológico do DACT ainda possui algumas questões-chave que continuam em aberto, tais como: (i) carência cartográfica e melhor caracterização das associações TTG; (ii) Quais as fontes específicas dos diversos pulsos magmáticos deste domínio; (iii) Maior detalhe dos eventos/processos que ocorreram durante o Sideriano; (iv) Melhor definição dos períodos magmáticos durante a evolução paleoproterozoica e dos limites geográficos deste domínio; (v) Aprofundamento do ambiente tectônico específico para cada suíte magmática reconhecida; (vi) Qual o significado geotectônico do DACT com relação a evolução crustal do Cráton São Francisco e seu enquadramento global em termos do Supercontinente Columbia. Assim, a presente Tese pretende suprir algumas lacunas existentes destas questões geológicas abordadas.

1.3. Escopo da Tese

Esta Tese está organizada em cinco capítulos, ademais anexos (materiais suplementares) com os dados U-Pb. O primeiro capítulo informa sobre a contextualização geológica da tese, além de suas principais finalidades e objetivos, e as metodologias utilizadas para o alcance dos resultados. O conjunto dos resultados obtidos está organizado e apresentado na forma de dois artigos publicados no ano de 2020, e que constam no segundo e terceiro capítulos.

O segundo capítulo foi um artigo publicado no *Journal Precambrian Research* intitulado "*The Siderian Crust (2.47-2.3 Ga) of the Goiás Massif and its Role as a Building Block of the São Francisco Paleocontinent*". Este artigo trata sobre o significado da evolução magmática, principalmente das associações de rochas TTG, durante o Sideriano e seu enquadramento com as rochas do Cráton São Francisco.

O terceiro capítulo foi um artigo publicado no *Journal of South American Earth Science* intitulado "*The 2.26 to 2.18 Ga Arc-Related Magmatism of the Almas-Conceição do Tocantins Domain: An Early Stage of the São Francisco Paleocontinent Assembly in Central Brazil*". Este artigo trata a respeito dos diversos pulsos magmáticos dos metagranitoides durante o período acrescionário Riaciano, além de sua perspectiva com relação aos orógenos cronocorrelatos do Cráton São Francisco.

O quarto capítulo apresenta as principais conclusões e contribuições científicas da tese. Algumas respostas às questões geológicas inicialmente propostas são discutidas. Adicionalmente, é feita uma proposta mais ampla, do que foi mostrado nos artigos publicados, sobre as definições das unidades litoestratigráficas e do quadro evolutivo do Domínio Almas-Conceição do Tocantins.

O quinto capítulo contém as referências bibliográficas utilizadas na tese.

1.4. Geologia Regional e Local

Em função de que os artigos publicados e presentes nos capítulos 1 e 2 possuem o detalhamento deste tópico, um sumário a respeito da contextualização e conhecimento geológico da região estudada será abordado a seguir. A pesquisa desta tese discorre sobre as principais referências bibliográficas da literatura até meados do ano de 2020. Contudo, não detalha a recente contribuição de Martins-Ferreira *et al*., (2020), e neste sentido, a respectiva publicação será melhor descrita no presente subitem.

A Província Tocantins é um sistema orogênico desenvolvido durante a Orogenia Brasiliana-Pan-Africana devido à colisão de três paleocontinentes: Amazônico, São Francisco, e o Paranapanema (Almeida *et al*., 1981; Hasui *et al*., 2012; Fuck *et al*., 2017). O bloco Parnaíba, segmento crustal de menor dimensão, também está relacionado ao processo de aglutinação do Gondwana Ocidental pela "colagem" principal destes três paleocontinentes (Castro *et al*., 2013).

Domínios paleoproterozoicos estão expostos na porção norte da zona externa do Orógeno Brasília (Fig. 1.1), nos estados de Goiás e Tocantins, tendo sido formados como parte ocidental do paleocontinente São Francisco (Dardenne, 2000; Cruz *et al*., 2003; Cordeiro e Oliveira, 2017; Cuadros *et al*., 2017a, b; Martins-Ferreira *et al*., 2020). Nas concepções mais atuais, os domínios

abordados neste trabalho compõem o Bloco Cavalcante-Natividade (CNB) na Fig. 1.1, que é subdividido nos domínios Almas-Conceição do Tocantins (DACT) e Cavalcante-Arraias (DCA) na Fig. 1.2 (Fuck *et al*., 2014 ; Sousa *et al*., 2016; Cordeiro & Oliveira, 2017).

O DACT foi chamado de Terreno Granito-*Greenstone* do Tocantins e caracterizado como domos granito-gnaisses cercados por faixas de *greenstone belts*, interpretado como formado em ambiente de subducção no início do Paleoproterozoico (Cruz e Kuyumjian, 1998; Kuyumjian *et al*., 2012). A unidade mais antiga do DACT é o Grupo Riachão do Ouro (GRO), uma sequência metavulcano-sedimentar que consiste na Formação Córrego do Paiol na base e na Formação Morro do Carneiro no topo. Metagranitoides com idade de 2,45 Ga foram identificados como constituintes do Complexo Ribeirão das Areias (Cruz *et al*., 2003), e caracterizados como uma série TTG de Alto Al intrusiva no GRO. Esses autores também descreveram dois tipos de rochas que compõem série granítica cálcioalcalina de baixo K com idades de 2,2 Ga, denominadas de Suítes 1 e 2.

A Suíte Conceição do Tocantins, definida por Sousa *et al*. (2016), incluí conjunto de granitoides cálcioalcalinos relacionados a um arco magmático gerado entre 2,3 e 2,16 Ga. Adicionalmente, esta suíte é intrudida pelo magmatismo sin-colisional da Suíte Aurumina entre 2,17-2,15 Ga, e que constituí a Suíte Xobó e o Corpo Granito Príncipe.

Martins-Ferreira *et al*. (2020) nomearam o DACT de Terreno Almas-Conceição do Tocantins e demonstraram que a Formação Morro do Carneiro representa uma bacia orogênica de *back-arc* depositada entre 2,23 e 2,21 Ga, com valores de Hf epsilon variando de positivo a negativo (+6,34 a -7,96). Esses autores também indicaram que os anfibolitos da Formação Córrego do Paiol foram formados em ambiente relacionado à subducção, similar ao contexto de supra-subducção.

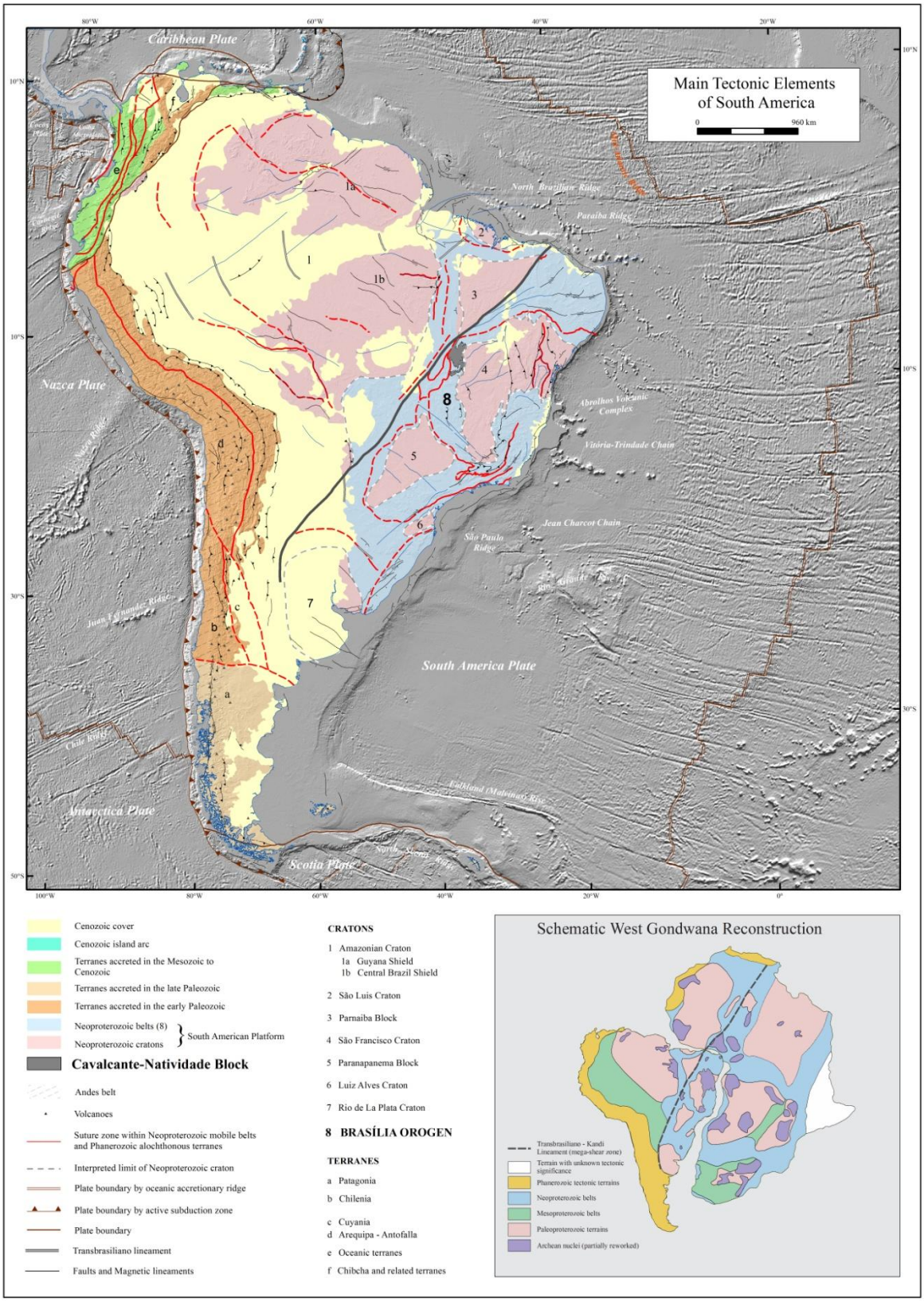

Figura 1.1 - Mapa tectônico esquemático da América do Sul, mostrando a localização do Bloco Cavalcante-Natividade na Porção Norte do Orógeno Brasília (8), destacado em cor cinza (modificado de Cordani *et al*., 2016).

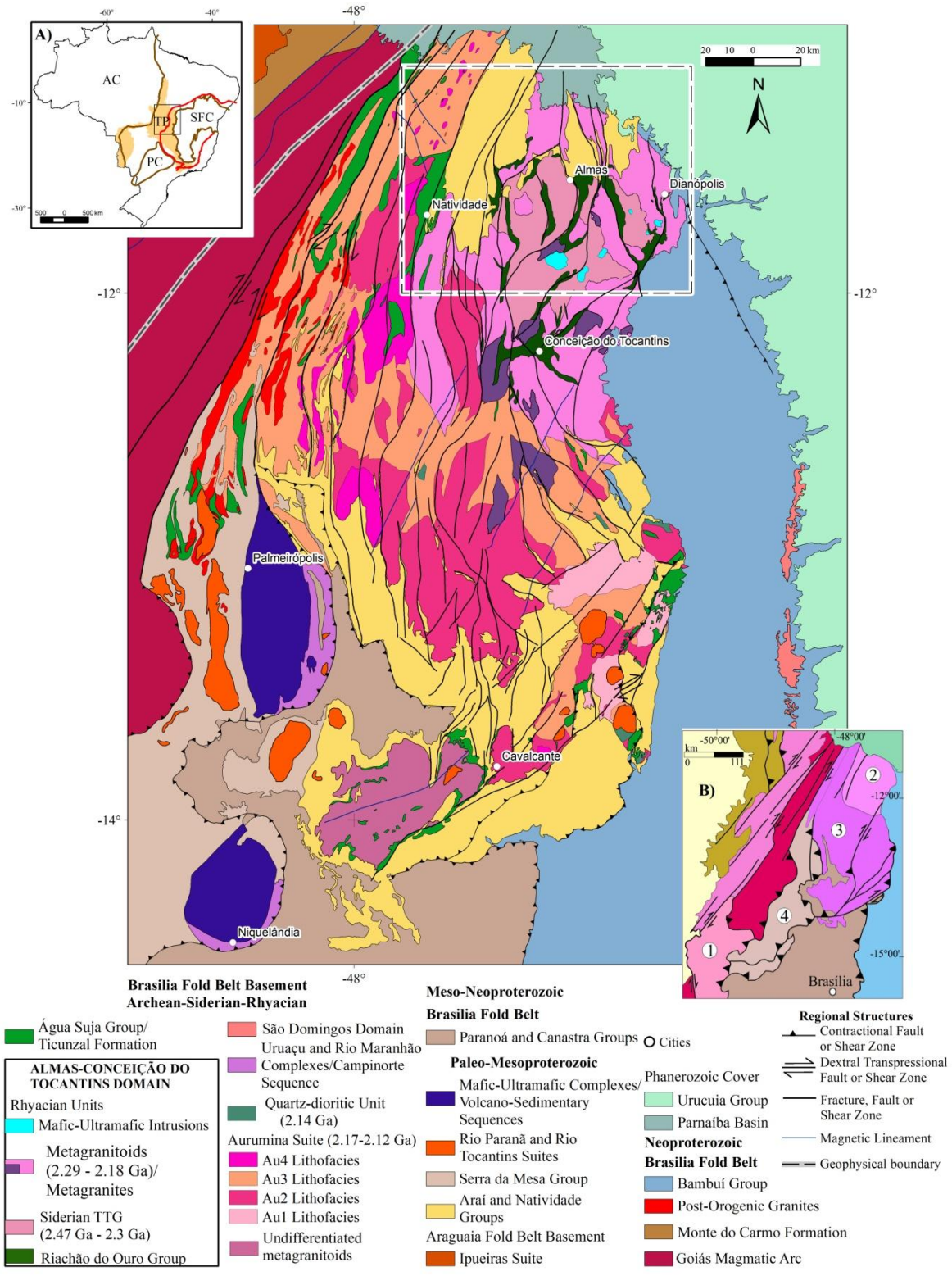

Figura 1.2 - Divisão geotectônica da Faixa Brasília Setentrional. Modificado de Saboia *et al.*, (2020b). As unidades que compõem o Domínio Almas-Conceição do Tocantins (DACT) estão destacadas no retângulo de linha preta. Legenda da figura. (A) TP: Província Tocantins. A linha em vermelho corresponde ao limite da região pericratônica do Paleocontinente São Francisco. (B) Domínos tectônicos do Orógeno Brasília: 1-Domínio Crixás-Goiás, 2-Domínio Almas-Conceição do Tocantins, 3-Domínio Cavalcante-Arraias, 4 -Domínio Campinorte.

Martins-Ferreira *et al*. (2020) classificaram os metagranitoides do Terreno Almas-Conceição do Tocantins em: (i) batólitos Siderianos representados pelo Porto Alegre (metagranodioritos, 2,47 Ga), Rio do Peixe (metatonalitos, 2,47 Ga) e Granodiorito Ribeirão das Areias (2,46 Ga). Estas rochas possuem valores εHf (t) predominantemente positivos, mas também valores negativos, entre -7,4 a +6,3. (ii) Serra do Pilão (metatonalitos e metagranodioritos, 2,39 Ga). As amostras deste batólito apresentaram valores de εHf (t) positivos entre +0,1 a +4,3. (iii) rochas Riacianas da Suíte Serra do Boqueirão (metatonalitos, metagranodioritos e metadioritos, 2.201 a 2.204 Ma) e Tonalito Ribeirão das Areias (2,21 Ga). As amostras da Suíte Serra do Boqueirão apresentam valores de εHf (t) positivos e negativos, entre -2,7 a 0,39. Os autores também concluíram que todos os grupos de granitoides possuem assinatura cálcioalcalina e foram formados em ambientes de arco magmático oceânico e/ou continental do tipo Cordilheiriano, e que correspondem a um orógeno acrescionário desenvolvido entre 2,5 a 2,2 Ga na margem ocidental do Paleocontinente São Francisco. O modelo geodinâmico proposto é relacionado com eventos magmáticos alternados de *flare-ups* e de quiescência, baseado no trabalho de Ducea *et al*. (2015). Três eventos magmáticos acrescionários foram reconhecidos: um mais velho com idades entre 2.476 ± 9 Ma a 2.462 ± 13 Ma, um intermediário de 2.390 ± 14 Ma, e um mais jovem com idades entre 2.235 ± 26 Ma a 2.201 ± 5 Ma. Estes autores também detalharam quatro episódios evolutivos distintos: (S1) 2,52-2,46 Ga, indica adição de material juvenil. (S2) 2,43-2,37 Ga, sugere participação predominante de material crustal retrabalhado e contribuição subordinada de material juvenil. (R1, Sideriano a Riaciano) 2,32-2,26 Ga e (R2) 2,24-2,20 Ga, são indicativos de magmas derivados predominantemente de crosta reciclada e/ou contaminada.

Na porção oeste da área estudada ocorrem unidades litoestratigráficas do Domínio Cavalcante-Arraias, representadas pela sequência metavulcano-sedimentar do Grupo Água Suja (2,17 Ga, Queiroz, 2001; Lima, 2014) e pelos metagranitoides da Suíte Aurumina (2,17-2,11 Ga, Sousa *et al*., 2016; Cuadros *et al*., 2017b). O DACT foi fortemente afetado por processos orogênicos durante o Paleoproterozoico e Neoproterozoico, registrados como metamorfismo regional (fácies xisto verde a anfibolito), dobramentos em escala quilométrica, extensas zonas de cisalhamento transpressionais, além da deformação associada ao Lineamento Trans-Brasiliano (Borges *et al*., 1999; Kuyumjian & Araújo Filho, 2005; Fuck *et al*., 2017).

1.5. Metodologia de Trabalho

Este trabalho possui enfoque regional (área de estudo com ~11.000 km^2) respaldado pelo mapeamento geológico em escala 1:250.000 desenvolvido por este autor na Folha Dianópolis, através do Serviço Geológico do Brasil (SGB-CPRM). A oportunidade de pesquisa decorre da cooperação científica entre os orientadores desta tese, Profs. Drs. Claudinei Gouveia e Elton Dantas da UnB em conjunto com instituições de fomento científico (citadas nos reconhecimentos dos artigos publicados), e o SGB-CPRM. Para alcançar o objetivo proposto foi necessário o desenvolvimento de uma abordagem que envolveu o tratamento e integração dos novos dados e os disponíveis na literatura (cartográficos, petrográficos, geocronológicos e litoquímicos). O desdobramento do conjunto dos resultados obtidos também contou com a colaboração dos coautores dos artigos publicados, profissionais que fazem parte da mesma linha de pesquisa dos orientadores da tese e do SGB-CPRM.

A metodologia de trabalho utilizou técnicas de mapeamento geológico sistemático (cartografia e petrografia), geocronologia U-Pb (SHRIMP-*Sensitive High Resolution Ion Microprobe* e LA-ICPMS-*Laser Ablation Inductively Coupled Plasma Mass Spectrometry*) e de litogeoquímica de rocha total (elementos maiores por XRF, elementos traços e ETR por ICP).

1.5.1. Mapeamento Geológico

Os métodos de trabalho utilizados na execução do projeto de mapeamento geológico da Folha Dianópolis (SC.23-Y-C, Saboia & Meneghini, 2019) seguiram a sistemática estabelecida pelo SGB-CPRM, e são descritos em detalhes por Medeiros & Rosa-Costa (2020). Basicamente envolvem as seguintes etapas: (i) Preliminar constitui na aquisição, interpretação e integração de produtos de sensoriamento remoto (imagens de radar, satélite, aerogeofísicas) e de dados e mapas geológicos disponíveis na literatura. É feita a elaboração do mapa geológico preliminar em ambiente SIG; (ii) Atividades de campo e análises laboratoriais os trabalhos de campo foram executados realizando-se, sempre que possível, perfis geológicos transversais ao arcabouço lito-estrutural das unidades geológicas. São feitas as descrições dos afloramentos com coletas de amostras representativas para os estudos petrográficos, litoquímicos e geocronológicos; e (iii) Final e produtos gerados envolve a integração dos dados de campo e de laboratórios, analisados e interpretados em conjunto.

1.5.2. Geocronologia U-Pb em Zircão

O método U-Pb em zircão é uma ferramenta de grande importância nas geociências, pois informa a história temporal das rochas e consequentemente determina a idade de cristalização de rochas ígneas de diversas composições. Os avanços nas técnicas analíticas nas últimas décadas, em especial por LA-ICP-MS e microssonda iônica (do inglês, SIMS), fornecem informações dos domínios do zircão como etapas de cristalização e eventos superpostos da rocha em maior detalhe quando comparados com as técnicas de diluição isotópica (ID-TIMS). Assim, as técnicas de análises pontuais e de maior resolução espacial produzem idades que contribuem de forma significativa para a identificação de fases de cristalização e metamorfismo dos diferentes eventos geológicos. Destaca-se que a cavidade (*spot*) gerada pela microssonda iônica permite uma leitura mais precisa da fração do zircão analisada, enquanto que a cavidade analisada pelo método LA-ICP-MS possui maior volume e pode implicar num erro analítico mais elevado (Kröner *et al*., 2014).

A concentração de zircão a partir das amostras selecionadas foi realizada nos laboratórios de preparação da CPRM (SUREG-GO) e da UnB. Em ambos os locais a rocha foi reduzida via britador e extraída a fração inferior a 500 µm através de peneiramento. O material recolhido no peneiramento foi bateado para a concentração dos minerais pesados. O concentrado passou pelo separador isodinâmico Frantz e a fração não magnética a 1,8 amperes foi levada ao microbateamento em placa de petri. A partir do concentrado final, os minerais de interesse foram separados manualmente em lupa binocular. Para a confecção dos *mounts*, cristais de zircão foram fixados em fita dupla face (cerca de 50). Os cristais foram embutidos em resina epóxi (a frio), desgastados para a exposição do interior dos grãos e polidos em pasta de diamante 0,25 µm. Os cristais de zircão foram imageados por microscópio eletrônico de varredura (MEV) usando catodoluminescência e/ou elétrons retroespalhados (*backscattered electrons*-BSE).

As determinações realizadas no LA-ICP-MS foram realizadas no Laboratório de Geocronlogia da Universidade de Brasília e seguiram o procedimento apresentado por Buhn *et al*. (2009). Para a limpeza dos *mounts* foi utilizado banho com ácido nítrico diluído (3%), água Nanopure® em ultrassom e por último em acetona para extração de qualquer resíduo de umidade. As análises isotópicas foram realizadas no LA-MC-ICP-MS Neptune (Thermo-Finnigan) acoplado ao Nd-YAG (λ=213nm) Laser Ablation System (New Wave Research, USA). A ablação dos grãos foi realizada em *spot* 25-40 µm, com freqüência de 10 Hz e fluência de 0,19 a 1,02 J/cm^2. O material pulverizado foi carreado por um fluxo de He (~0,40 L/min) e Ar (~0,90 L/min). Em todas as análises foi utilizado o padrão internacional GJ-1 para a correção da deriva do equipamento, assim como o fracionamento entre os isótopos de U e Pb. Para a verificação da

acurácia foram realizadas análises nos padrões FC-1, Temora, 91500 ou UQZ. Os dados foram adquiridos em 40 ciclos de 1 segundo. O procedimento de coleta de dados seguiu a seqüência de leitura: - 1 branco, 1 padrão, 4 ou 8 amostras, 1 branco e 1 padrão. Em cada leitura foram determinadas as intensidades do sinal das massas ^{202}Hg, ^{204} (Pb+Hg), ^{206}Pb, ^{207}Pb, ^{208}Pb e ^{238}U. A redução dos dados brutos, que inclui as correções para branco, deriva do equipamento e chumbo comum, foram realizadas em planilha EXCEL (Oliveira, 2015), confeccionada no próprio laboratório e os dados reportados conforme recomendações de Horstwood *et al*. (2016). As idades foram calculadas, bem como os gráficos foram criados utilizando os recursos do ISOPLOT 4.15 (Ludwig, 2012).

As análises de microssonda iônica foram realizadas no GeoLab SHRIMP da Universidade de São Paulo. Nesse laboratório foram confeccionadas as montagens de grãos e obtidas imagens de catodoluminescênia em microscópio eletrônico de varredura para a investigação prévia das estruturas internas dos grãos a serem analisados. O equipamento utilizado para as análises foi o modelo SHRIMP II e a metodologia analítica seguiu os procedimentos descritos por Williams (1998) e Williams & Meyer (1998). Para normalização da concentração de U-Pb-Th foi utilizado o padrão internacional de zircão SL13 (238 ppm) e o *bracketing* da razão ^{206}Pb/^{238}U foi executado com a utilização do padrão natural Temora 2, de idade 416,78 Ma (Black *et al*., 2003). As condições de análises foram: *spot size* = 24 μm, 6 *scans*, *dead time* = 25ηs e *source slit* = 80μm. Para a redução dos dados foi utilizado o programa Squid 1.06 (Ludwig, 2002) e para os cálculos das idades e plotagem dos pontos optou-se pelo programa Isoplot 4 (Ludwig, 2012). As incertezas relatadas em tabelas e figuras são fornecidas no nível 1σ e 2σ, respectivamente, e as idades finais são cotadas no nível de confiança de 95% (2σ).

1.5.3. Litoquímica

Os processos magmáticos, tais como fusão parcial, assimilação e contaminação, são relacionados ao controle das variações geoquímicas no magma precursor das rochas ígneas (Brown *et al*., 1984). Logo, as variações dos elementos químicos, principalmente de elementos menores como ETR, LILE e HFSE, são amplamente aplicadas em estudos de petrogênese de granitóides e fornecem importantes informações sobre a fonte do magma e de seu ambiente tectônico (Pearce *et al*., 1984; Harris *et al*., 1986; Chappell & White, 1992).

Os granitóides são os tipos de rocha mais abundantes na crosta continental e sua classificação pode ser complexa, uma das razões é que dificilmente são originados de uma única fonte, sendo mais comum uma origem por misturas de fontes crustais e mantélicas (Patiño

Douce, 1999; Frost *et al*., 2001). Neste contexto, o estudo da geoquímica de granitóides constitui uma excelente ferramenta para uma melhor compreensão sobre a evolução da crosta continental, e dos processos magmáticos envolvidos.

As análises dos elementos maiores em pastilha fundida foram realizadas por fluorescência de raios X (XRF) no laboratório SGS GEOSOL em Vespasiano, Minas Gerais (Brasil), de acordo com o método analítico XRF79C pré-estabelecido. As polpas (~2 gramas por amostra) foram secas em estufa e pesadas após resfriamento em um frasco contendo fluxo de tetraborato de lítio. A amostra foi então transferida para um cadinho de platina e homogeneizada. Após homogeneização, iodeto de lítio foi adicionado antes da fusão em máquina automática e da análise por XRF. As análises de elementos traços foram realizadas por espectrometria de massa com plasma indutivamente acoplado (ICP-MS/ICP-OES) no laboratório SGS GEOSOL em Vespasiano, Minas Gerais (Brasil), de acordo com os métodos analíticos IMS95A e ICM14B pré-estabelecidos. Para a análise IMS95A, as polpas (~10 gramas por amostra) foram pesadas e então fundidas em um cadinho de grafite pela adição de metaborato de lítio ($LiBO_2$). Após a fusão o fundido foi transferido para um béquer contendo uma solução de ácido nítrico (HNO_3) e ácido tartárico ($C_4H_6O_6$) em volumes iguais antes da homogeneização e dissolução total sob agitação, e da leitura da solução por ICP-MS. Para a análise ICM14B, a decomposição das amostras foi feita através de abertura por água régia (HCl e HNO_3) e leitura por ICP-MS e ICP-OES.

Os padrões utilizados para as análises geoquímicas correspondem aos seguintes materiais de referência presentes nos certificados de análise do laboratório SGS GEOSOL: AMIS0183, GBM995-2-R, GRE-03, IPT122, JK 28, SARM3, SG-077, SG-121, SG_122, SG-142 and TILL-3. Os resultados das análises geoquímicas foram plotadas usando o software GCDkit (Janousek *et al*., 2006).

Capítulo 2

2. THE SIDERIAN CRUST (2.47-2.3 Ga) OF THE GOIÁS MASSIF AND ITS ROLE AS A BUILDING BLOCK OF THE SÃO FRANCISCO PALEOCONTINENT

André Menezes Saboia[1], Claudinei Gouveia de Oliveira[2], Elton Luiz Dantas[2], Pedro Cordeiro[3], Jaime Estevão Scandolara[1], Joseneusa Brilhante Rodrigues[1], Isabela Moreno Cordeiro de Sousa[2]

[1]Geological Survey of Brazil (andre.saboia@cprm.gov.br)

[2]University of Brasília, Brazil

[3]Pontificia Universidad Católica de Chile

Abstract

The basement of the northern Brasília Belt, in Central Brazil, is dominated by large volumes of TTG magmatism generated during the Early Paleoproterozoic, and represents a continental block formed prior to the welding of the São Francisco paleocontinent during the Rhyacian, holding important information concerning the mechanisms and products of Paleoproterozoic crustal growth and amalgamation. New U-Pb zircon geochronological data was obtained from metagranitoids and mafic-ultramafic intrusions from the Almas-Conceição do Tocantins Domain (ACTD). This was coupled with geochemical data from the metagranitoids to better constrain the processes of continental crust evolution in this region during the Siderian period. Two main plutonic episodes were recognized in the mapped area: (i) an early suite (2.47 Ga) dominated by tonalites and trondhjemites with subordinate biotite granites (Ribeirão das Areias Complex - RAC); and (ii) a later suite (2.30 Ga) including tonalites and trondhjemites (Ribeirão Itaboca Suite - RIS). Most of the RAC trondhjemite-tonalite-granodiorite (TTG) rocks are marked by fractionated REE patterns with high $(La/Yb)_N$ = 15 – 107 and samples have medium to high Sr/Y ratio (28 - 257). These TTG include both high- and low-Al types and high- and medium-pressure groups. The RIS TTG suite displays higher HREE contents with high $(La/Yb)_N$ = 65 – 89 and high Sr/Y ratio (59 - 95) and contains the high-Al type and the medium pressure group. In spite of the wide age gap between them, both RAC and RIS are characterized by TTG rocks formed in a subduction-like tectonic setting. The biotite granites are related to a magmatic stage after the TTG formation. Mafic rocks of the Gameleira Suite have an abundance of zircon, interpreted as crustal contamination, with dominant $^{207}Pb/^{206}Pb$ age populations of 2.48 and 2.30 Ga, and are interpreted to be associated with an extensional magmatic event following the Siderian period. Regional geotectonic correlations within the São Francisco Craton based on

data compiled from the literature indicate a significant volume of Siderian crust generation that has been overlooked in continental amalgamation models and that TTG magmatism is a more common geochemical signature in Paleoproterozoic rocks than has been previously suggested.

Keywords: TTG rocks; Biotite granites and hybrid granitoids; Brasília Belt; Goiás Massif; U-Pb Geochronology; Whole-rock geochemistry.

2.1. Introduction

The Neoarchaean-Paleoproterozoic transition is marked by a fundamental change in the geodynamics of plate tectonics, associated with thinner oceanic crust produced over time due to cooling of the mantle (Martin, 1986; Van Hunen et al., 2008; Condie and Kröner, 2008; Condie and O´Neill, 2010; Condie and Kröner, 2013; Laurent et al., 2014). As a consequence, the volume of TTG magmatism at the end of the Archaean diminished significantly and was surpassed by calc-alkaline magmatism in Paleoproterozoic terranes (Condie, 2008; Condie, 2014; Martin et al., 2014; Moyen et al., 2016; Halla et al., 2017; Moyen and Laurent, 2018). However, TTG rocks still formed during the Paleoproterozoic around the world (e.g. in the North China Craton, the Mineiro Belt in Brazil and the West African Craton; Yang and Santosh, 2015; Diwu et al., 2014; Barbosa et al., 2018a; Sakyi et al., 2020).

The global transition from TTG to calc-alkaline magmatism coincides with a global magmatic slowdown event in the Early Proterozoic (ca. 2.45–2.20 Ga, Condie et al., 2009; Condie and Aster, 2010; Partin et al., 2014; Pehrsson et al., 2014; Teixeira et al., 2015), suggesting important planetary consequences associated with changes in the regime of crustal recycling.

In this context, Siderian to Rhyacian magmatic and metamorphic rocks from the Almas-Conceição do Tocantins Domain (ACTD) of central Brazil, provide an opportunity to investigate the tectonic evolution of orogenic systems at the Archaean–Proterozoic boundary. Additionally, this domain represents one of the building blocks of the São Francisco paleocontinent, which amalgamated from 2.2 to 2.0 Ga, meaning that the results of this study can also provide important insights into how these terranes were later incorporated into supercontinents (Cruz et al., 2003; Fuck et al., 2014; Cordeiro and Oliveira, 2017).

This work contributes to the discussion on the geodynamic evolution of this region during the transition from the Archaean into the Proterozoic by detailing the petrography, geochronology (by U-Pb in zircon) and geochemistry of Siderian-Rhyacian felsic and mafic-ultramafic magmatism within the ACTD. Additionally, we provide a refined geological map of

the domain along with an interpretation of the geotectonic evolution of these rocks within the context of bordering terranes.

2.2. Tectonic Setting and Regional Geology

The Brasília Belt is an orogenic system developed during the Brasiliano-Pan African Orogeny due to the collision of three paleocontinents: the Amazonian to the northwest, the São Francisco to the east and the Paranapanema to the southwest, which is presently covered by the Paraná Basin (Hasui et al., 2012; Bizzi et al., 2003; Dardenne, 2000; Fig. 2.1A). Archaean and Paleoproterozoic domains are exposed in the northern portion of the Brasília Belt in the states of Goiás and Tocantins (Fig. 2.1), having formed as part of the western São Francisco paleocontinent during a Rhyacian Orogeny (i.e. the Goiás Massif; Cordeiro and Oliveira, 2017).

The northernmost and least understood part of the Goiás Massif, the ACTD (Fig. 2.1B), comprises a ~65,000 km2 collage of Paleoproterozoic terranes (Fuck et al., 2014; Fuck et al, 2017; Cordeiro and Oliveira, 2017; and references therein). The cartographic limits of the ACTD (Fig. 2.1) are according to the geological mapping of the Almas-Cavalcante Complex in the Arraias sheet (SD.23-V-A), and Dianópolis sheet (SC.23-Y-C) (Saboia et al, 2014; Abdallah and Meneghini, 2017; Saboia and Meneghini, 2019).

Correia Filho and Sá (1980) divided the granite-gneiss terrane of the ACTD into two associations: a) a granitic-migmatitic association and 2) a migmatitic-amphibolitic association. These authors also characterised a set of granitoids bodies under the name of acid-to intermediate rocks. Other works grouped and characterized the granite-gneiss rocks in the region under the name of Goiano Complex (Costa, 1985) and Alto Paranã Complex (Borges, 1998).

The ACTD contains granite-gneiss domes surrounded by greenstone belts, interpreted to have formed in a subduction environment in the early Paleoproterozoic (Cruz and Kuyumjian, 1998; Cruz et al., 2003; Kuyumjian et al., 2012). The oldest unit of the ACTD is the Riachão do Ouro Group, a greenstone volcano-sedimentary sequence consisting of the basal Córrego do Paiol Formation (mafic and ultramafic metavolcanic rocks) and the upper Morro do Carneiro Formation (phyllites, BIF's, quartzites, metacherts, metaconglomerates and felsic metavolcanic rocks), both with greenschist to amphibolite facies metamorphism (Costa, 1985; Cruz and Kuyumjian, 1998; Borges et al., 1999).

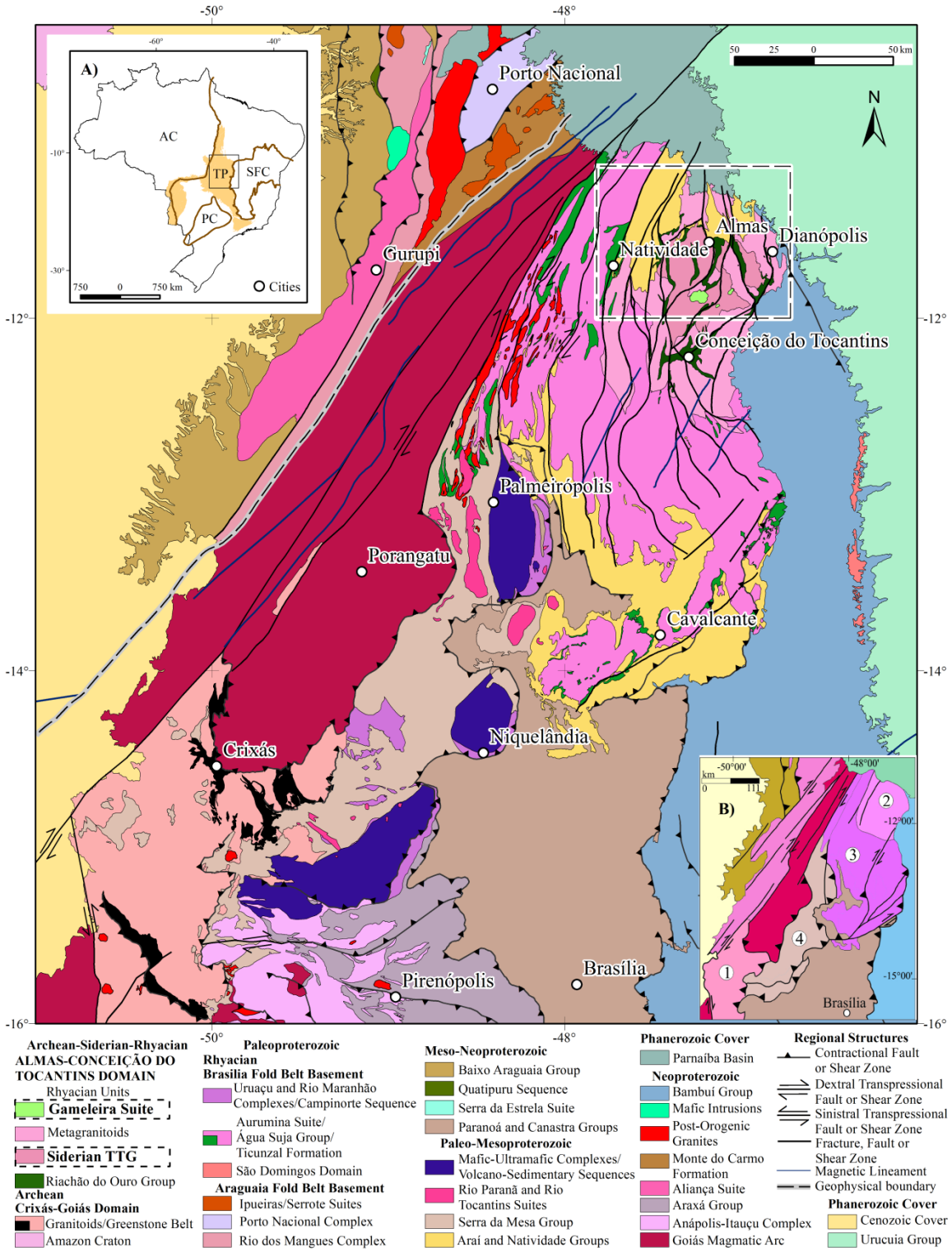

Figure. 2.1 - Geotectonic division of the Northern Brasília Belt. Modified from: Bizzi et al. (2003); Alvarenga et al. (2007); Frasca et al. (2010, 2018); Abdallah and Meneghini, (2017); Saboia et al. (2014); Ribeiro and Alves (2017). In the legend, the units in the dashed rectangles are the subject of this work. On the figure the rectangle with a dashed line indicates the study area and location of Figure 2. (A) TP-Tocantins Province, AC-Amazon Craton, SFC-São Francisco Craton, PC- Paranapanema Craton. (B) Major geotectonic domains. Modified from: Bizzi et al. (2003); Fuck et al. (2014); Cordeiro and Oliveira, (2017). 1 - Crixás-Goiás Domain, 2 – ACTD, 3 - Cavalcante Arraias Domain, 4 - Campinorte Domain. The Goiás Massif

corresponds to the domains 1, 2, 3 and 4.

Nd isotope data produced a T_{DM} age of 2.58 Ga for a metadacite dike that cross-cuts the metabasaltic rocks (Cruz and Kuyumjian, 1999), and 2.51 Ga for metabasalts of the Córrego do Paiol Formation (Saboia and Meneghini, 2019). A felsic volcanic rock from the Morro do Carneiro Formation close to the Almas region was dated (U-Pb in zircon) at 2206 ± 13 Ma (Dardenne et al., 2009). A minimum age for the Riachão do Ouro Group is provided based on the presence of xenoliths of this unit hosted within granitoids from the Ribeirão das Areias Complex, which is dated at 2.47-2.45 Ga (Cruz et al., 2003; Martins-Ferreira et al., 2017). Important auriferous occurrences are associated with this volcano-sedimentary sequence in shear zones (Kuyumjian et al, 2012).

Cruz and Kuyumjian (1998) and Cruz et al., (2003, and references therein) named and described three types of low-K calc-alkaline intrusives into the Riachão do Ouro Group, listed below: (i) the Ribeirão das Areias Complex (U-Pb titanite age of 2.45 Ga and $\varepsilon Nd(t) = +0.58$) and (ii) Suite 2 (U-Pb zircon age of 2.2 Ga and Nd isotope data with T_{DM}= 2.76 to 2.53 Ga and $\varepsilon Nd(t)$= -4.95 to -0.88) are peraluminous, biotite-rich and composed of tonalites, trondhjemites, granodiorites, and subordinate monzogranites. According to the authors above, these two units were generated by the partial melting of metabasalts either sourced from the subducted oceanic crust or newly underplated basaltic crust resulting in the formation of a garnet-amphibolite or eclogite restite, (iii) Suite 1 (U-Pb zircon age of 2.2 Ga and Nd isotope data with T_{DM}= 2.54 to 2.45 Ga and $\varepsilon Nd(t)$= -1.37 to -0.15) is rich in amphibole, has low aluminium, is metaluminous, and is composed predominantly of tonalites. According to the authors above, this suite was derived from partial melting of an ultramafic source with the formation of a pyroxene and olivine residue in a mantle wedge environment over the subduction zone.

The medium- and small-sized layered mafic-ultramafic bodies of the studied region (1.5 to 10 km of length) are called the Gameleira Suite. They consist mainly of gabbros, peridotites, pyroxenites, and serpentinites locally deformed and metamorphosed (Correia Filho and Sá, 1980; CPRM, 2000). Recent works have demonstrated the magmatic complexity of the ACTD, in terms of the petrological, geochronological and geochemical characterization of Siderian (2.47 to 2.3 Ga) and Rhyacian (ca. 2.26 to 2.18 Ga) units that make up this domain (Fuck et al., 2014; Lima, 2014; Sousa et al., 2016; Abdallah and Meneghini, 2017; Saboia and Meneghini, 2019).

In the western portion of the studied area, the ACTD is covered or in tectonic contact with the metavolcano-sedimentary Água Suja Group (2.17 Ga, maximum deposition age) and it is intruded by the metagranitoids of the Aurumina Suite with magmatism between 2.10 to 2.16 Ga (Silva, 1987; Queiroz, 2001; Abdallah and Meneghini, 2017; Cuadros et al., 2017b). This domain is also covered by Meso-Neoproterozoic metasedimentary basins (Natividade and

Bambuí Groups) and Phanerozoic sedimentary basins (Parnaíba and São Francisco), besides being intruded by Cretaceous mafic dikes (Correia Filho & Sá, 1980; Hasui, 1990; Saboia, 2009). The region was strongly affected by orogenic processes in the Paleoproterozoic and Neoproterozoic, registered as regional metamorphism (greenschist to amphibolite facies), kilometer-scale folds and extensive transpressional shear zones (Borges et al., 1999; Kuyumjian; Araújo Filho, 2005; Kuyumjian et al., 2012; Saboia and Meneghini, 2019). The western portion of the area is strongly marked by deformation associated with the Trans-Brasiliano Lineament (Dardenne and Saboia, 2007; Fuck et al., 2017).

2.3. Local Geology

This work focuses on three units from the ACTD: the Ribeirão das Areias Complex (Cruz et al., 2003, and references therein), the Ribeirão Itaboca Suite (defined in this work) and the Gameleira Suite (Correia Filho and Sá, 1980).

2.3.1. Ribeirão das Areias Complex (RAC)

This unit forms an approximately 58 km long NNE-trending crustal segment that is exposed as a flatland in the central part of the mapped area (Fig. 2.2). It is composed of multiple large sigmoidal-shaped batholiths oriented NNW-SSE to NNE-SSW. Contact relationships of the RAC are dominantly by fault or undetermined, however, this unit is interpreted as intrusive into the Riachão do Ouro Group based on the presence of metavolcanic xenoliths within the complex.

The RAC comprises mesocratic and leucocratic metatonalites and metatrondhjemites with subordinate metagranodiorites (Fig. 2.3A, B). The nuclei of batholiths preserve igneous textures whereas their borders are foliated with banded structures. In addition to the rock types described above, this unit also includes subordinate medium to very coarse-grained metagranodiorite and metamonzogranite intrusions (mapped as Ribeirão das Areias intrusive bodies - RAib in Fig. 2.2), which might crop out as up to 500 m high hills against the generally flat landscape.

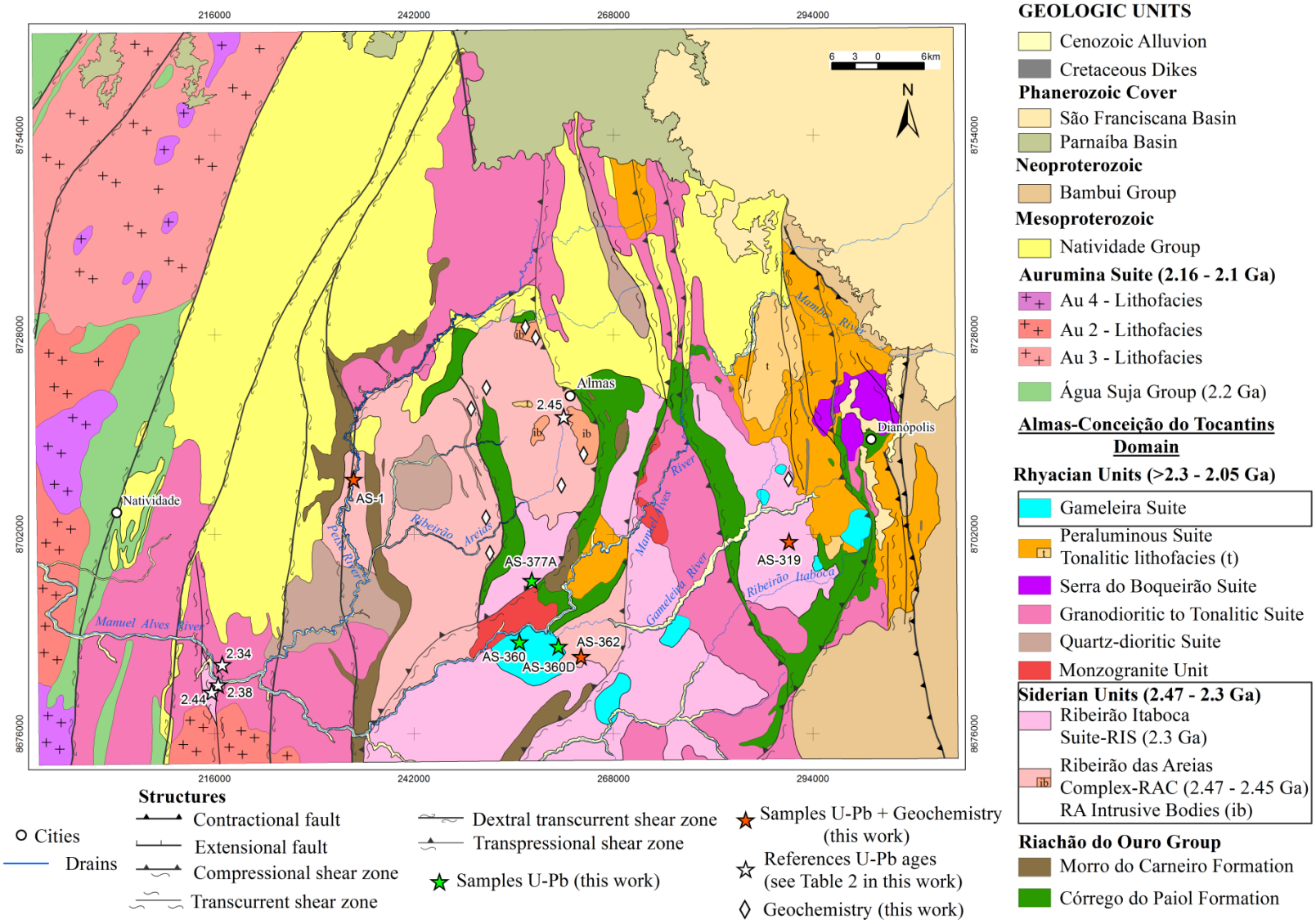

Figure 2.2 - Schematic geological map of the studied area, indicating the locations of the geochronological and geochemical data (Modified from Saboia et al., 2014). The units of the map that are inside the rectangles in the legend are the subject of this work.

2.3.2. Ribeirão Itaboca Suite (RIS)

The Ribeirão Itaboca Suite also is exposed as a flat region dominantly in the center-eastern part of the studied area, with additional isolated occurrences near the Príncipe and the Conceição do Tocantins villages that were described in previous works (Fuck et al., 2014; Lima, 2014; Sousa et al., 2016). The contact relationship with the RAC is unknown and its stratigraphic position was defined based on geochronological data (Table 2). In previous works, this unit was inserted in the migmatitic-amphibolitic association, as an undivided granite-gneiss complex or as part of Suite 1 and 2 granitoids (Correia Filho and Sá, 1980; Cruz et al., 2003).

The RIS includes mesocratic and leucocratic biotite metatonalites and tonalitic gneisses with subordinate foliated metatrondhjemites and metagranodiorites (Fig. 2.3C, D). This unit is also characterized by migmatitic gneisses showing banding, dilation, stromatic structures, mafic enclaves, and the formation of metatexites and diatexites migmatites (sensu Sawyer, 2008).

2.3.3. Gameleira Suite

The mafic-ultramafic rocks of the Gameleira Suite occur as generally NNE-NE trending plutons and a few stocks, exposed in the central-eastern portion of the studied area. These rocks are in tectonic contact or intrusive into the other studied units.

The Gameleira Suite is dominantly composed of metanorites, metagabbro-norites and meta-olivine gabbro-norites with cumulate and subophitic textures and rhythmic layering structures (Fig. 2.3E, F). They are mesocratic to melanocratic usually with isotropic and massive structure. The Barra do Gameleira Intrusion is the most conspicuous occurrence, represented by an 8 x 10 km semi-circular shaped layered intrusion with preserved magmatic cross-stratification but otherwise metamorphosed locally to the amphibolite and granulite facies (Correia Filho and Sá, 1980) and having a NNW foliation related to a ductile deformation. Subordinate, peridotites, pyroxenites, and serpentinites are also described as occurring throughout the mapped area (Correia Filho and Sá, 1980; CPRM, 2000).

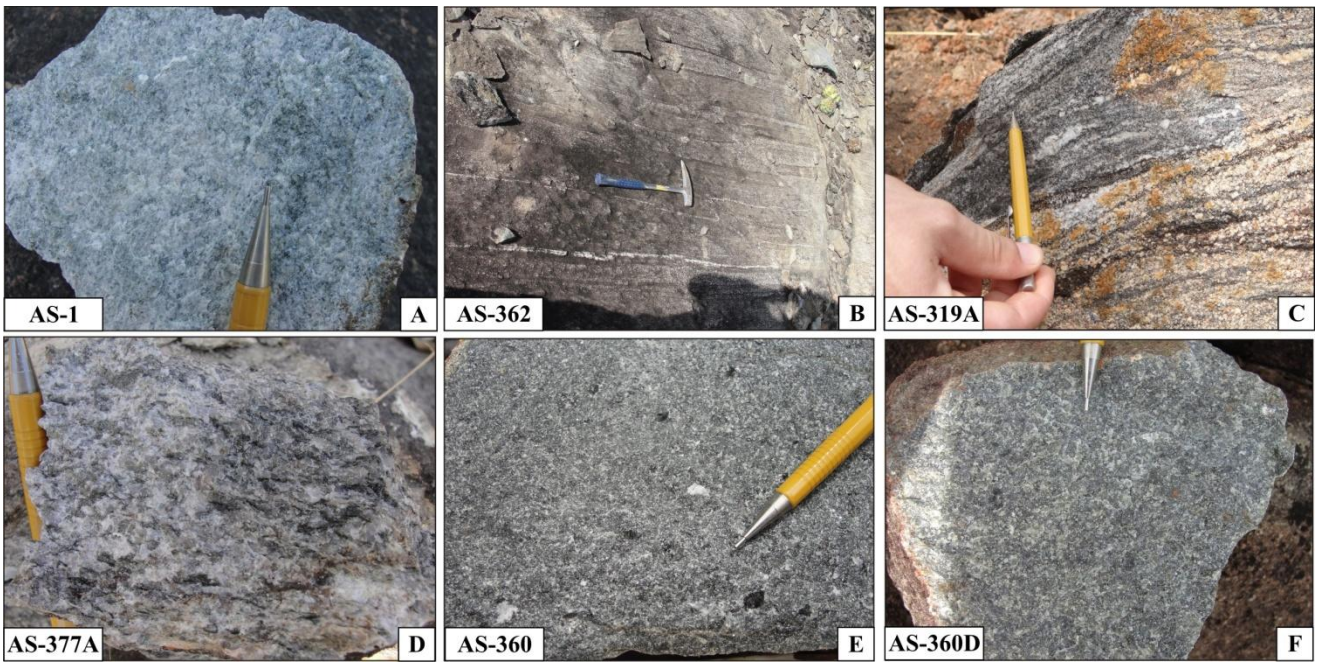

Figure 2.3 - Field aspects of the rocks dated in this study. (A) Ribeirão das Areias metagranodiorite with medium- to coarse-grained and inequigranular texture. (B) Ribeirão das Areias tonalitic-gneiss with banded structure. (C) Ribeirão Itaboca medium- to coarse-grained tonalitic-gneiss with stromatic structure. (D) Ribeirão Itaboca medium- to coarse-grained, foliated, biotite metatonalite. (E) Gameleira Suite isotropic, inequigranular, magnetic and slightly porphyritic gabbronorite. (F) Gameleira Suite isotropic medium grained olivine-gabbronorite. Field/sample point is shown in the lower left corner of corresponding photos, for reference.

2.4. Methods

2.4.1. U-Pb LA-MC-ICPMS and SIMS (SHRIMP) Geochronology

In order to detail the Siderian magmatic events of the studied area we analyzed representative samples of the: (a) Ribeirão das Areias Complex: AS-1 (by SHRIMP II with zircon imaged by cathodoluminescence-CL) and AS-362 (by LA-MC-ICP-MS with zircon imaged by back-scattered electron-BSE); (b) Ribeirão Itaboca Suite: AS-319 (by LA-MC-ICP-MS with zircon imaged by CL) and AS-377A (by LA-MC-ICP-MS with zircon imaged by BSE); (c) Gameleira Suite: AS-360 (by LA-MC-ICP-MS with zircon imaged by BSE) and AS-360D (by LA-MC-ICP-MS with zircon imaged by BSE). Tables with analytical data are in the supplementary materials section (Tables A-F). The new ages obtained in this work and the available geochronological data in the literature are summarized in Table 2.2 and sample locations are depicted on Figure 2.2. For analysis by LA-MC-ICP-MS (Laser Ablation Multi-Collector–Inductively Coupled Plasma-Mass Spectrometer) and SHRIMP (Sensitive High - Resolution Ion Microprobe) samples were broken with a jaw crusher and powdered to approximately 500 µm. Heavy mineral concentrates were obtained by panning and were

subsequently purified using a Frantz isodynamic separator. Zircon grains were selected from the least magnetic fraction and while the objective was to sample all the populations of zircon grain based on appearance (colour, shape, size, etc), the best grains of each population were selected (clear, lacking fractures or inclusions). These grains were set in epoxy resin mounts and their surface was then polished to expose the grain interiors for imaging via Scanning Electron Microscope (SEM) using cathodoluminescence (CL) and/or backscattered electron imaging (BSE).

The U–Pb analyses by LA-ICP-MS were carried out using a Thermo Scientific Neptune coupled to an Nd-YAG laser (λ = 213 nm) ablation system (New Wave Research, USA) at the Geochronology Laboratory of the University of Brasília. Analytical procedures follow those outlined in Bühn et al., (2009), where the epoxy mounts were cleaned in an HNO3 solution (3%) and ultraclean water bath. Ablation was done with a spot size of 25–30 µm, at a frequency of 10 Hz and fluence of 2.0–6.0 J/cm^2. The ablated material was carried by Ar (0.90 L/min) and He (0.40 L/min) in analyses of 40 cycles of 1 s. Unknown analyses were bracketed by measurements of the international standard GJ-1 (^{207}Pb/^{206}Pb = 608.3 Ma, ^{206}Pb/^{238}U = 600.7 Ma and ^{207}Pb/^{235}U = 602.2 Ma, according Jackson et al. 2004), following the sequence 1 blank, 1 standard, 4 unknown, 1 blank and 1 standard. Accuracy was controlled using the standard 91500 (ID-TIMS 1065.4 ± 0.3 Ma - Wiedenbeck et al., 1995). Raw data were reduced using Chronus (Oliveira, 2010), an add-in for Excel®. In the data reduction process, Chronus performed corrections for background, mass fractionation, and instrumental mass-bias drift. For this the sample-standard bracketing (Albarède et al., 2004) method was applied and the uncertainties calculated by quadratic addition of the individual uncertainties. The down hole fractionation was corrected by Chronus (Oliveira, 2010) using the method of intercept, derived from the least squares (Košler et al., 2002; Bevington and Robinson, 2003). Ages were calculated using ISOPLOT 4.1 (Ludwig, 2012). The samples were analyzed in four sessions, and results obtained for the 91500 are presented in supplementary data and summarized in Table G.

Samples for SHRIMP analyses were mounted with Temora zircon standard crystals. CL images were obtained in order to reveal internal structures of the zircon grains. Ion microprobe analyses were carried out using SHRIMP II at the University of São Paulo. SHRIMP analytical methods and data treatment follow those described by Williams (1998) and Williams and Meyer (1998). The analysis were performed using a spot size of 24 µm. Data were processed using SQUID and ISOPLOT 4.1 (Ludwig, 2012). The analytical data of the primary (Temora zircon) and secondary (SL-13 zircon) standards are included in the supplementary material (Table H).

2.4.2. Whole-rock Geochemistry

The whole-rock geochemistry of 13 representative metagranitoids was studied to establish the tectonic setting and geochemical features of the felsic Siderian magmatism of the ACTD (Table 2.1). The rocks studied refer to eleven samples of Ribeirão das Areias Complex, including RAib intrusions (AS-1, AS-210, AS-210A, AS-332, AS-333, AS-335, AS-344, AS-348, AS-352, AS-362 and AS-362A) and two samples of Ribeirão Itaboca Suite (AS-317A and AS-319A). Major element analyses were carried out by X-ray fluorescence (XRF) at the SGS GEOSOL laboratory in Vespasiano, Minas Gerais (Brazil), according to its pre-established XRF79C analytical method. Pulps (~2 grams per sample) were oven-dried and weighed after cooling into a jar containing lithium tetraborate flux. The sample was then transferred to a platinum crucible and homogenized. After homogenization, lithium iodide was added prior to fusion in an automatic machine, and analysis by XRF. Trace element analyses were carried out by inductively coupled plasma mass spectrometry (ICP-MS) at the SGS GEOSOL laboratory in Vespasiano, Minas Gerais (Brazil), according to its pre-established IMS95A analytical method. Pulps (~10 grams per sample) were weighed and then fused in a graphite crucible by adding lithium metaborate. After fusion the melt was transferred to a beaker containing a solution of nitric acid and tartaric acid in equal volumes before homogenization and total dissolution under agitation, and analysis of the solution by ICP-MS. The standards used for the geochemical analyses correspond to the following reference materials present in the certificates of analysis by the SGS GEOSOL laboratory: AMIS0183, GBM995-2-R, SARM3, SG-077, SG-121, SG-142 and TILL-3. Geochemical analyses were plotted using the GCDkit software (Janousek et al., 2006).

2.5. Results

2.5.1. Geochronology of Ribeirão das Areias Complex: samples AS-1 and AS-362

The NNE trending, medium grained, granoblastic metagranodiorite AS-1 (Fig. 2.3A) was collected under the Rio do Peixe bridge on the TO-280 road (UTM 234129E; 8709166N). It is composed of quartz, plagioclase, microcline, and biotite with accessory titanite, opaque minerals, apatite and zircon. Sericite, clinozoisite, epidote, chlorite and carbonate represent the secondary mineral assemblage. Zircon grains are clear, prismatic, 50-120 µm in size, lack inclusions or fractures, and show strong and continuous oscillatory zoning under CL (Fig. 2.4A).

Unit/Rock Type	RAC/ Gran. * TTG	RAC – Raib/ Granit. B.G	RAC – Raib/ Granit. B.G	RAC – Raib/ Gran. TTG	RAC/ Tonal. TTG	RAC/ Gran. TTG	RAC/ Tonal. TTG	RAC/ Tonal. TTG	RAC/ Trond. TTG	RAC/ Tonal. * TTG	RAC/ Trond. TTG	RIS/ Tonal. TTG	RIS/ Tonal. * TTG
Sample	AS-01	AS-210	AS-210A	AS-332	AS-333	AS-335	AS-344	AS-348	AS-352	AS-362	AS-362A	AS-317A	AS-319A
SiO_2	69.10	72.50	71.80	69.20	67.70	73.80	69.70	74.10	72.20	67.00	71.80	69.60	70.20
Al_2O_3	14.30	15.00	15.20	15.40	16.10	13.80	15.50	14.50	15.80	15.90	14.70	16.00	15.30
Fe_2O_3	4.46	2.25	2.08	3.06	4.00	2.11	3.38	1.86	1.72	3.82	2.43	4.33	3.67
MgO	1.61	0.74	0.53	0.64	1.03	0.27	0.91	0.25	0.42	1.05	0.48	0.99	1.06
CaO	2.72	0.45	0.68	2.52	3.67	1.66	3.13	1.72	1.89	3.45	2.56	3.77	3.17
Na_2O	3.32	4.59	4.55	4.56	4.46	4.49	4.22	5.44	5.65	4.74	4.84	3.94	3.94
K_2O	2.03	3.88	3.52	2.32	1.43	2.49	1.92	1.48	1.82	1.39	1.28	1.52	1.35
TiO_2	0.46	0.22	0.20	0.31	0.40	0.11	0.34	0.12	0.20	0.43	0.23	0.43	0.37
P_2O_5	0.11	0.06	0.07	0.11	0.12	0.05	0.10	0.04	0.07	0.15	0.06	0.13	0.05
MnO	0.05	0.04	0.03	0.04	0.05	0.05	0.04	0.02	0.04	0.04	0.03	0.05	0.04
LOI	1.26	1.01	0.83	0.88	1.09	0.60	1.05	0.64	0.71	1.40	0.96	0.43	0.54
SUM	99.42	100.74	99.49	99.04	100.05	99.43	100.29	100.17	100.52	99.37	99.37	101.19	99.69
Ni	10.10	1.00	9.00	8.00	10.00	9.00	13.00	1.00	9.00	16.00	11.00	22.00	18.00
Co	8.50	1.40	2.40	4.80	8.90	3.10	6.40	2.20	3.00	8.70	3.90	8.20	8.60
Ba	406.00	993.00	863.00	716.00	589.00	492.00	400.00	364.00	389.00	473.00	370.00	536.00	479.00
Rb	45.20	78.00	67.70	36.80	33.10	55.50	52.30	37.80	26.30	33.80	27.40	60.80	47.40
Sr	312.50	320.70	378.30	493.50	410.50	206.00	389.70	196.50	962.30	439.90	296.80	678.80	436.60
Nb	8.35	2.05	1.21	3.66	4.33	4.93	3.46	3.13	0.98	2.89	2.18	5.19	5.02
Ta	3.29	0.23	0.10	0.39	0.32	1.43	0.74	0.78	0.12	0.11	0.10	0.69	0.59
Zr	176.70	136.70	116.10	117.00	163.00	60.30	149.40	82.10	108.60	196.80	92.70	216.90	125.10
Hf	4.33	3.25	2.66	3.13	4.30	2.40	3.72	2.52	2.72	4.69	2.48	5.72	3.19
Cu	4.70	3.10	16.50	5.90	2.40	1.50	2.50	10.10	2.60	28.80	3.40	5.90	5.30
Pb	3.10	5.10	7.00	4.70	1.70	2.70	1.00	7.10	5.30	1.40	0.90	3.70	4.30
Zn	36.00	10.00	22.00	16.00	61.00	20.00	29.00	12.00	11.00	62.00	26.00	57.00	51.00
Th	3.40	7.90	7.70	8.40	5.60	2.40	2.60	2.80	3.70	7.30	3.20	13.90	9.60
U	0.19	2.48	2.15	1.34	0.56	0.72	2.09	1.39	0.56	0.47	0.40	1.12	0.68
Ga	14.40	18.00	19.20	17.80	20.80	17.00	18.00	16.70	17.80	22.20	18.90	20.10	18.60
Cs	1.18	0.96	0.86	0.32	0.41	0.58	0.76	0.47	0.48	0.30	0.14	2.29	0.89
Y	11.15	17.89	4.52	5.96	7.35	6.88	3.63	4.33	3.75	5.78	1.96	7.14	7.34
La	9.80	191.10	32.60	28.60	35.60	14.00	20.10	10.00	32.40	44.60	17.90	67.90	39.80
Ce	19.00	95.60	49.10	68.30	57.10	16.20	35.80	20.40	49.80	72.20	22.70	131.90	70.40
Pr	2.08	23.74	5.10	5.57	6.73	2.27	3.27	1.72	5.44	6.72	2.64	12.31	6.66
Nd	7.70	77.60	14.30	19.20	22.90	8.20	10.50	5.70	18.30	21.00	8.40	48.60	27.20
Sm	1.90	9.20	2.50	3.00	3.70	1.80	1.80	1.20	2.80	2.70	1.20	6.10	3.80
Eu	1.03	2.41	0.64	0.77	0.95	0.51	0.58	0.43	0.78	0.67	0.38	1.53	1.37
Gd	2.45	6.71	1.52	2.13	2.69	1.84	1.42	1.21	2.00	2.10	0.92	3.24	2.36
Tb	0.33	0.68	0.18	0.26	0.33	0.35	0.21	0.18	0.22	0.25	0.10	0.44	0.31
Dy	1.73	3.00	0.80	1.24	1.70	1.28	0.86	0.89	0.90	1.21	0.41	1.33	1.15
Ho	0.48	0.51	0.16	0.24	0.29	0.33	0.17	0.16	0.14	0.22	0.07	0.29	0.28
Er	1.37	1.27	0.42	0.60	0.72	0.63	0.33	0.37	0.30	0.50	0.14	0.61	0.43
Tm	0.28	0.16	0.03	0.09	0.10	0.19	0.08	0.06	0.03	0.07	0.03	0.17	0.11
Yb	1.30	0.90	0.30	0.50	0.60	0.60	0.30	0.30	0.20	0.40	0.20	0.50	0.40
Lu	0.20	0.12	0.03	0.07	0.06	0.19	0.07	0.03	0.03	0.03	0.03	0.16	0.11
K_2O/Na_2O	0.61	0.85	0.77	0.51	0.32	0.55	0.45	0.27	0.32	0.29	0.26	0.39	0.34
Sr/Y	28.03	17.93	83.69	82.80	55.85	29.94	107.36	45.38	256.61	76.11	151.43	95.07	59.48
(La/Yb)n	4.97	139.87	71.58	37.68	39.08	15.37	44.13	21.96	106.71	73.45	58.96	89.46	65.54
Eu/Eu*	1.46	0.94	1.0	0.93	0.92	0.86	1.11	1.09	1.01	0.86	1.11	1.05	1.4

Table 2.1 - Major and trace element data for the studied samples. Oxides (wt. %) and Trace elements (ppm). Normalization values are from Masuda et al. (1973). Acronyms are: (RAC) Ribeirão das Areias Complex with (RAib) Ribeirão das Areias intrusive bodies, (RIS) Ribeirão Itaboca Suite, (Trond.) Trondhjemite, (Tonal.) Tonalite, (Gran.) Granodiorite, (Granit.) Granite,

(B.G) Biotite granites, (TTG) TTG rock, (*) Samples with U-Pb analyzes.

Fourteen zircon grains were investigated by SHRIMP II (Table A, see supplementary material). The most concordant data (seven spots) were used to define the concordia age (MSWD=1.6) of 2473 ± 12 Ma, which is interpreted as the crystallization age (Fig. 2.5A). Th/U ratios range from 0.38 to 0.78.

Sample AS-362 (UTM 263793E; 8686067N) corresponds to a medium grained tonalitic-gneiss with decimetric scale banding (Fig. 2.3B) and blastomylonitic texture. Quartz, plagioclase and biotite are the main minerals with titanite, opaque minerals and zircon as accessory minerals. Sericite, zoisite, epidote, chlorite and carbonate represent the secondary mineral assemblage. The zircon recovered from this sample is prismatic, presents some inclusions and abundant fractures. The grains are around 100 µm. Oscillatory zoning is the main structure observed in BSE images (Fig. 2.4B).

Thirty seven spots on thirty crystals were conducted by LA-MC-ICP-MS (Table B). All crystals have Th/U ratios compatible with igneous rock, between 0.16 and 0.57, except for spot 1.1 that has a ratio of 0.04. Data from the 28 spots with the most consistent results were used in the age calculation. Its regression (Fig. 2.5B) has an upper intercept of 2478 ± 9 Ma associated with an MSWD of 0.72, interpreted as the crystallization age. The lower intercept of 533 ± 38 Ma may be related to a later thermal event.

2.5.2. Geochronology of Ribeirão Itaboca Suite: samples AS-319 and AS-377A

Sample AS-319 (Fig. 2.3C) is a medium- to coarse-grained, granolepidoblastic tonalitic biotite-gneiss collected about 16 km southwest of Dianópolis city (UTM 290901E; 8701080N). Essential minerals are quartz, plagioclase, K-feldspar and biotite whereas opaque minerals and zircon are accessory. Secondary minerals are white mica, chlorite, zoisite, sericite and carbonate.

Zircon grains extracted from this sample are prismatic crystals 50-250 µm in length. They are light pink, clear, and with few inclusions or fractures. CL images show well-developed oscillatory zoning (Fig. 2.4C), which together with the high Th/U ratios (usually >0.1), indicate a magmatic origin for the zircon. The U-Pb isotopic content of twenty-six zircon grains from this sample was determined by LA-MC-ICP-MS (Table C). The majority of the spots have an age of ~ 2.3 Ga, with only 5 presenting $^{207}Pb/^{206}Pb$ ages between 2400 and 2600 Ma.

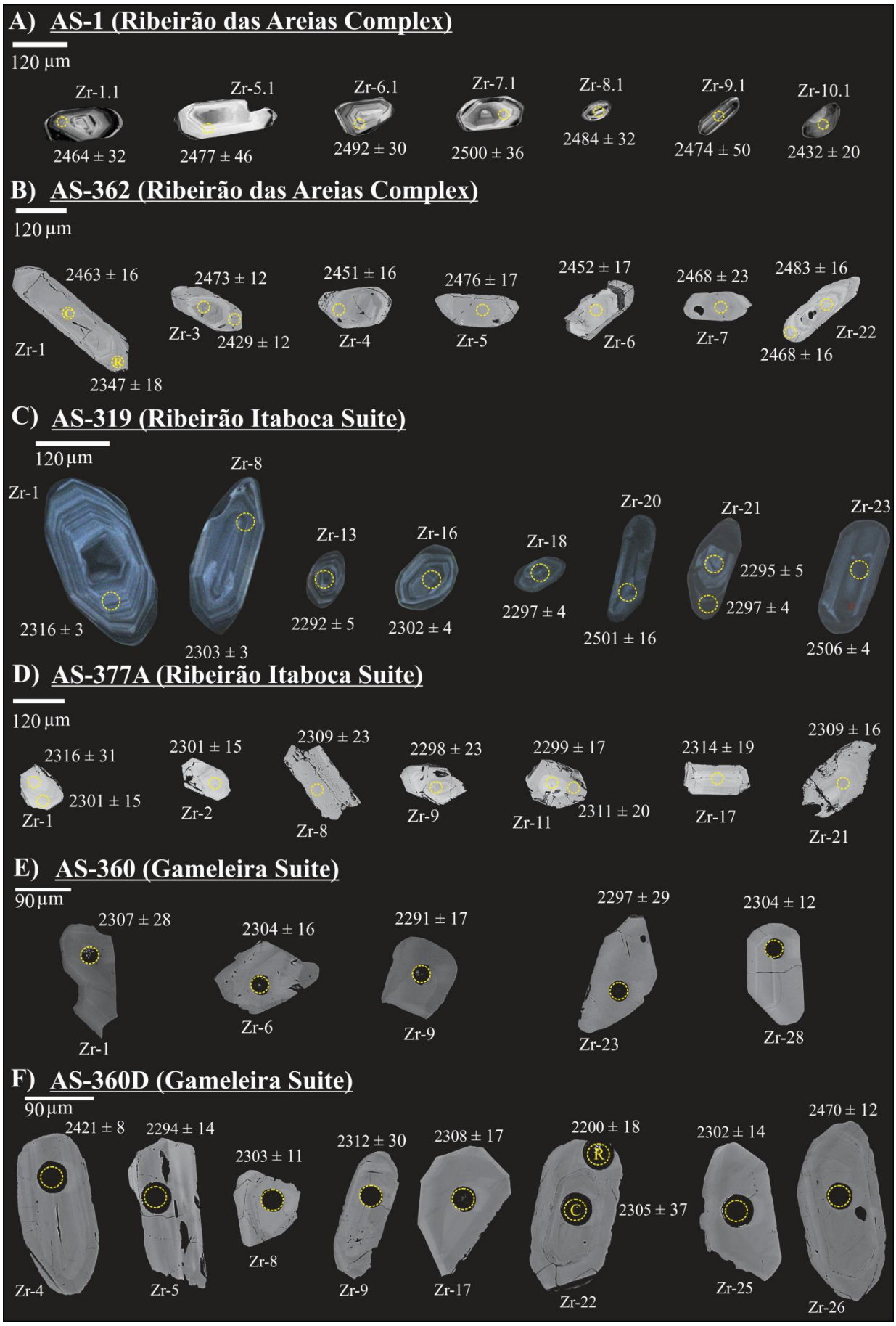

Figure 2.4 - SEM images of analyzed zircon crystals. The yellow dotted circles indicate the spot

analyzes and their $^{207}Pb/^{206}Pb$ apparent ages and uncertainties (2 sigma) are expressed in Ma. Zr = number of analyzed zircon (see supplementary material). (A) CL images of selected zircons for AS-1 sample (Ribeirão das Areias Complex). (B) BSE images of selected zircons for AS-362 sample (Ribeirão das Areias Complex). (C) CL images of selected zircons for AS-319 sample (Ribeirão Itaboca Suite). (D) BSE images of selected zircons for AS-377A sample (Ribeirão Itaboca Suite). (E) BSE images of selected zircons for the AS-360 sample (Gameleira Suite). (F) BSE images of selected zircons for the AS-360D sample (Gameleira Suite). C-core and R-rim.

The five most concordant analyses from the main group were used to calculate the concordia age of 2299 ± 3 Ma, (MSWD = 0.51, probability of concordance of 0.87; Fig. 2.5C). This result is interpreted as the crystallization age of the igneous protolith. Selected grains yield Th/U between 0.23 and 0.38. The older group could be interpreted as inherited zircons, potentially from the RAC.

Sample AS-377A (UTM 257616E; 8695079N) is a coarse-grained, foliated biotite metatonalite (N13°E trend; Fig. 2.3D) composed of quartz, plagioclase and biotite with accessory zircon and opaque minerals. Zircon grains are bipyramid prisms with fractures and some inclusions. BSE images reveal discrete oscillatory zoning and some homogeneous crystals (Fig. 2.4D).

This sample was investigated by LA-MC-ICP-MS (Table D). Thirty one analyzed spots were used for age calculations. The results obtained are distributed along a line with different degrees of lead loss. Regression along this line is associated with an MSWD of 0.60 and has upper and lower intercepts of 2307 ± 5 Ma and 239 ± 120 Ma, respectively (Fig. 2.5D). The first age is interpreted as the crystallization age for this sample and the younger suggests present day lead loss.

2.5.3. Geochronology of Gameleira Suite: Samples AS-360 and AS-360D

Samples AS-360 and AS-360D were collected on the northwestern (UTM 255749E; 8687991N) and eastern border (UTM 260835E; 8687410N) of the Barra do Gameleira intrusion, respectively.

Sample AS-360 is a fine- to medium grained isotropic gabbronorite with equigranular to slightly porphyritic and hipidiomorphic textures (Fig. 2.3E). Plagioclase (andesine and labradorite) and clinopyroxene (augite) are the main minerals, while orthopyroxene, opaque minerals and zircon are accessory minerals. Secondary minerals are amphibole, bastite, sericite, zoisite and epidote.

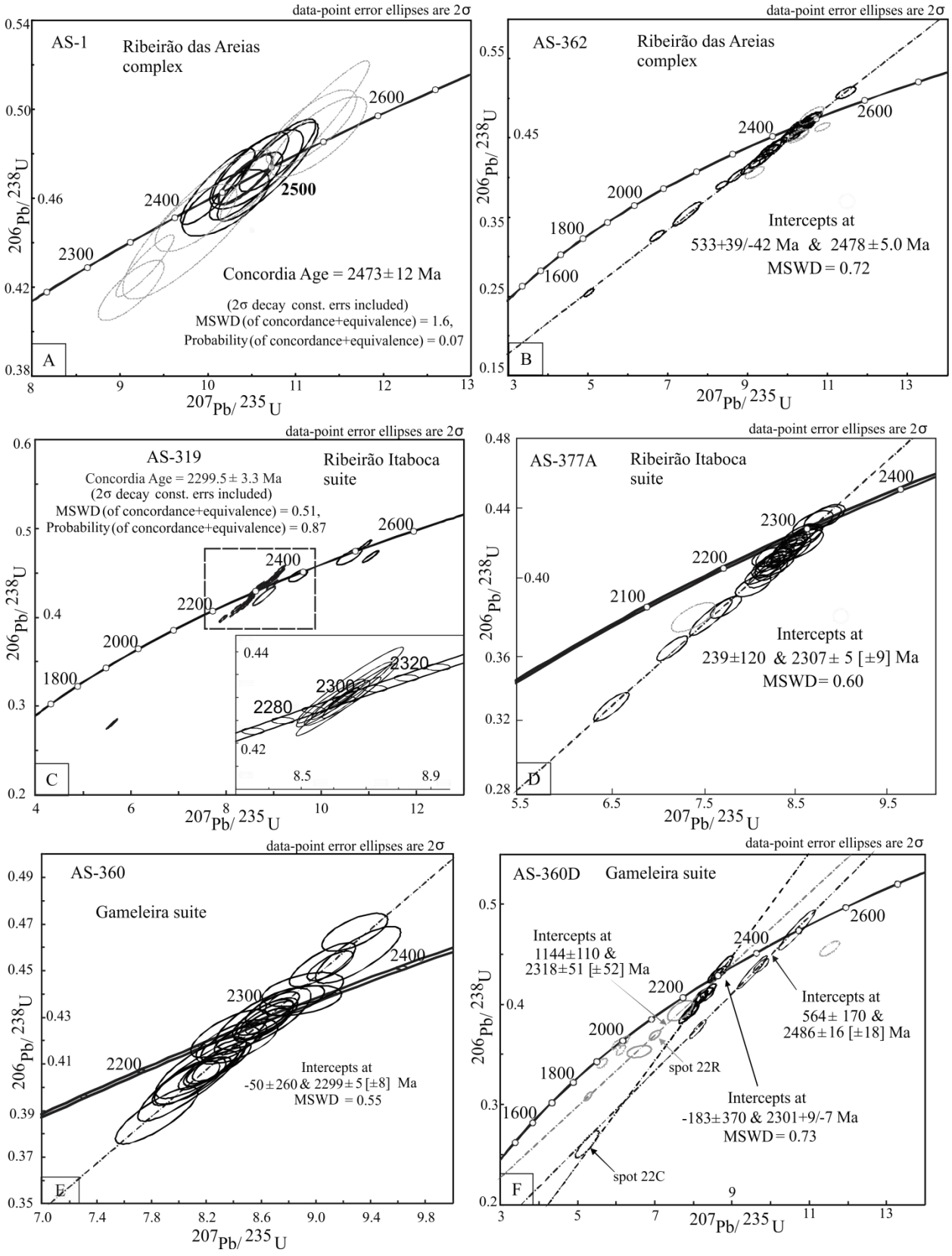

Figure 2.5 - (A) U-Pb concordia diagram for AS-1 sample (Ribeirão das Areias Complex). Dashed grey ellipses represent data not used in age calculation. (B) Concordia diagram for AS-362 sample (Ribeirão das Areias Complex). (C) U-Pb concordia diagram for AS-319 sample (Ribeirão Itaboca Suite). (D) U-Pb concordia diagram for AS-377A sample (Ribeirão Itaboca Suite). (E) U-Pb concordia diagram for the AS-360 sample (Gameleira Suite), the analysis discarded by high analytical error was not included in the concordia. (F) U-Pb concordia diagram

for the AS-360D sample (Gameleira Suite). Dashed grey ellipses represent data not used in age calculations.

This sample contains small and clear zircon fragments or short prismatic crystals (60-80μm). BSE images reveal homogenous internal structures or discrete sector/oscillatory zonation (Fig. 2.4E). Twenty-seven LA-MC-ICP-MS (Table E) isotopic analyses are nearly collinear on the concordia diagram. The data regress to yield an upper intercept age of 2299 ± 5 Ma with an MSWD = 0.55 (Fig. 2.5E), whereas the lower intercept indicates modern lead loss. Their Th/U values range from 0.20 to 0.8.

Sample AS-360D is a medium grained isotropic olivine-gabbronorite with equigranular and hipidiomorphic textures (Fig. 2.3F). Plagioclase, orthopyroxene, clinopyroxene and olivine are the main minerals, whereas opaque minerals and zircon are accessory. Secondary minerals are sericite, iddingsite, bastite and zoisite. The zircon grains in this sample are quite similar to those in sample AS-360. They also occur as small fragments or short prismatic crystals, which may be homogeneous or present some inclusions and fractures (Fig. 2.4F), but a few crystals present medium prisms (~3:1) with discrete oscillatory zoning, and features that appear to be thin rims (e.g. grains 22 and 26).

Analysis of these crystals shows some dispersion (Table F). Twelve out of 23 analyses (Th/U between 0.4 and 0.82) performed by LA-MC-ICP-MS yield an upper intercept of 2302 + 9/-7 Ma (MSWD = 0.73; Fig. 2.5F). Four analyses from zircon of the minor group are collinear and regress to yield an upper intercept age of 2486 +16/-18 Ma (MSWD = 0.51; Fig. 2.5F) interpreted as crustal contamination originating from the RAC. Most of the possible rims are too thin to be analyzed. An analysis was attempted at the rim of grain 22. The result obtained was discordant, but roughly aligned with three others results, which point out to the upper intercept of 2318 ± 51 Ma. Considering the uncertainties, this is the same age obtained for the main group. The core of grain 22 was also analyzed and presented a very discordant result (35.33%), with a $^{207}Pb/^{206}Pb$ apparent age of 2305 Ma and an abnormally high Th/U ratio of 1.42. This data was discarded in the age calculations, due to inconsistent behavior.

2.5.4. Geochemistry of the Ribeirão das Areias Complex and Ribeirão Itaboca Suite

Rocks from the ACTD have been classified as TTG in the past by Cruz et al. (2003, and references therein) and in the normative An–Ab–Or classification diagram (Fig. 2.6a; O'Connor, 1965) most samples indeed plot within the tonalite and trondhjemite fields.

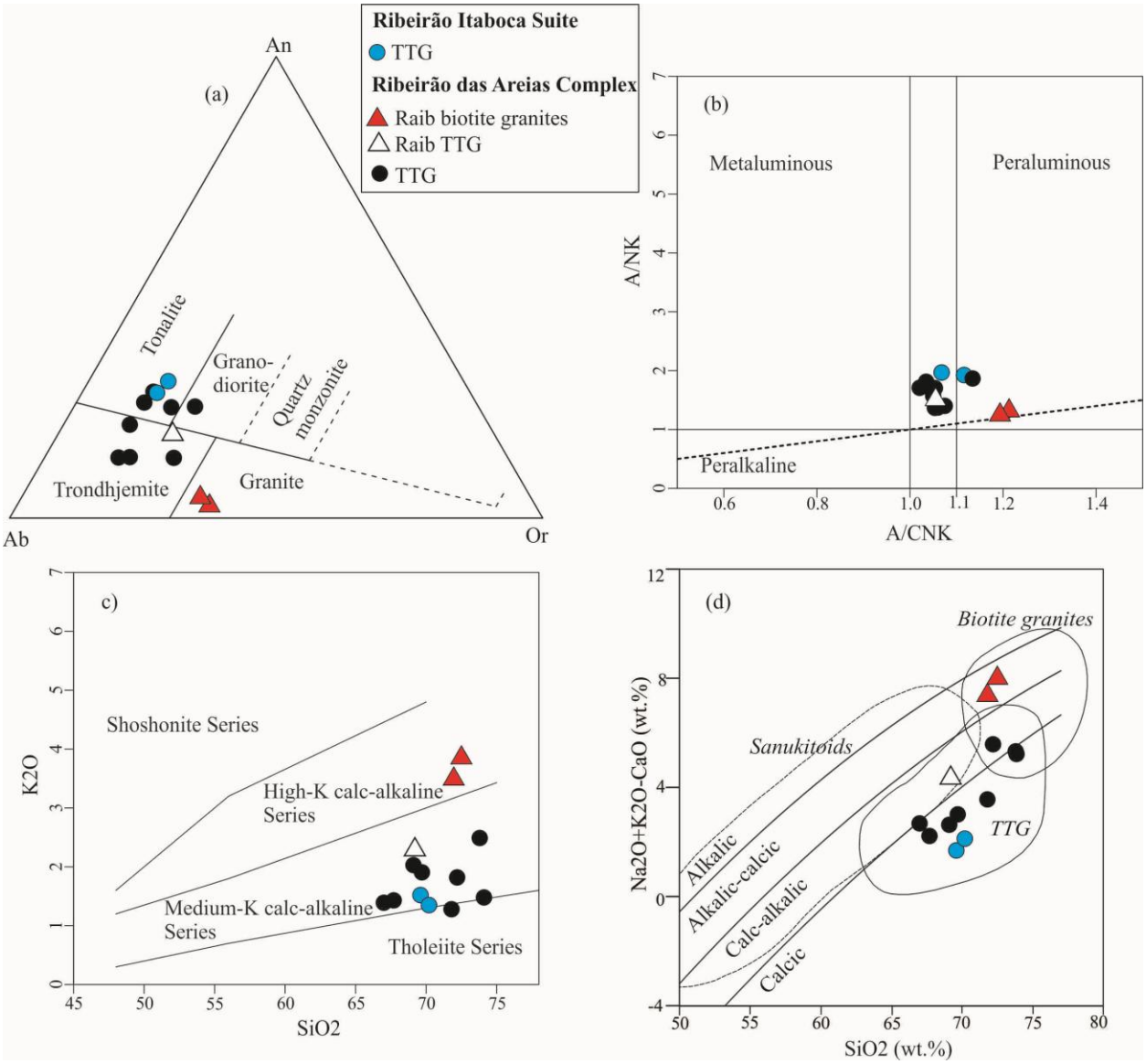

Figure 2.6 - Diagrams with the classification of the rocks of Ribeirão das Areias Complex and Ribeirão Itaboca Suite based on major elements. (a) Normative feldspar triangle (O'Connor, 1965). (b) A/NK vs. A/CNK (Shand, 1943). (c) SiO_2 vs. K_2O (Peccerillo and Taylor, 1976). (d) MALI index (Na_2O+K_2O-CaO) vs. SiO_2 diagram of Frost et al., (2001), fields from Laurent et al., (2014).

Samples AS-210 and AS-210A of the Ribeirão das Areias Complex (RAib) plot predominantly in the granite field. All of the studied rocks are felsic (67–74% SiO_2), peraluminous (Fig. 2.6b; Shand, 1943) and belong mainly to the medium-K calc-alkaline series (Fig. 2.6c; Peccerillo and Taylor, 1976), whereas most samples of RAib belong to the high-K calc-alkaline series and are strongly peraluminous. In Fig. 2.6d (MALI index of Frost et al., 2001 with fields from Laurent et al., 2014) most samples fall into the calcic and calc-alkalic fields, with the TTG rocks being calcic. The two RAib samples are alkalic-calcic and plot in the field of biotite granites.

Moyen et al., (2003) proposed discriminant diagrams for the typology of Archean rocks

using major elements based on samples from the Dharwar Craton. When the samples of this study are plotted on these (Fig. 2.7a), it is possible to identify each type, although there is some overlap between the groups. The studied TTG rocks mainly plotted in the fields of TTG & adakites with overlaps in the sanukitoids & enriched TTG and classic Archaean TTG fields in Fig. 2.7a. In the same figure, samples AS-210 and AS-210A of RAib fall close to the biotite granite field.

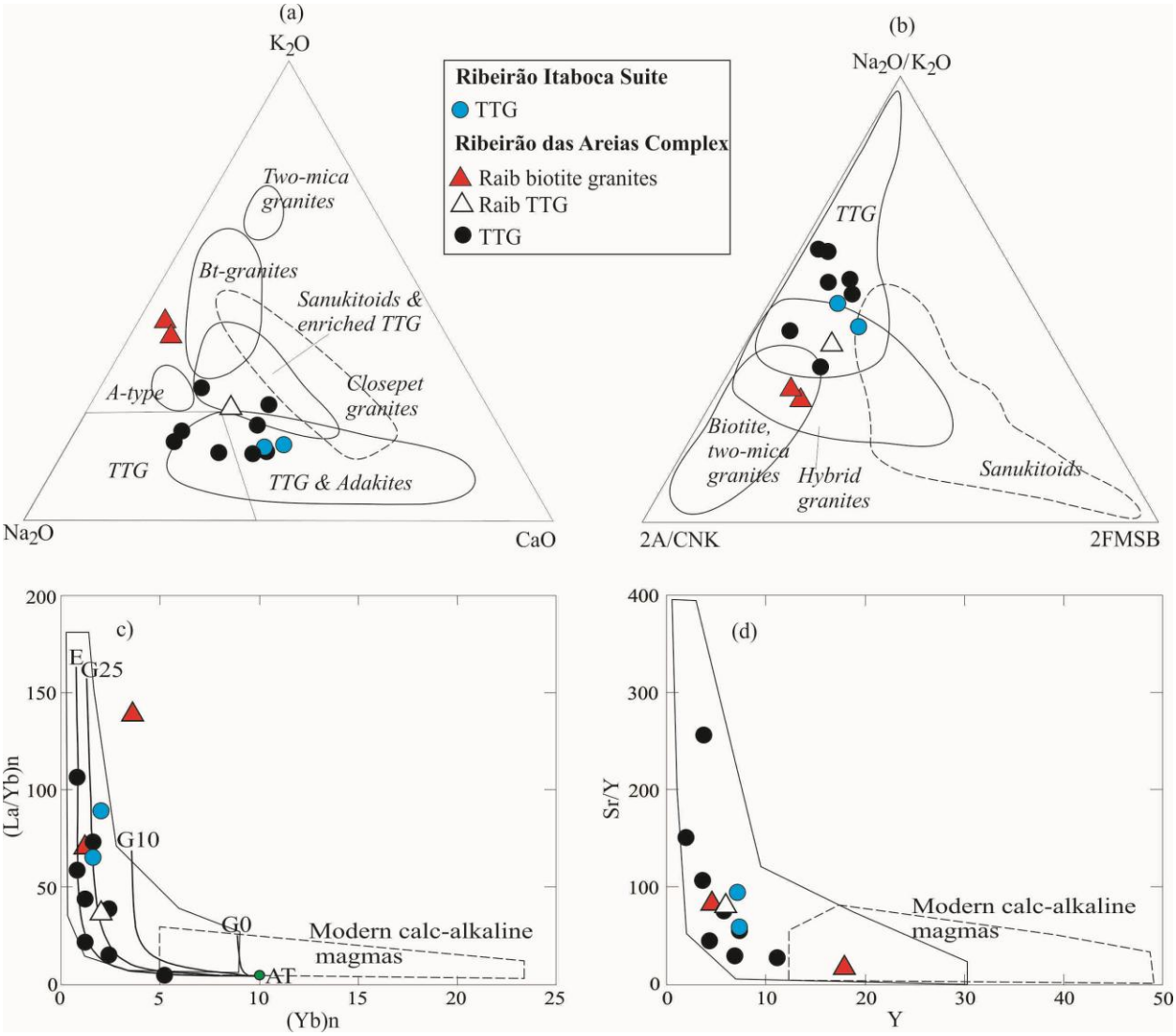

Figure 2.7 - Geochemical characteristic (major and trace elements) of Ribeirão das Areias Complex and Ribeirão Itaboca Suite. (a) Ternary diagram K_2O-Na_2O-CaO (Barker and Arth, 1976), with fields from Moyen et al. (2003). (b) Ternary classification diagram of Laurent et al. (2014). (c) La/Yb_N vs. Yb_N diagram and (d) Sr/Y vs. Y diagram (Martin et al., 1983; Drummond and Defant, 1990; Moyen and Martin, 2012). Normalization values are from Masuda et al. (1973). 2FMSB=2∗(FeOt+MgO)∗(Sr+Ba); A/CNK=(molar Al_2O_3/[CaO+Na_2O+K_2O] ratio); AT-Archean tholeiitic source; G0-Garnet-free amphibolite; G10 and G25- 10% and 25% garnet-bearing amphibolite; E- Eclogite.

Laurent et al., (2014) used samples of late-Archean granitoids from South Africa together with

those from other Archean cratons worldwide to suggest the use of a synthetic ternary diagram for purposes of classification, in which each pole represents a key geochemical characteristic of granitoids produced through one of these processes: Na_2O/K_2O vs. FMSB vs. A/CNK (Fig. 2.7b). In Figure 2.7b, most of the studied samples fit in the TTG field and some samples overlap with hybrid granites (Fig. 2.7b), but samples (AS-210 and AS-210A) of RAib fall in the biotite and two mica granites field. According to Figures 2.6d, 2.7a and 2.7b, samples AS-210 and AS-210A of RAib can be classified as biotite granites or hybrid granitoids (Moyen et al., 2003; Laurent et al., 2014).

The La/Yb_N vs. Yb_N diagram (Fig. 2.7c) proposed by Martin et al., (1983) to distinguish between Archean and post-Archean rocks shows that most of the samples from both RAC and RIS plot along the Y-axis in the high-Al_2O_3 Archaean TTG field. This pattern suggests a basaltic melting path defined by an Archean tholeiitic source transformed into: (i) eclogite restites (samples AS-348, AS-352 and AS-362A); and (ii) about 25%-garnet bearing amphibolite restite (samples AS-319A, AS-344, AS-333, AS-335 and AS-362. Drummond and Defant (1990) originally suggested a Sr/Y vs. Y diagram (Fig. 2.7d), these are commonly used to show "distinct" trondhjemite-tonalite-dacite (TTD) and arc andesite, dacite and rhyolite (ADR) compositional fields. Low Y and high Sr signatures in these Paleoproterozoic granitoids highlight their compositional difference from modern calc-alkaline magmas (Fig. 2.7d).

REE and multielement patterns were also useful to highlight some of the geochemical traits of the observed TTG samples (Fig. 2.8a, 2.8b and Table 2.1). TTG samples of RAC display REE patterns with medium to high LREE values (La = 10 – 45 ppm) and low HREE values (Yb = 0.2 – 0.6 ppm), corresponding to rather fractionated REE patterns resulting in high La/Yb ratios $(La/Yb)_N$ = 15 – 107, with the exception of sample AS-1 $(La/Yb)_N$ = 5. They have medium to high Sr contents (196 – 962 ppm) and low Y values (1.9 – 11 ppm) that confers a medium to high Sr/Y ratio (28 - 257). Samples show negative Nb and P anomalies, and most samples have slight to strong negative Ti anomalies. Samples lack significant Eu anomalies (Eu/Eu* = 0.8 – 1.1), but sample AS-1 has a positive Eu anomaly (Eu/Eu* = 1.4).

TTG samples of RIS display fractionated REE patterns with high LREE values (La = 40 – 68 ppm) and low HREE values (Yb = 0.4 – 0.5 ppm), that results in high La/Yb ratios $(La/Yb)_N$ = 65 – 89. They have high Sr contents (437 – 679 ppm) and low Y values (7.1 – 7.3 ppm), with a high Sr/Y ratio (59 - 95). Samples show negative Nb and P anomalies, and do not exhibit marked negative Ti anomalies. They have weakly positive Eu anomalies (Eu/Eu* = 1 – 1.4).

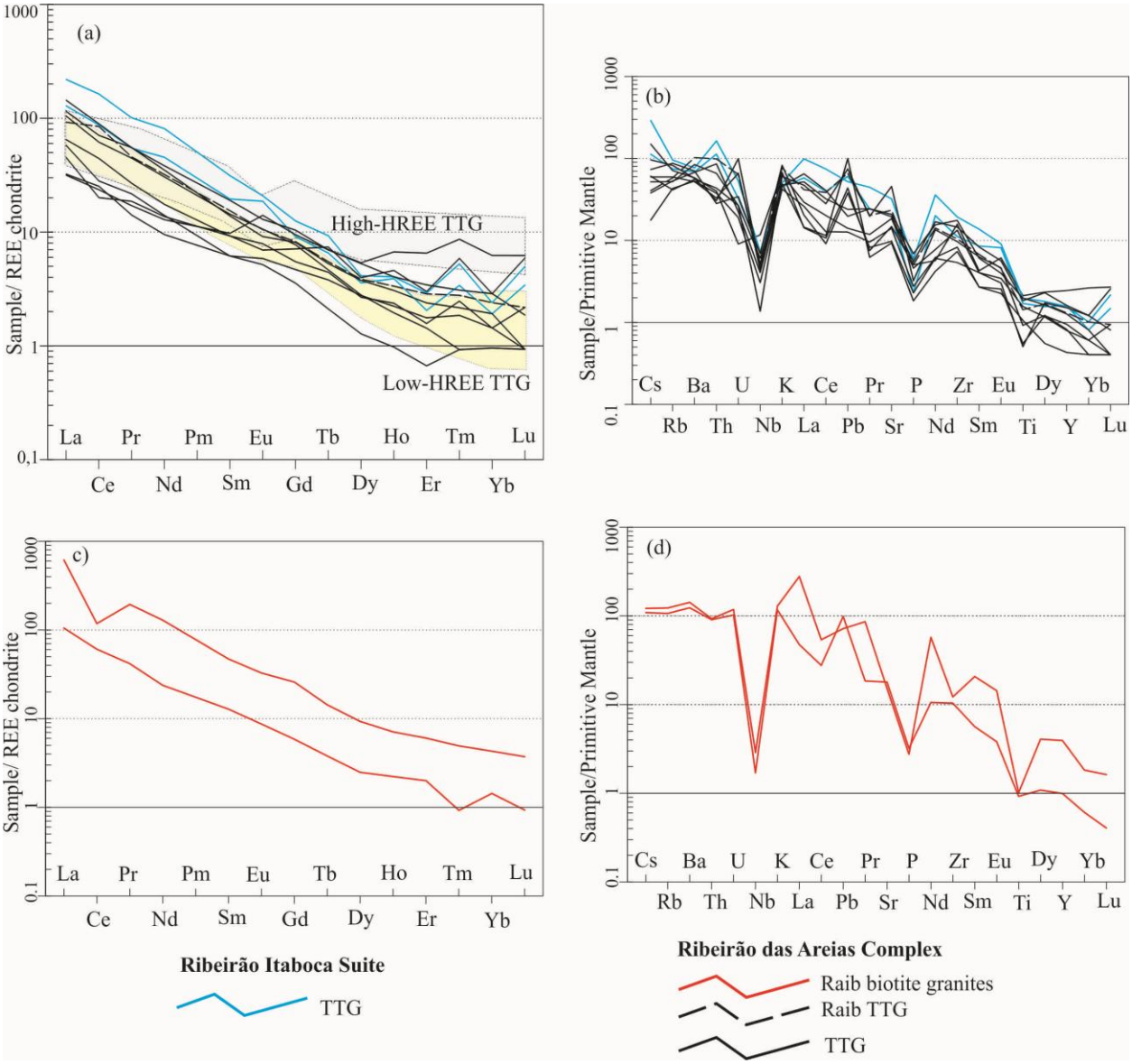

Figure 2.8 - Geochemical characteristic (multielementary diagrams) of Ribeirão das Areias Complex and Ribeirão Itaboca Suite. (a) Chondrite-normalized REE pattern (Boyton, 1984) for the TTG rocks in this work. Fields of High-HREE TTG and Low-HREE TTG from Halla et al. (2009). (b) Primitive mantle normalized trace element pattern (Sun and McDonough, 1989) for the TTGs rocks in this work. (c) Chondrite-normalized REE pattern (Boynton, 1984) for the biotite granites of RAib. (d) Primitive mantle normalized trace element pattern (Sun and McDonough, 1989) for the biotite granites of RAib.

TTG rocks from this study belong to the low-HREE TTG type (Fig. 2.8a) akin to the field presented by Halla et al. (2009), however, sample AS-1 of RAC belongs to the high-HREE type.

The spidergram of the biotite granites of RAib (Fig. 2.8c, 2.8d and Table 2.1) shows fractionated REE patterns with high La/Yb ratios $(La/Yb)_N$ = 71 – 140, and low to high Sr/Y ratio (18 - 84). In terms of other trace elements, the samples show negative Nb, P anomalies and have slight to strong negative Ti anomalies.

2.6. Discussion

2.6.1. Age and Geochemical Evidence for Subduction Magmatism in the ACTD

Previous studies in the ACTD identified important magmatic pulses during the Siderian period (Table 2.2), which are exemplified by the 2.45 Ga subduction-related RAC (Cruz et al., 2003), and 2.38-2.34 Ga tonalitic rocks (Fuck et al., 2014; Lima 2014). The well-defined ages presented in this work reveal that the TTG magmatic pulses were emplaced at ca. 2.47–2.30 Ga. TTG rock-forming events occurring during the early Paleoproterozoic are not exclusive to the ACTD, and have been described in others parts of the São Francisco pericraton including in the Mineiro Belt (Teixeira et al., 2015; Barbosa et al., 2019).

Regarding the dated mafic rocks of the Gameleira Suite, the 2.47 Ga zircon crystals of sample AS-360D are medium prisms (~3:1) and with discrete oscillatory zoning, while the 2.3 Ga population crystals are fragments or short prisms (~ 2:1) with homogeneous or discrete sector/oscillatory structure. With our data we cannot safely affirm that this zircon is of a mafic origin. If, on the one hand, the data from sample AS-360 are quite consistent and homogeneous, on the other hand, the result obtained for the AS-360D is atypical for an igneous rock. This sample has zircon crystals of different ages and morphological types, which makes the interpretation very difficult.

The zircon crystals of samples AS-360 and AS-360D that provided ages of ~ 2.3 Ga are very similar morphologically and have features common in mafic rocks (short prism and homogeneous or diffuse internal structure). At first this age seemed to represent the age of crystallization of the body, but due to the wide variety of ages in zircon from sample AS-360D, it seems consistent to interpret that all the zircon (of both samples) as crustal contamination. So at this point, we interpret that the zircon populations present in the AS-360 and AS-360D samples are all crustal contamination, and that the Gameleira Suite corresponds to a magmatic event occurring after the Siderian period.

As exemplified in section 2.2 the addressed region has undergone a complex structural and metamorphic history that involved regional tectonothermal events from the Paleoproterozoic to the Neoproterozoic. Kuyumjian et al., (2012 and references therein) concluded that the mineralization of the Córrego do Paiol Mine was developed in the final phase of Brasiliano Orogenesis at 563 ± 15 Ma (Ar^{40}-Ar^{39} on hydrotermal chlorite and muscovite). One of the investigated units, sample AS-362, a tonalitic-gneiss from the RAC, also yielded a Brasiliano age. The lower intercept age of 533 ± 38 Ma for this sample indicates both the presence and the importance of the Brasiliano thermal event in the studied region.

Variations of Sr/Y and La/Yb ratios (Fig. 2.9a) can be used to divide our TTG samples

into two groups based on pressure intensity (Moyen and Martin, 2012): (i) the high-pressure TTG field (sample AS-352, with Sr/Y=257); and (ii) the medium pressure TTG field (the other ten samples AS-1, AS-317A, AS-319A, AS-332, AS-333, AS-335, AS-344, AS-348, AS-362 and AS-362A). Based on the Al_2O_3 content (for rocks with $SiO_2 \geq 70\%$, Table 2.1) two subgroups of TTG can be defined (Barker and Arth, 1976): the high-Al_2O_3 trondhjemitic group (Al_2O_3>15%) for samples AS-317A, AS-319A, AS-344 and AS-352; the low-Al_2O_3 trondhjemitic group (Al_2O_3<15%) for samples AS-335, AS-348 and AS-362A.

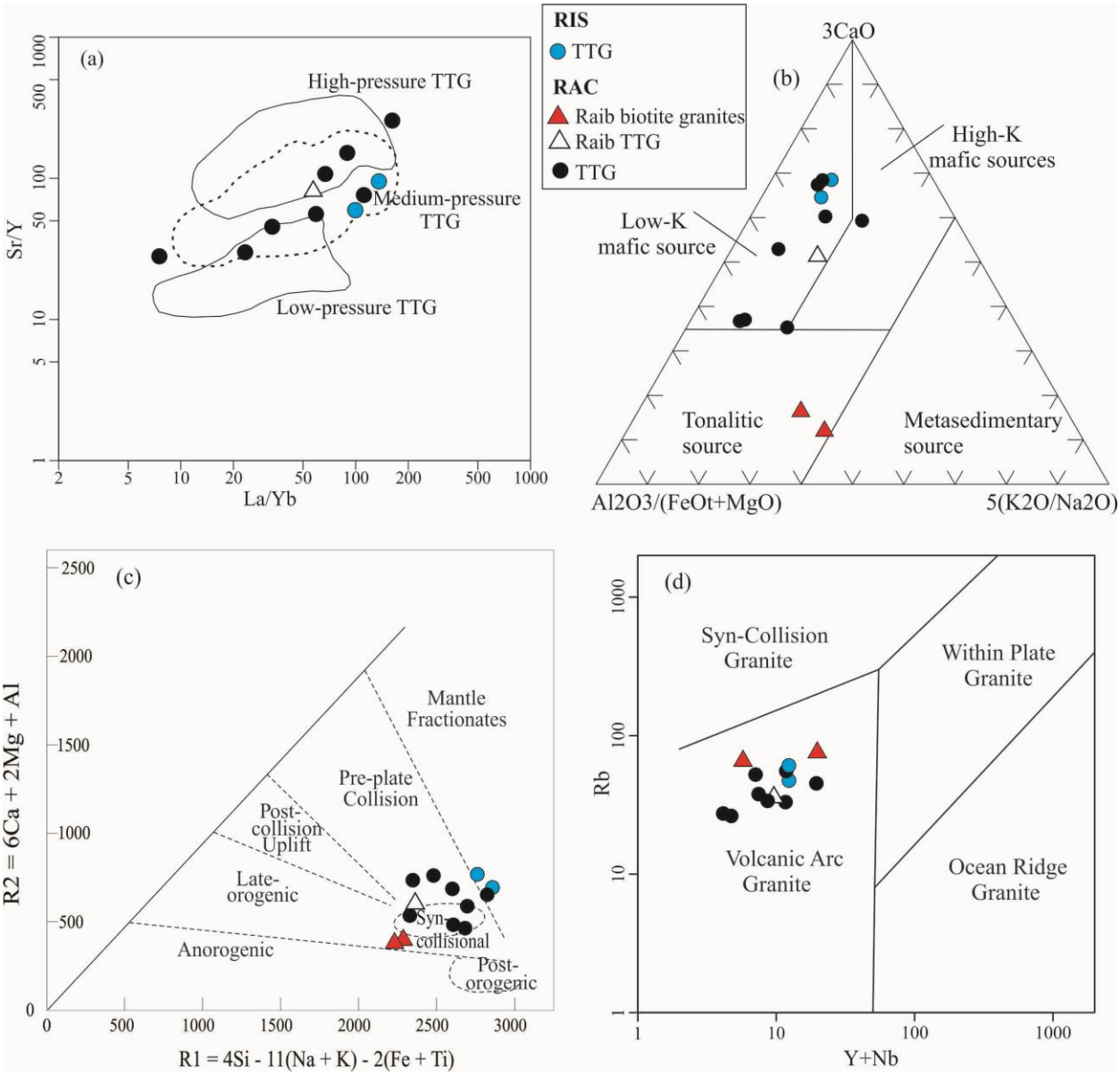

Figure 2.9 - Geochemical characteristic of Ribeirão das Areias Complex and Ribeirão Itaboca Suite based on trace elements. (a) Sr/Y vs. La/Yb diagram (fields from Moyen and Martin, 2012). (b) Ternary diagram Al_2O_3/(FeOt + MgO); 3∗CaO; 5∗(K_2O/Na_2O) of Laurent et al. (2014). (c) Multicationic diagram R1-R2 according to Batchelor and Bowden (1985). (d) Rb vs. (Y+Nb) tectonic discriminant diagram (Pearce et al, 1984).

According to Martin et al. (2005), Moyen and Martin (2012) and Laurent et al. (2014, and references therein), there are important discriminating characteristics for TTG rocks, such as: high Na_2O contents (3.0-7.0 %), 0.5 %< K_2O < 2%, and correlated low K_2O/Na_2O (≤ 0.6) ratios. $(La/Yb)_N$ ratios are greater than 15, Sr/Y ratios are 20 to 500, and they also lack significant Eu and Sr anomalies. Recently Moyen (2019) indicated there are no absolute parameters for the classification of TTG rocks, however there are similar characteristics among these rocks around the world. This author pointed out that some of the granitic to granodioritic rocks that are part of the TTG series are more similar to potassic biotite granites, which contrast with the sodic tonalites and trondhjemites. Thus, according to the works cited above and as noted in Fig. 2.6d, 2.7a and 2.7b (section 2.5.4) the RAib granitic rocks of this study (samples AS-210 and AS-210A) are considered to be biotite granites (or hybrid granitoids) and distinct from the TTG series.

The TTG rocks in this study are predominantly related to low-K mafic sources, only sample AS-1 is derived from more high-K mafic sources, whereas the biotite granites were generated from tonalitic sources (Fig. 2.9b). According to the multicationic diagram of Fig. 2.9c (Batchelor and Bowden, 1985), the studied TTG rocks show compositions that allow them to be related to the subduction (pre-plate collision) and syn-collisional settings. In this diagram the biotite granites of RAib have different distribution, suggesting a late-orogenic tectonic setting. All samples fall in the Volcanic Arc Granite (VAG) field in the Rb vs Y+Nb diagram (Fig. 2.9d) reflecting their low HFSE contents, and this is also consistent with the hypothesis of arc-derived rocks. Most of the studied rocks have negative Nb, P and Ti anomalies, and these negative anomalies on mantle-normalized trace element diagrams have been attributed to geochemical features of subduction zones and arc settings (Castillo et al., 2007, and references therein). Based on the geochemical characteristics exemplified above, we infer a tectonic setting related to subduction for the TTG rocks of this study.

Our interpretation of post-Archean TTG rocks in a subduction tectonic setting allows for a correlation with the geodynamic model of the evolution of late-Archean granitoids of Laurent et al. (2014). In this model, several pulses of TTG magmatism occur in the first stage where the subduction of the basaltic oceanic crust takes place under an older continental crust or in an intra-oceanic setting. The presence of high- and medium-pressure TTG rocks derived from mafic sources (Figures 2.7c and 2.9a) indicates that the subduction tectonic setting would be the most likely for the genesis of these rocks. The second magmatic stage of the model corresponds to the emplacement of granitoid types (such as biotite granites and hybrid granitoids) in a continental collision to post-collisional extension tectonic settings. Although in this work we haven't dated the RAib rocks, the geochemical signature of biotite granites formed from tonalitic/crustal

sources (Fig. 2.9b) and the comparison with similar Archaean occurrences, favor the interpretation of generation of these rocks after the TTG formation event.

2.6.2. Crustal Evolution of the Siderian Magmatism in ACTD

Previous works in the ACTD have reported sparse Sm-Nd or Lu-Hf data able to constrain source characteristics of the Siderian and Rhyacian magmatism. A single Siderian sample is reported with $\varepsilon Nd_{(t)}$ of -3.10 (Fuck et al., 2014) whereas Rhyacian samples show $\varepsilon Nd_{(t)}$ ranging from -5.12 to +0.21 (Sousa et al., 2016), suggesting crustal reworking involved in both magmatic events. This previously published data, together with our new ages and geochemical data obtained for the mapped area are compatible with the following evolution phases:

During the Neoarchean Era (> 2.5 Ga) magmatism and deposition of the Riachão do Ouro Group took place, as supported by data of Kuyumjian et al. (2012 and references therein).

During the early Siderian, subduction of basaltic oceanic crust generated the Ribeirão das Areias Complex TTG magmatism, which in turn, intruded the Riachão do Ouro Group.

This first stage of subduction continued until ~ 2.3 Ga with the formation of TTG rocks of the Ribeirão Itaboca Suite. It suggests a period of at least 170 Ma of TTG emplacements, with at least two main pulses of TTG magmatism represented by the RAC and the RIS. Inherited zircon ages suggest that the RIS assimilated older crust during the youngest TTG magmatism pulse. Biotite granites in this study represent a latter magmatic stage, possibly emplaced after the last TTG magmatism pulse. As exemplified by Laurent et al. (2014 and references therein), a continent-continent collision is not necessary to explain the crustal thickening and consequent required heat source for the generation of magmas with crustal components.

The mafic intrusions of the Gameleira Suite carried inherited zircon from the RAC and RIS. Tectonic quiescence, during and after emplacement, is suggested by preserved igneous structures such as rhythmic layering and cross-stratification. Therefore, an extensional tectonic setting after the Siderian period is proposed for this magmatic event.

After the Siderian/early Rhyacian period, the ACTD witnessed widespread Rhyacian magmatism associated with the formation of the western margin of the São Francisco Paleocontinent (Cordeiro and Oliveira, 2017). This Rhyacian Orogeny reworked the oldest units of most of the current ACTD and other Goiás Massif domains in subduction-driven orogens and generated the emplacement of various granitoid units and depositional processes from ~2.26 to 2.10 Ga (Fuck et al., 2014; Sousa et al., 2016; Cordeiro and Oliveira, 2017; Abdallah and Meneghini, 2017; Cuadros et al, 2017a; Cuadros et al, 2017b; Saboia and Meneghini, 2019).

2.6.3. Comparison with other Sideran Terranes in the São Francisco Craton and Pericraton

Other Siderian terranes in the São Francisco Craton (SFC) and pericraton share geological similarities with those within the ACTD. In this discussion, the craton and pericraton will be compartmentalized in three sectors (Fig. 2.10), according to Souza et al. (2003) and Hasui et al. (2012).

In the western sector, Siderian magmatism is restricted to the Mineiro Belt (Table 2.2) with U-Pb zircon ages of 2472 ± 11 to 2414 ± 29 Ma for the Cassiterita orthogneiss and 2356 ± 3 to 2350 ± 4 Ma for the Lagoa Dourada Suite. The Cassiterita orthogneiss comprises rocks with TTG affinity interpreted as a juvenile intra-oceanic arc (Barbosa, 2015; Alkmim and Teixeira 2017). The Lagoa Dourada Suite consists of a series of biotite-hornblende tonalites and biotite trondhjemites, which originated from melts derived from a juvenile and short-lived tholeiitic basalt source (Seixas et al., 2012; Alkmim and Teixeira 2017). This suite includes the Resende Costa peraluminous orthogneiss which has TTG-like assemblages derived from a short-lived slightly depleted tholeiitic source subjected to minor crustal assimilation in an oceanic arc setting (Teixeira et al., 2015). Barbosa et al., (2019) presented ages (U-Pb zircon, Table 2.2) of 2472 ± 11, 2419 ± 13, 2462 ± 14 and 2414 ± 29 Ma for the Cassiterita orthogneiss, and reaffirmed the similar chemical and isotopic composition with the Resende Costa-Lagoa Dourada TTG units. The $\varepsilon_{Hf(t)}$ and $\varepsilon_{Nd(t)}$ for the Cassiterita orthogneiss and the Lagoa Dourada Suite indicate the formation of juvenile crustal segments with limited crustal assimilation in both events (Teixeira et al., 2015; Barbosa et al., 2019). Therefore, even though formed at different stages in the Siderian, both the Cassiterita orthogneiss and the Lagoa Dourada Suite attest to juvenile events of intra-oceanic arc formation. Moreira et al., (2018) presented Lu-Hf analyses in zircon grains from the Lagoa Dourada Suite, consistent with a juvenile origin. The same authors noticed that the zircon grains from the Resende Costa Suite have two clear domains, the cores are ca. 2.35 Ga and the rims are ca. 2.13 Ga. The interpreted magmatic titanite grains from the same sample yielded ages within uncertainty of the zircon rims.

In the southern Gavião Block (central sector, Fig. 2.10), granitoids of Rio do Paulo Suite have a U-Pb zircon age (Table 2.2) of 2324 ± 6 Ma (Cruz Filho and Martins, 2013; Wosniak and Oliveira, 2013).

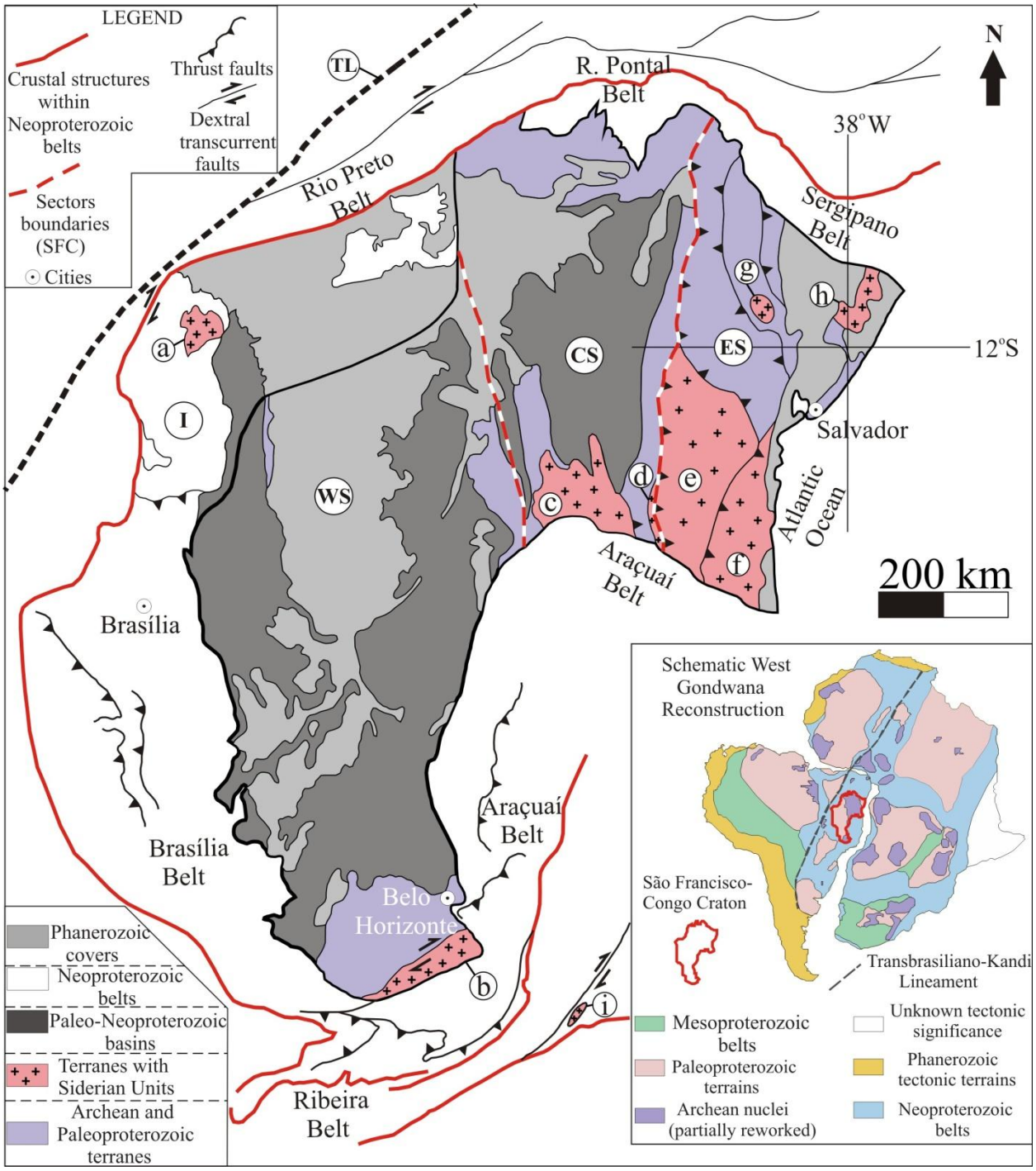

Figure 2.10 - Location of Siderian terranes (~ 2.5 to 2.3 Ga) within the São Francisco Craton, Pericraton and marginal Brasiliano Belts. Legend: (I) Northern Paleoproterozoic basement of the Brasília Belt, (WS) Western sector, (CS) Central sector, (ES) Eastern sector, (a) Siderian units (this study) of the ACTD, (b) Mineiro Belt, (c) Southern Gavião Block, (d) Contendas-Mirante Domain in the Gavião Block, (e) Jequié Block, (f) Southern Itabuna–Salvador–Curaçá Belt, (g) Serrinha Block (Curral Granitoid), (h) Northern Salvador-Esplanada-Boquim Belt, (i) Mafic basement inlier of the Ribeira Belt, (TL) Transbrasiliano-Kandi Lineament. Modified from Hasui et al. (2012) and Cordani et al. (2016).

Locality	Unit	Rock type	Method	Age (Ma)	Tectonic Setting	Reference
ACTD	RAC	Metagranodiorite	U - Pb SHRIMP II (Zr)	2473 ± 6	Subduction-like	This work
ACTD	RAC	Tonalitic-gneiss	U - Pb SHRIMP II (Zr)	2478 ± 5 [± 9]	Subduction-like	This work
ACTD	RIS	Tonalite gneiss	U - Pb LA-ICPMS (Zr)	2299.5 ± 3.3	Subduction-like	This work
ACTD	RIS	Metatonalite	U - Pb SHRIMP II (Zr)	2308 ± 5 [± 8]	Subduction-like	This work
ACTD	Gameleira Suite	Gabbronorite	U - Pb LA-ICPMS (Zr)	2301 + 9/-7 (inherited zircons)	Extensional	This work
ACTD	Gameleira Suite	Gabbronorite	U - Pb LA-ICPMS (Zr)	2299 ± 5 (inherited zircons)	Extenional	This work
ACTD	RAC	Trondhjemite	U - Pb SHRIMP (Tit)	2455±14	Subduction-related	1
ACTD	Basement of ACTD	Tonalite	U - Pb LA-ICP-MS (Zr)	2446±68	-	2
ACTD	Basement of ACTD	Tonalite gneiss, granite gneiss	U - Pb ID-TIMS (Zr)	2386 ± 24; 2379 ± 6	-	3
ACTD	Rio do Moleque Suite	Tonalite	U - Pb LA-ICPMS (Tit)	2342 ± 26	Oceanic arc	4
MB	Cassiterita Suite	Metatonalites	U - Pb SHRIMP and LA-ICPMS (Zr)	2472 ± 11, 2419 ± 13; 2462 ± 1; 2414 ± 29	Oceanic arc	5
MB	Lagoa Dourada Suite	Tonalite, Trondhjemite	U - Pb ID-TIMS (Zr)	2356 ± 3; 2350 ± 4	Intra-oceanic	6
MB	Resende Costa Suite	Tonalites and granodiorites	U - Pb LA-ICPMS (Zr)	2352 ± 11 (core ages)	Intra-oceanic	7
MB	Resende Costa Suite	Tonalites and granodiorites	U - Pb LA-ICPMS (Zr)	2151 ± 31 (rims ages)	Intra-oceanic	7
MB	Resende Costa Suite	Orthogneiss (trondhjemites)	U - Pb LA-ICPMS (Zr)	2351 ± 48; 2317 ± 16	Oceanic arc	8
SGB	Rio do Paulo Suite	-	U - Pb LA-ICPMS (Zr)	2324 ± 6	-	9

SGB	Aracatu Granitoid	Trondhjemite	U - Pb TIMS evaporation (Zr)	2380	Continental magmatic arc	10
CMDGB	Pé de Serra de Contendas Granitoid	-	Pb-Pb (Zr)	2500; 2300	-	11
CMDGB	Rio Jacaré Sill	-	Pb-Pb (Wr)	2474±72	Intraplate (?)	12
JB	Heterogeneous Orto- and Paragranulites	Granulite-charnockite	Pb-Pb (Zr)	2461±1	-	13
SISCB	Ipiaú Monzonite	-	Pb-Pb (Zr)	2450 ± 1	-	12
SISCB	Ibirapitanga-Ubaitaba Granitoids	-	Pb-Pb (Zr)	2450	-	11
SB	Curral Granitoid	Granodiorite	Pb-Pb (Zr)	2468 ± 3	-	14
NSEBB	Charnockitic of Monzogranitic Composition (MCh)	charnockite monzogranitic	U - Pb LA-ICPMS (Zr)	2473 ± 13	Continental magmatic arc	15
RB	Basement inlier	Mafic granulite	U - Pb ID-TIMS (Zr)	2.427 ± 9	Oceanic	16

Table 2.2 - Summary of the available geochronological data of the studied geological units and new data obtained in this work. It also includes the available geochronological data for the Siderian terranes within the São Francisco Craton, Pericraton and marginal Brasiliano Belts. References: 1 – Cruz et al., (2003); 2 – Sousa et al., (2016); 3 - Fuck et al., (2014); 4 - Lima (2014); 5- Barbosa et al., (2019); 6 - Seixas and Stevenson (2012); 7 - Moreira et al., (2018); 8 - Teixeira et al., (2015); 9 - Cruz Filho and Martins (2013); 10 - Cruz et al., (2016); 11 - Souza et al., (2004); 12 - Barbosa and Sabaté (2004); 13 - Barbosa et al., (2012); 14 - Rios et al., (2008); 15 - Barbosa et al., (2018); 16 - Heilbron et al., (2016). Acronyms are: (ACTD) Almas-Conceição do Tocantins Domain; (MB) Mineiro Belt; (SGB) Southern Gavião Block; (CMDGB) Contendas-Mirante Domain Gavião Block; (JB) Jequié Block; (SISCB) Southern Itabuna–Salvador–Curaçá Belt; (SB) Serrinha Block; (NSEBB) Northern part of the Salvador-Esplanada-Boquim Belt; (RB) Ribeira Belt; (Zr) zircon; (Tit) titanite; (Wr) whole-rock.

Based on U-Pb dating and geochemical data, Cruz et al., (2016) grouped the Rio do Paulo Suite with the Aracatu Granitoid (2.38 Ga) and others granitoids of Rhyacian age in the Group 1/Bom Sucesso Suite with ages between 2324 ± 6 to 2091 ± 6.6 Ma. The Nd isotopes (εNd(t)) with Archean model ages and negative values are compatible with crustal recycling for the Aracatu Granitoid of Group 1 (Cruz et al., 2016). These authors suggested that between 2.38 and 2.12 Ga a magmatic arc (Western Bahia Magmatic Arc) was installed on the eastern continental margin of the Gavião paleoplate and a subduction zone also developed to the west producing the rocks

of Group 1. The striking geochronological and geochemical similarities between the Western Bahia Magmatic Arc and equivalent rocks in the Mineiro Belt and Mantiqueira Complex allowed Cruz et al., (2016) to propose these arcs as part of the same orogenic system. In the southeast portion of the Gavião Block (Contendas-Mirante Domain) the Pé de Serra de Contendas Granitoid (Souza et al., 2004) is represented by hastingsite-biotite granite (2500 Ma, Pb-Pb zircon age, Table 2) with calc-alkaline high K composition and subordinate alkaline aegerine granite/syenite (2300 Ma, Pb-Pb zircon age).

The eastern sector, unlike other sectors highlighted in Figure 2.10, has an abundant record of Siderian magmatism. In the Jequié Block (eastern sector, Fig. 2.10) some granulite–charnockite rocks have Pb-Pb zircon ages of 2461± 1 to 2560 ± 2 Ma (Barbosa et al., 2012 and references therein; Table 2.2). In the southern part of the Serrinha Block (eastern sector) the Curral Granitoid (2862± 5 to 2468 ± 3Ma, Pb-Pb zircon age) has a composition ranging from tonalite to granodiorite and monzogranite with low potassium calc-alkaline affinities (Rios et al., 2009 and references therein). In the southern part of the Itabuna–Salvador–Curaçá Belt, numerous intrusive bodies of monzonite with shoshonitic affinity crop out, such the Ipiaú Monzonite with an age of 2450 ± 1 Ma (Pb–Pb evaporation on zircon, Table 2.2; Barbosa and Sabaté, 2004 and references therein). The Ibirapitanga-Ubaitaba Granitoids (2450 Ma, Pb-Pb zircon age) are composed of granulitic rocks with high potassium to shoshonitic and calc-alkaline affinities (Souza et al., 2004). In the northern part of the Salvador-Esplanada-Boquim Belt some acidic granulites made of charnockites with monzogranitic composition yielded U-Pb ages for the formation of the protholith of the granite at 2473 ± 13 Ma (Barbosa et al., 2018b). According to these authors, these rocks are composed of calc-alkaline high K-shoshonitic series and formed in a continental magmatic arc setting.

In the Contendas-Mirante Domain of the Gavião Block the Rio Jacaré Sill (2474±72 Ma, Table 2.2) is a layered mafic–ultramafic body.

A mafic granulite composed of a metamafic unit within a reworked basement inlier of the Ribeira Belt, has a tholeiitic chemical signature and a zircon age of 2.427 ± 9 (Heilbron et al., 2017, Table 2.2).

Therefore, Siderian magmatism in various locations of the São Francisco craton and pericraton registered important similarities. First, the ACTD, Mineiro Belt and Western Bahia Magmatic Arc (Aracatu Granitoid) show granitoids formed between 2.47-2.3 Ga. However, an important distinction between them is that only Siderian rocks from the Mineiro Belt and the Mantiqueira Complex (Cutts et al., 2019) are compatible with juvenile crust formation whereas the other Siderian belts registered crustal reworking. Second, the RAC and RIS metagranitoids in this study show striking correlation with the Cassiterita - Resende Costa-Lagoa Dourada units of

the Mineiro Belt, which share in common both TTGs geochemical signature and footprint of subduction environments. In terms of absolute age, the RAC (2.47 – 2.45 Ga; Table 2) coincides with the Cassiterita Suite (2472 - 2414 Ma) and the RIS (2.30 Ga) is younger than the Lagoa Dourada Suite (2350 Ma) and Resende Costa Suite (2317 Ma). However, the ages of 2386 to 2342 Ma (Table 2) reported by Fuck et al. (2014) and Lima (2014) may be related to the RIS.

This comparison between belts in the São Francisco craton and epicraton suggest that the Siderian Orogen in the ACTD is synchronous with that in the eastern sector of the São Francisco Craton registered in the Salvador-Esplanada-Boquim Orogen (Barbosa et al., 2018b) and the Western Bahia Magmatic Arc (Cruz et al., 2016). They are suggestive of subduction-related magmatism during the Siderian period in the proto-São Francisco paleocontinent. Contemporaneously, juvenile crust was being formed in the Mineiro Belt (Minas Accretionary Orogeny) likely as an intra-ocean arc system (Teixeira et al., 2015, 2017a, 2017b). Limited geochemical and geochronological data, particularly in the eastern sector, restricts the scope of interpretation on these proto-São Francisco terranes. Therefore, additional geochronological, isotopic and geochemical data are needed to establish and consolidate these correlations.

The contemporaneity and geochemical similarities between various Siderian terranes of the São Francisco craton and pericraton (Fig. 2.10) could be indicating a unified "proto-São Francisco" landmass whereby these terranes aggregated around an Archean core. An equivalent example can be found in the Rae craton (Canada) where the Arrowsmith Orogeny (2.5-2.3 Ga) included an Andean-type accretionary orogen amalgamated to a supercraton (Berman et al. 2013 and references therein). However, very little is known of the basement underneath the São Francisco Basin except that it has been a single landmass since the amalgamation of the São Francisco paleocontinent, after 2.05 Ga (Heilbron et al., 2017b; Fuck et al., 2017). Therefore, we hypothesize two possibilities involving Siderian terranes of the São Francisco craton and pericraton. The first hypothesis includes that the Siderian Orogeny preserved within the ACTD developed on the margins of an Archean proto-São Francisco landmass which would encompass the Gavião Block, Quadrilátero Ferrífero, the basement of the Mineiro Belt and terranes currently hidden underneath the São Francisco Basin. The second hypothesis is that the Siderian rocks of the ACTD represented a microcontinent amalgamated to the São Francisco paleocontinent during a Rhyacian Orogeny from 2.18 to 2.08 Ga.

2.7. Conclusions

The Ribeirão das Areias Complex-RAC (2.47 Ga) and The Ribeirão Itaboca Suite-RIS (2.3 Ga) are characterized by TTG rocks with subordinate biotite granites for the RAC. A

subduction-like tectonic setting is proposed for the formation of the TTG rocks whereas the biotite granites postdating the formation of TTG. We infer that the transition from TTG magmatism to the calc-alkaline magmatism probably occurred after the last TTG pulse from RIS (2.3 Ga).

The mafic rocks of the Gameleira Suite have inherited zircons with ages of 2.48 and 2.30 Ga and are interpreted to be associated with an extensional magmatic event after the Siderian period.

Regional correlation with others terranes in the São Francisco Craton can be established with the Mineiro Belt, Salvador-Esplanada-Boquim Orogen and Western Bahia Magmatic Arc. The Siderian Orogen of the studied region is representative of significant crustal growth related to the building blocks of the Columbia Supercontinent.

Acknowledgements

We thank the Institute of Geosciences of the University of Brasilia (IG/UnB) and the Geological Survey of Brazil (CPRM) for the field work support and the laboratory analysis. The CNPq (Conselho Nacional de Desenvolvimento Científico e Tecnológico) is acknowledged for grants provided to CGO (process number 305769/2019-7). We are grateful to Dr. Wilson Teixeira for handling this paper and for the detailed reviews by Dr. Kathryn Cutts and an anonymous reviewer and their valuable suggestions and corrections that helped improve earlier versions of this work. This study was financed in part by the Coordenação de Aperfeiçoamento de Pessoal de Nível Superior - Brasil (CAPES) - Finance Code 001 and the INCT Estudos Tectônicos.

Capítulo 3

3. THE 2.26 TO 2.18 Ga ARC-RELATED MAGMATISM OF THE ALMAS-CONCEIÇÃO DO TOCANTINS DOMAIN: AN EARLY STAGE OF THE SÃO FRANCISCO PALEOCONTINENT ASSEMBLY IN CENTRAL BRAZIL

André Menezes Saboia[1], Claudinei Gouveia de Oliveira[2], Elton Luis Dantas[2], Jaime Estevão Scandolara[1], Pedro Cordeiro[3], Joseneusa Brilhante Rodrigues[1], Isabela Moreno Cordeiro de Sousa[2]

[1]Geological Survey of Brazil (andre.saboia@cprm.gov.br)

[2]University of Brasília, Brazil

[3]Pontificia Universidad Católica de Chile

Abstract

Paleoproterozoic (Rhyacian) rocks dominate within the basement of the Neoproterozoic Brasília Belt and their genesis has been attributed to the orogenic amalgamation event that assembled the São Francisco-Congo paleocontinent from 2.18 to 2.07 Ga. However, the tectonic framework and genesis of the building blocks involved in this continent-wide amalgamation event are unclear, particularly in relation to terranes from the Almas-Conceição do Tocantins Domain, in the Goiás Massif, central Brazil. This work provides new whole-rock chemical and geochronological data, which indicate the generation of felsic to intermediate magmatism around 2.29 and 2.28 Ga corresponding to the Monzogranitic Unit and the Quartz-dioritic Suite, respectively. Later magmatic events occurred in a continental arc setting, around 2.2 Ga represented by metaluminous to peraluminous I-type magmatism of the Granodioritic to Tonalitic Suite (GTS) and the Serra do Boqueirão Suite. Around 2.18 Ga a peraluminous I-type magmatism took place and generated the Peraluminous Suite (PS). Our data show that after an earlier Siderian magmatic event around 2.45 Ga, reported in previous works, the Almas do Conceição do Tocantins Domain oversaw additional Rhyacian events of magmatic activity around 2.29 Ga to 2.18 Ga. Regional geotectonic correlations with the São Francisco Craton and other pericratonic belts indicate coeval magmatic events taking place during the early stages of the Columbia Supercontinent amalgamation.

Keywords: I-type granites, Paleoproterozoic basement, Brasília Belt, U-Pb Geochronology, Whole-rock geochemistry

3.1. Introduction

Continental crust is generated by magmatism dominantly within arc-related settings formed along subduction zones whereas the contribution of accretionary and collisional orogens to the formation of continental crust remain contentious (Cawood et al., 2009, 2013). Through partial melting and mixing of continental crust and mantle sources, such settings are important sources of felsic magmatism and the consequent diversity of granites (Frost et al., 2001).

Mixing of igneous and sedimentary sources originates peraluminous to strongly peraluminous granites (Barbarin, 1999; Collins and Richards, 2008). Peraluminous granites can be either generated by partial melting of metasedimentary rocks (S-type) or igneous rocks (I-type), a well-documented process in experimental petrology (Patiño Douce, 1999; Clemens and Stevens, 2012). Thus, the recycling of older igneous/sedimentary sources to generate new continental crust is a complex process that offers an opportunity to understand how the cycles of continental amalgamation and break-up evolved throughout Earth's history.

Widespread Paleoproterozoic felsic magmatic activity, particularly within 2.18 and 2.03 Ga, is linked to the amalgamation of the São Francisco (-Congo) Paleocontinent, one of the building blocks of the Columbia Supercontinent (Zhao et al., 2004; Cordeiro and Oliveira, 2017). Within such time span, older crustal blocks were welded together with multiple contemporaneous intra-oceanic arcs. However, contemporaneous orogenic systems are widely restricted to South American and African terranes, which still have obscure crustal recycling mechanisms.

Here we present geologic, geochronological (U-Pb in zircon) and whole-rock geochemical data for the Rhyacian magmatism related to the Almas-Conceição do Tocantins Domain. This area corresponds to the western part of the São Francisco palecontinent which, unlike the cratonic core, was affected by later deformation and is henceforth referred to as the São Francisco pericraton. We also discuss the role of magmatism associated with crustal recycling for generating multiple types of granitoids and the implications of this magmatism for the assembly of the São Francisco paleocontinent.

3.2. Geological Setting

The Almas-Conceição do Tocantins Domain (Fig. 3.1B) is the northeastern most portion of the Goiás Massif, a ~65.000 km2 collage of dominantly Paleoproterozoic terranes cropping out as the basement of the Brasília Belt (Fuck et al, 2014; Cordeiro and Oliveira, 2017; and

references therein). In the Neoproterozoic, The Goiás Massif represented the western edge of the São Francisco paleocontinent (Fig. 3.1A) during its collision against the Amazonian paleocontinent (Cordeiro and Oliveira, 2017; Hasui et al., 2012; Bizzi et al., 2003; Dardenne, 2000). This collision is part of the Brasiliano Orogeny, which shaped the Brasília Belt into its present tectonic framework and decreasingly affected Goiás Massif rocks from west to east towards the São Francisco Craton.

The Almas-Conceição do Tocantins Domain (Fig. 3.1) is dominated by an older volcano-sedimentary sequence and Paleoproterozoic metagranitoids from ~2.45 to 2.2 Ga (Cruz et al., 2003). Rocks from this domain have been previously referred as composing a granite-greenstone terrane (Kuyumjian et al., 2012), but in this work we follow the nomenclature proposed by Fuck et al. (2014) and Cordeiro and Oliveira (2017) with its cartographic limits according to the geological map of the Almas-Cavalcante Complex in the Arraias Sheet and Dianópolis Sheet (Saboia et al., 2019; Abdallah and Meneghini, 2017).

The understanding of the geological-tectonic aspects of the region evolved due to recent works and interpretation in terms of petrological, geochronological and geochemical characterization of the magmatism related to the Almas-Conceição do Tocantins Domain. Among these approaches, we highlight new ages obtained from Siderian magmatism (2.47 to 2.3 Ga), and a better definition of the Rhyacian units (ca. 2.26 to 2.18 Ga) that make up this domain (Fuck et al., 2014; Lima, 2014; Sousa et al., 2016; Saboia et al, 2019; Abdallah and Meneghini, 2017). Therefore, the Almas Conceição do Tocantins can be divided into:

a) The Riachão do Ouro Group, a greenstone volcano-sedimentary sequence, constituted of basal mafic and ultramafic metavolcanic rocks of the Córrego do Paiol Formation and upper phyllites, banded iron formations, quartzites, metacherts, metaconglomerates and felsic metavolcanic rocks of the Morro do Carneiro Formation (Correia Filho and Sá, 1980; Costa, 1985; Cruz and Kuyumjian, 1998; Borges et al., 1998). A minimum age for the Riachão do Ouro Group is provided by xenoliths of this group hosted within granitoids from the Ribeirão das Areias Complex aged close to 2.45 Ga (Cruz et al., 2003).

b) The Ribeirão das Areias Complex, interpreted as fragments of a poorly studied tonalitic basement of the Almas-Conceição do Tocantins Domain with a U-Pb titanite age of 2455±14 Ma (Cruz et al., 2003). The metagranitoids of this complex are biotite-rich, peraluminous, and encompass tonalites, trondjhemites and granodiorites (Cruz et al., 2003).

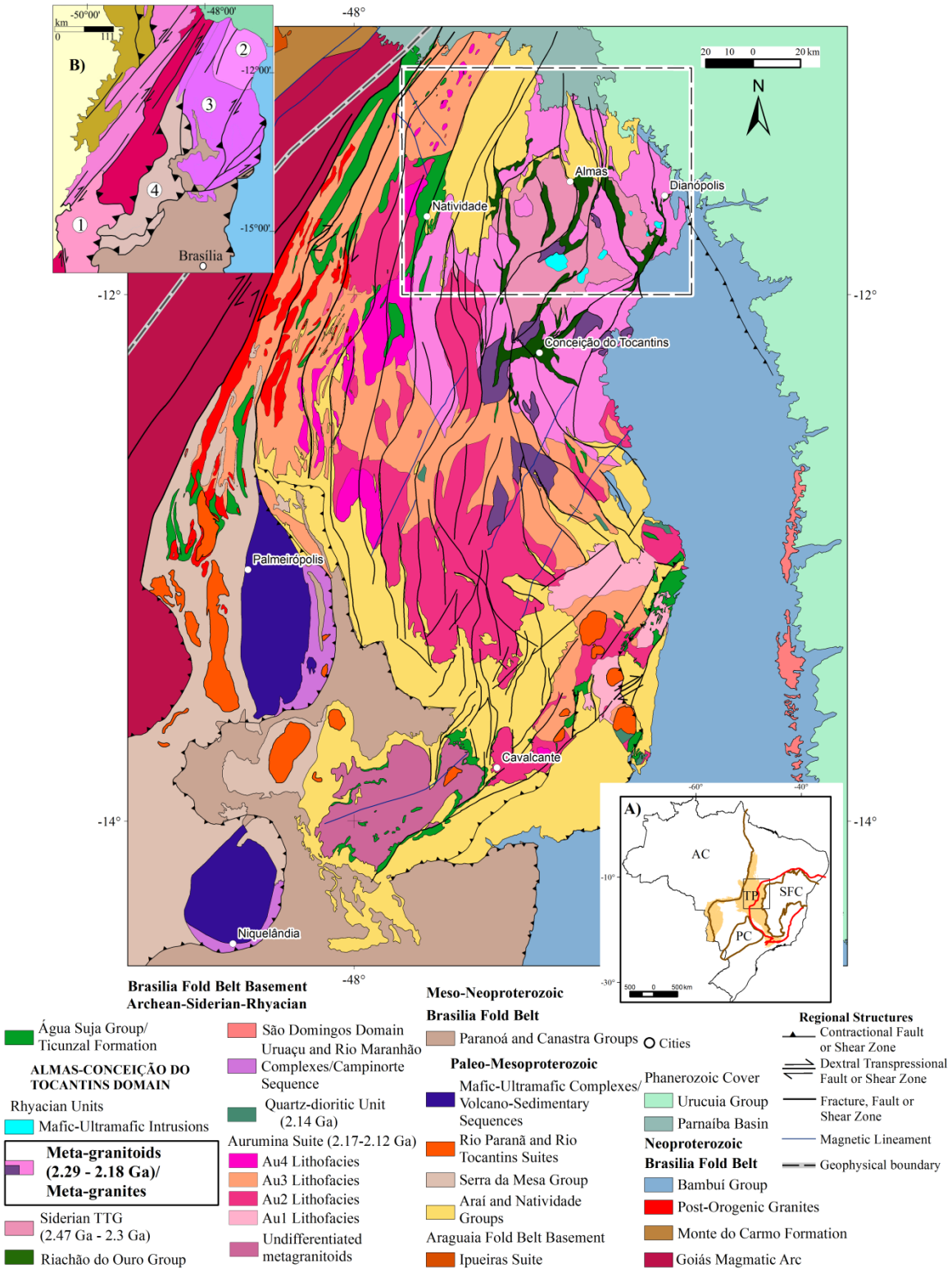

Figure 3.1 - Geotectonic division of the Northern Brasília Belt. Modified from: Bizzi et al. (2003), Alvarenga et al. (2007), Frasca et al. (2010, 2018); Abdallah and Meneghini (2017), Saboia et al. (2019), and Ribeiro and Alves (2017). The units inside the rectangle are the ones covered in this paper. The units in the black rectangle are the subject of this work. The rectangle with a dashed line indicates the study area and location of Figure 2. (A) TP-Tocantins Province, AC-Amazonian Craton, SFC-São Francisco Craton, PC- Paranapanema Craton. The red line represents the boundary of the São Francisco paleocontinent (pericraton) according to Pereira and Fuck (2005). (B) Major geotectonic domains. Modified from: Bizzi et al. (2003); Fuck et al.

(2014); Cordeiro and Oliveira, (2017). 1 - Crixás-Goiás Domain, 2 – Almas - Conceição do Tocantins Domain, 3 – Cavalcante-Arraias Domain, 4 - Campinorte Domain. The Goiás Massif corresponds to the domains 1, 2, 3 and 4.

c) The Suite 1 and Suite 2 of Cruz et al. (2003). Suite 1 (2.2 Ga with T_{DM}= 2.54 to 2.45 Ga and εNd(t)= -1.37 to -0.15) is amphibole-rich, metaluminous, composed dominantly of meta-tonalites. Suite 2 (2.2 Ga with T_{DM}= 2.76 to 2.53 Ga and εNd(t)= -4.95 to -0.88) is biotite-rich, peraluminous and composed of meta-tonalites, meta-trondhjemites, meta-granodiorites, and subordinate meta-monzogranites. The Conceição do Tocantins Suite, proposed by Sousa et al. (2016), encompasses Suites 1 and 2 from Cruz et al. (2003) and other tonalites and granodiorites formed from 2.22 to 2.16 Ga.

d) The Gameleira Suite comprises medium- and small-sized mafic-ultramafic layered plutons intruding gneissic-migmatitic basement rocks with meta-gabbros, meta-peridotites, meta-pyroxenites and serpentinites (Correia Filho and Sá, 1980).

In the western portion of the studied area, the Almas-Conceição do Tocantins Domain is locally covered by younger units or is in tectonic contact with the metavolcano-sedimentary Água Suja Group (2.17 Ga). The domain is additionally intruded by metagranitoids of the 2.12-2.16 Ga Aurumina Suite (Silva, 1987; Queiroz, 2001; Fuck et al., 2014; Sousa et al., 2016; Abdallah and Meneghini, 2017; Cuadros et al., 2017a, b). The Almas-Conceição do Tocantins Domain is also covered by Meso-Neoproterozoic metasedimentary basins (Natividade and Bambuí groups) and Phanerozoic sedimentary basins (Parnaíba and São Franciscana), besides being intruded by Cretaceous mafic dikes (Correia Filho and Sá, 1980; Hasui, 1990; Saboia, 2009). The mapped region was strongly affected by orogenic processes in the Paleoproterozoic and Neoproterozoic registered as regional metamorphism (greenschist to amphibolite facies), kilometer-scale folds and extensive transpressional shear zones (Borges et al., 1999; Kuyumjian and Araújo Filho, 2005). The western portion of the area is strongly marked by deformation related to the Transbrasiliano Lineament (Fuck et al., 2017).

3.3. Local Geology

Several Rhyacian units occur within the Almas-Conceição do Tocantins Domain with ages spanning from 2.3 to 2.1 Ga. The description of these units will follow a geochronological order from the oldest to the youngest according to ages from this work and the literature. Geological units mapped in this work and their general macroscopic and petrographic features are summarized in Table 3.1 and Fig. 3.3 and 3.4.

3.3.1. Monzogranitic Unit

The Monzogranitic Unit corresponds to a set of elliptic to semi-circular granitic bodies located in the central-eastern portion of the mapped area (Fig. 3.2). This unit is composed mainly of medium- to coarse-grained, light to pink, inequigranular to porphyritic meta-granites (Fig. 3.4A). The Pau Ramalhudo body (Correia Filho and Sá, 1980) is the most conspicuous intrusion of this unit as a NE-SW oriented 11.5 km long pluton.

3.3.2. Quartz-dioritic Suite

The Quartz-dioritic Suite occurs in the central-western part of the studied area and it is composed of two large bodies and few narrows strips of quartz-meta-diorite, meta-gabbros and subordinate meta-tonalites (Abdallah and Meneghini, 2017).

3.3.3. Granodioritic to Tonalitic Suite (Hornblende-biotite meta-granitoids - GTS)

The Granodioritic to Tonalitic Suite is the largest unit in the study area and comprises foliated batholiths and mylonitized bodies along regional shear zones of NNW, NS, and NNE directions. This suite comprises part of the Suite 1 of Cruz et al. (2003), the Rio do Moleque and part of the Manuel Alves Suites defined by Corrêa et al. (2015), and the Conceição do Tocantins Suite proposed by Sousa et al. (2016). The main granitoid types are biotite meta-granodiorites and meta-tonalites with subordinate hornblende-biotite meta-tonalites, biotite meta-monzogranites and quartz-meta-diorite. Garnet may occur as an accessory mineral in some batholiths. Its porphyroclastic aspect and the presence of fractures and alterations on its borders indicate that it belongs to the primary mineralogy. These rocks contain mafic microgranular enclaves and usually have their igneous textures modified by processes of ductile deformation and recrystallization (Fig. 3.4C).

3.3.4. Serra do Boqueirão Suite

The Serra do Boqueirão Suite is characterized by mesocratic medium-to-coarse grained hornblende meta-tonalites with inequigranular textures and foliated structures (Fig. 3.4D). This unit was loosely inserted in the Suite 1 granitoids of Cruz et al. (2003) and its type locality is the Corrente Pluton (Correia Filho and Sá, 1980) next to the Dianópolis town.

Units	Age (Ga) crystallization	Petrography				
		Lithology	Texture aspects	Main mafic phase	Accessory minerals	Secondary minerals
Monzogranite Unit	2.29 ± 7[1]	Monzogranite to syenogranite	Medium-to-coarse grained; inequigranular, and porphyritic texture; foliated and mylonites; not magnetic	Biotite	Zircon and opaque	Sericite and chlorite
Quartz-dioritic Suite	2.28 ± 6.8[1]	Quartz-diorite-gabbro-tonalite	Medium-to-coarse grained; inequigranular texture; granoblastic; foliated and banding structures; magnetic	Hornblende, biotite	Zircon, magnetite and opaque	Sericite, chlorite, epidote, zoisite, carbonate
Granodioritic to Tonalitic Suite (GTS)	2.26 ± 9.6[2] - 2.16 ± 6[3]	Granodiorite-tonalite-quartz-diorite-monzogranite-	Medium-to-coarse grained; fine-to-medium- grained; inequigranular and porphyritic textures; hypidiomorphic; xenomorphic; recrystallized; granoblastic; porphyroclasts; foliated and mylonites; not magnetic	Biotite, hornblende,	Zircon, titanite, garnet, apatite, allanite, opaque	Sericite, muscovite, chlorite, epidote, zoisite, clinozoisite, carbonates, clay minerals
Serra do Boqueirão Suite	2.22[4] - 2.21 ± 13[1]	Tonalite	Medium-to-coarse grained; inequigranular texture; hypidiomorphic; granoblastic; foliated; not magnetic	Hornblende	Zircon and opaque	Sericite, chlorite, zoisite
Peraluminous Suite (PS)	2.2 ± 4[4]- 2.18 ± 5[1]	Granodiorite-tonalite-leuco-tonalite-monzogranite	Medium-to-coarse grained; inequigranular, equigranular and porphyritic texture; hypidiomorphic; xenomorphic; granoblastic; foliated, protomylonite and banding structures; not magnetic	Biotite	Zircon, muscovite, apatite, opaque, monazite	Sericite, white mica, chlorite, epidote, zoisite, titanite, carbonate

Table 3.1 - Summary of the main aspects of the studied geologic units. Age of crystallization according to: 1- this work; 2- Sousa et al. (2016); 3- Abdallah and Meneghini (2017); 4- Cruz et al. (2003; and references therein).

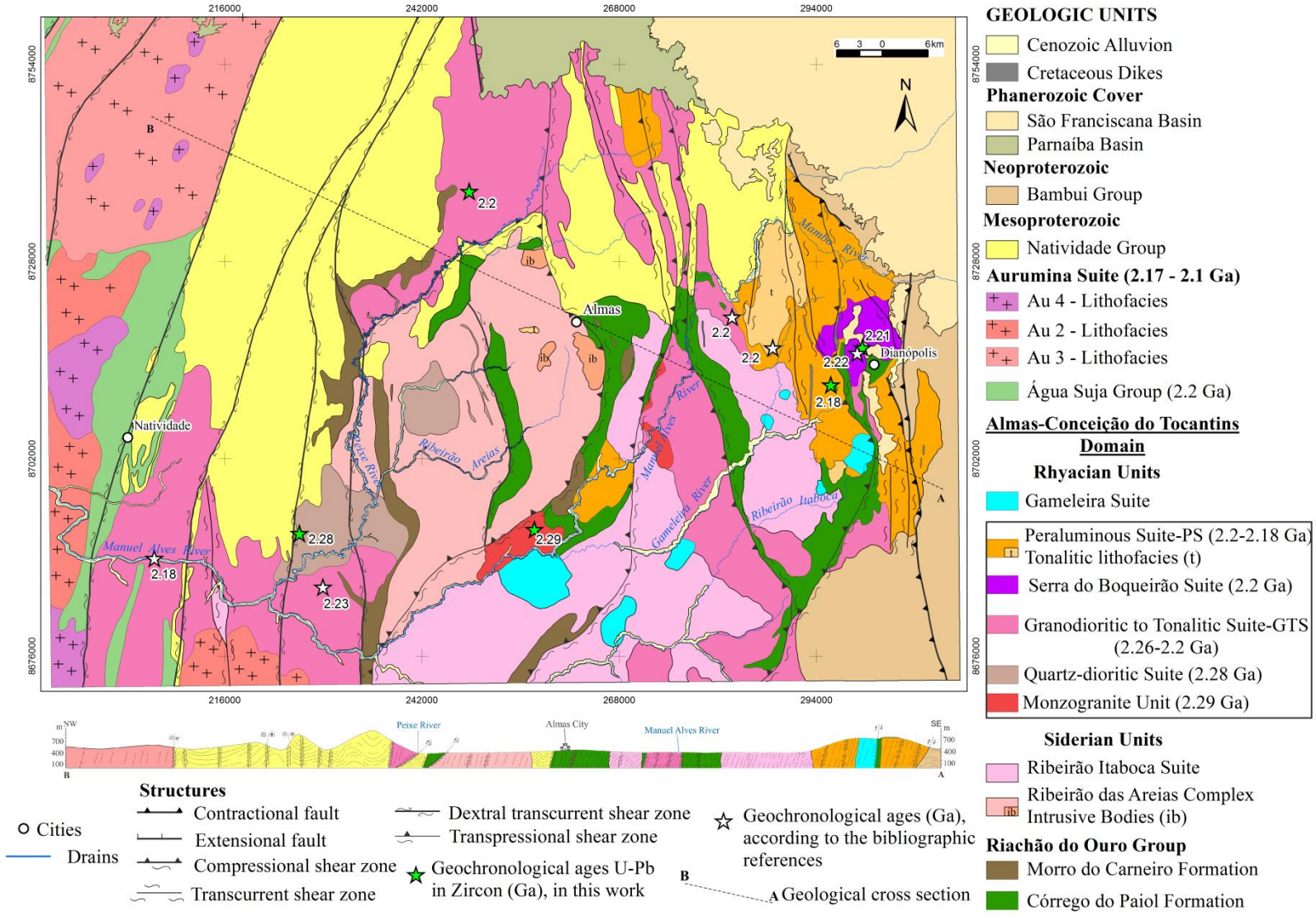

Figure 3.2 - Schematic geological map of the studied area, indicating the locations of geochronological data (Modified from Saboia et al., 2019). Units highlighted by the black outlined rectangle are covered in detail in this paper.

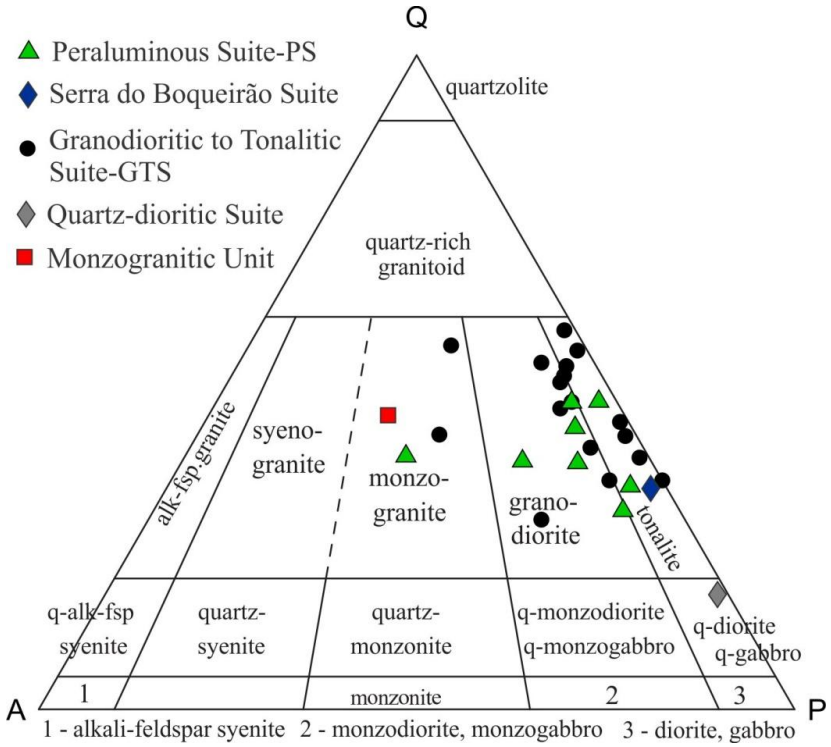

Figure 3.3 - QAP diagram (Streckeisen, 1976) for the studied samples.

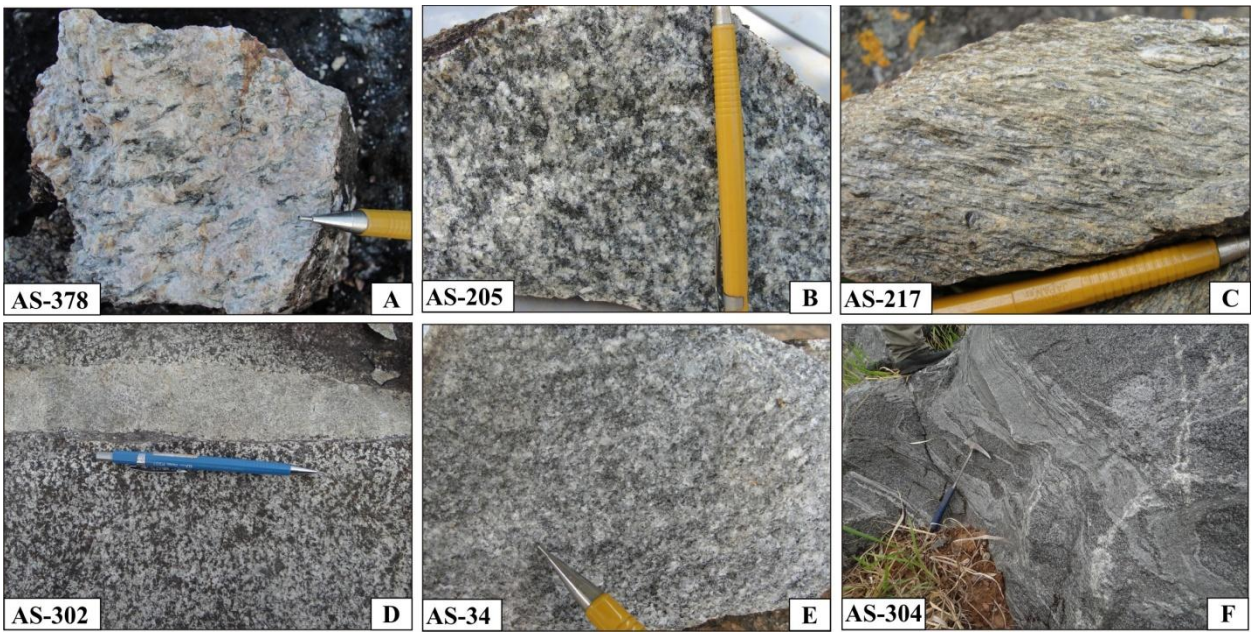

Figure 3.4 - Field aspects of the metagranitoids of the study area. (A) Foliated porphyritic biotite meta-monzogranite (Monzogranite Unit). (B) Isotropic magnetic biotite-hornblende quartz-meta-diorite (Quartz-dioritic Suite). (C) Mylonitic biotite meta-granodiorite (GTS). (D) Biotite-hornblende meta-tonalite with inequigranular texture (Serra do Boqueirão Suite), cut by leucocratic vein of the Peraluminous Suite. (E) Medium to coarse-grained, biotite meta-granodiorite with inequigranular and slightly porphyritic texture (PS). (F) Injection migmatitic facies (lithofacies 1 and 2) of the Peraluminous Suite. The acronym for the field/sample point is in the lower left corner of the figures.

3.3.5. Peraluminous Suite (Muscovite-biotite meta-granitoids - PS)

This Peraluminous Suite mainly forms a NS elongated batholith deformed by regional shear zones. According to Cruz et al. (2003) this unit is inserted in the Suite 2 granitoids and Abdallah and Meneghini (2017) describe this unit as consisting of peraluminous meta-granodiorites and meta-tonalites. Two distinct lithofacies were recognized: (1) dominant muscovite-biotite meta-granodiorite with subordinate meta-tonalite and meta-monzogranite, and (2) leucocratic meta-tonalite (biotite < 10%) stocks and late fine- to coarse-grained leucocratic veins. Igneous muscovite, belonging to the primary mineralogy is distinct from the metamorphic muscovite for presenting larger crystals, in which lamellae are not necessarily parallel to the foliation. Thin muscovite lamellae within the foliation planes are characteristical of metamorphic recrystallization. It is common in outcrops that both lithofacies occur associated and composing intercalated bands (Fig. 3.4 F).

3.4. Methods

3.4.1. U-Pb LA-MC-ICPMS and SIMS (SHRIMP) Geochronology

Four zircon U-Pb ages by Laser Ablation Microprobe Multi-Collector Inductively Coupled Plasma Mass Spectrometer (LAM-MC- ICPMS) and one by Secondary Ion Mass Spectrometer (SIMS) techniques were performed in the attempt to date the major magmatic events of the studied area. The new ages obtained in this work and the available geochronological data in the literature are reported in Table 3.1. Tables with analytical data are in the supplementary materials section (Tables I-N). The localization of the samples is shown in Fig. 3.2 and their coordinates are reported in Tables I-N. We analyzed five representative samples of the Almas-Conceição do Tocantins Domain units, and they will be described from the oldest to the youngest (as in section 3.3): Monzogranite Unit, Quartz-dioritic Suite, Granodioritic to Tonalitic Suite (GTS), Serra do Boqueirão Suite and Peraluminous Suite (PS). For zircon concentration samples were broken with a jaw crusher and powdered to approximately 500 µm. Heavy mineral concentrates were obtained by panning and were subsequently purified using a Frantz isodynamic separator. Zircon grains were selected from the least magnetic fraction. The best zircon grains were selected and set in epoxy resin mounts. Their surface was then polished to expose the grain interiors in order to be imaged on Scanning Electron Microscope (SEM) using cathodoluminescence (CL) and/or backscattering electrons (BSE).

The U–Pb analyses by LA-ICP-MS were carried out using a Thermo Scientific Neptune coupled to an Nd-YAG laser (λ = 213 nm) ablation system (New Wave Research, USA) at the Geochronology Laboratory of the University of Brasília. Analytical procedures follow those outlined in Bühn et al. (2009), where the epoxy mounts were cleaned in an HNO_3 solution (3%)

and ultraclean water bath. Ablation was done with a spot size of 25–30 µm, at frequency of 10 Hz and fluence of 2.0–6.0 J/cm^2. The ablated material was carried by Ar (0.90 L/min) and He (0.40 L/min) in analyses of 40 cycles of 1 s. Unknown analyses were bracketed by measurements of the international standard GJ-1, following the sequence 1 blank, 1 standard, 4 unknown, 1 blank and 1 standard. Accuracy was controlled using the standard 91500 (Wiedenbeck et al., 1995). Raw data were reduced using a homemade spreadsheet and corrections were done for background, instrumental mass-bias drift and common Pb. Ages were calculated using ISOPLOT 4.1 (Ludwig, 2012).

Samples for SIMS analyses were mounted with standard zircon crystals SL13 + FC1. Cathodoluminescence (CL) images were obtained in order to reveal internal structures of the zircon grains. Ion microprobe analyses were carried out using SHRIMP II at the University of São Paulo. The analytical methods and data treatment follow those described by Williams (1998) and Williams and Meyer (1998). The analyses were performed using a spot of 24 µm. Data were processed using SQUID and ISOPLOT 4.1 (Ludwig, 2012).

3.4.2. Whole-rock Geochemistry

Representative whole-rock geochemical analyses (26 samples) of the Granodioritic to Tonalitic Suite (GTS, 18 samples) and Peraluminous Suite (PS, 8 samples) are shown in Table 3.2. Major element analyses were carried out by X-ray fluorescence (XRF) at the SGS GEOSOL laboratory in Vespasiano, Minas Gerais (Brazil), and according to its pre-established XRF79C analytical method. The rock powder (~2 grams per sample) was dried in an oven and weighed after cooling in a jar containing lithium tetraborate flux. The sample was then transferred to a platinum crucible and homogenized. After homogenization lithium iodide was added before fusion in an automatic machine and analysis by XRF. Trace element analyses were carried out by inductively coupled plasma mass spectrometry (ICP-MS) at the SGS GEOSOL laboratory in Vespasiano, Minas Gerais (Brazil), and according to its pre-established IMS95A analytical method. The rock powder (~10 grams per sample) was weighed and then fused in a graphite crucible by adding lithium metaborate. After fusion the melt was transferred to a beaker containing a solution of nitric acid and tartaric acid in equal volumes before homogenization and total dissolution under agitation, and analysis of the solutions by ICP-MS. The standards used for the geochemical analyses correspond to the following reference materials present in the certificates of analysis by the SGS GEOSOL laboratory: AMIS0183, GBM995-2_R, GRE-03, IPT122, JK 28, SARM3, SG_077, SG_121, SG_122, SG_142 and TILL-3. The geochemical analyses were plotted using the GCDkit software (Janousek et al., 2006).

3.5. Results

3.5.1. Geochronology

3.5.1.1. Monzogranite Unit: Sample AS-378

Sample AS-378 is a pink, porphyritic, medium- to coarse-grained biotite meta-monzogranite from the Pau Ramalhudo Body (Fig. 3.4A) showing foliation along a N45°E trend. Quartz, K-feldspar, plagioclase and biotite are essential minerals whereas zircon is accessory and sericite with chlorite are subordinate. Zircon is represented by one family of medium bi-pyramidal crystals with some inclusions and abundant fractures and discrete oscillatory zonation under BSE images.

The isotopic composition of 33 spots on 30 zircon grains (Tab. I, see supplementary material) was determined by LA-MC-ICPMS, but four of them were discarded due to high error or common lead content. Data considered valid present similar $^{207}Pb/^{206}Pb$ ages with discordance between -9 and +19%. They present Th/U ratios from 0.34 to 0.91. Among the 29 data, those with the most consistent ages (15 spots) were selected and used in the regression, that yields an upper intercept age of 2297± 7 [±10] Ma with MSWD = 0.9 (Fig. 3.5A). This result is interpreted as the crystallization age of the Pau Ramalhudo meta-monzogranite.

3.5.1.2. Quartz-dioritic Suite: Sample AS-205

This outcrop is located at the base of the Santa Clara Ridge. Sample AS-205 is a magnetite-bearing, mesocratic, medium- to coarse-grained biotite-hornblende quartz-meta-diorite with granoblastic texture and slightly foliated structure (Fig. 3.4B). Essential minerals are plagioclase, hornblende, biotite and quartz. Magnetite and zircon are the accessory minerals, and sericite, epidote, zoisite, chlorite and carbonate are the secondary minerals.

Zircon recovered from this sample is prismatic and has well-developed pyramidal termination. BSE images reveal crystals with well-marked oscillatory zoning and others discretely zoned or homogeneous. Determined by LA-MC-ICPMS, the isotopic data from 40 analyzed spots (on 30 crystals) show a consistent group with varied discordance and Th/U from 0.21 to 0.78 (Tab. J). Data from 3 spots were discarded from the age calculation because they present behavior slightly different from the others. The regression of the 37 remaining analyses define an upper intercept of 2280 ± 7 [± 10] Ma with MSWD = 1.3 (Fig. 3.5B), interpreted as the crystallization age of the sample.

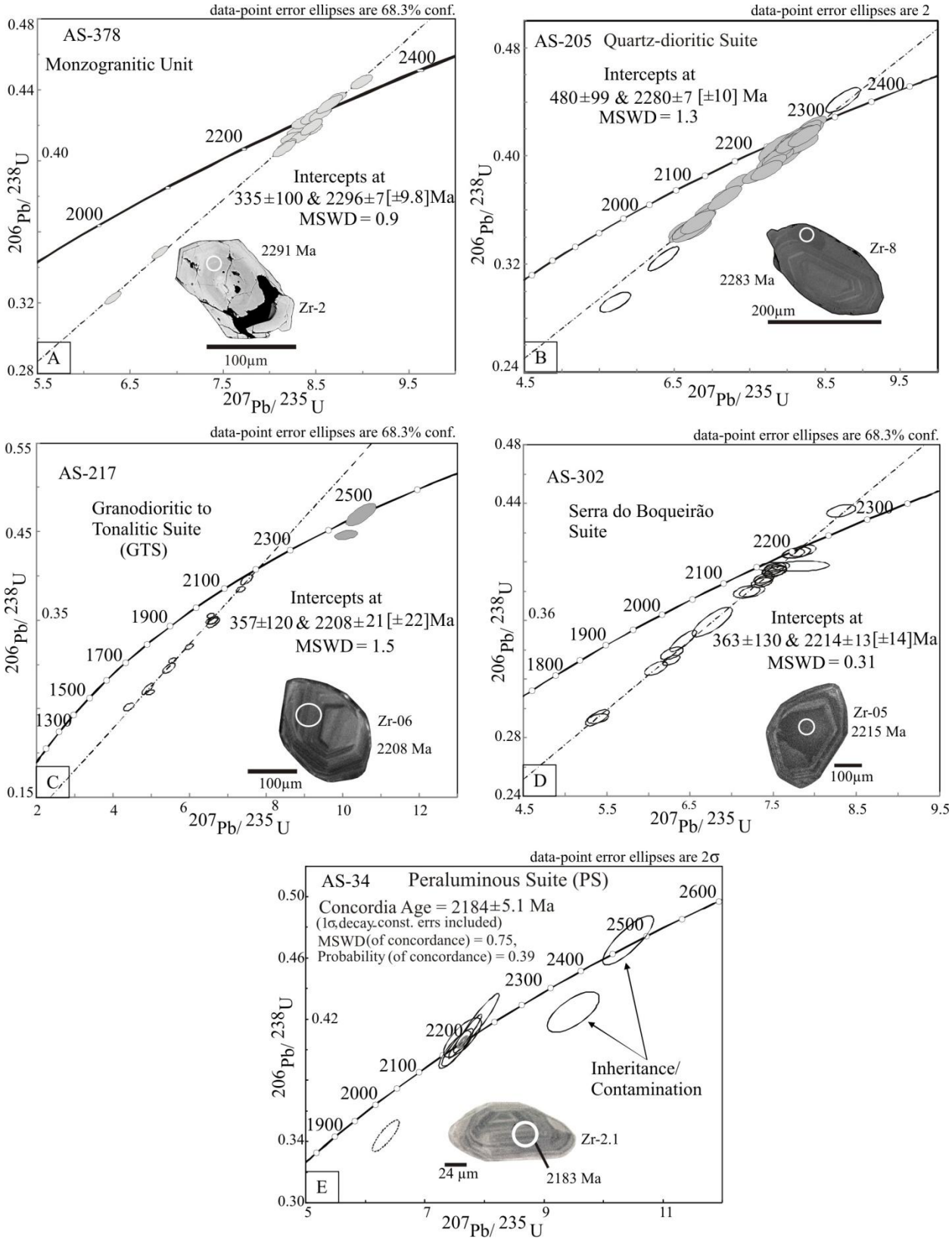

Figure 3.5 - (A) U-Pb Concordia diagram for AS-378 sample (Monzogranite Unit) with backscattered electrons (BSE) image of one analyzed zircon. (B) U-Pb Concordia diagram for AS-205 sample (Quartz-dioritic Suite) with BSE image of one analyzed zircon. (C) U-Pb Concordia diagram for AS-217 sample (GTS) with cathodoluminescence (CL) image of one analyzed zircon. (D) U-Pb Concordia diagram for AS-302 sample (Serra do Boqueirão Suite) with BSE image of one analyzed zircon. (E) U-Pb Concordia diagram for the AS-34 sample (PS) with CL image of one analyzed zircon. Zr= number, image and age of analyzed zircon.

3.5.1.3. Granodioritic to Tonalitic Suite (GTS): Sample AS-217

The analyzed sample is a proto-mylonite biotite meta-granodiorite (Fig. 3.4C) with granolepidoblastic texture, medium-grained and strongly foliated and sheared structure (N60°E trend). Quartz, plagioclase, microcline, and biotite are the main minerals, while zircon is the main accessory mineral. Sericite and zoisite represent the secondary assemblage.

Zircon extracted from this rock occurs as large bipyramidal prisms with some fractures and inclusions. Cathodoluminescense images show strong oscillatory zoning. A few crystals present dark or zoned core. This sample had 25 zircon crystals analyzed by LA-MC-ICPMS (27 spots), but data of twelve were discarded due to high analytical errors (Tab. L). Of the remainder, twelve spots were located in the zoned areas (Th/U between 0.09 and 0.24) and their regression indicates the upper intercept of 2208 ± 21 [± 22] Ma, interpreted as the crystallization age, with MSWD = 1.5 (Fig. 3.5C). Two spots located in cores presented $^{207}Pb/^{206}Pb$ apparent ages near 2.5 Ga and they are interpreted as inherited zircon.

3.5.1.4. Serra do Boqueirão Suite: Sample AS-302

This sample is from the Corrente Pluton, which occurs nearby the Dianópolis. The sample is a mesocratic hornblende meta-tonalite, medium-grained, with inequigranular and hipidiomorphic texture, and slightly foliated (Fig. 3.4D). Quartz, plagioclase and hornblende are the main minerals, and zircon is the accessory mineral. Zoisite, sericite and chlorite constitute the secondary minerals. The zircon grains are large pyramidal prisms with some inclusions and well-marked oscillatory zonation.

Twenty six spots had their isotopic composition determined by LA-MC-ICPMS. Four of them had their data discarded due to high analytical errors and the others were used in age calculation (Tab. M). The upper intercept of 2214 ± 13 [± 14] Ma with MSWD = 0.31 (Fig. 3.5D) was obtained by regression of all other data. This age is interpreted as the crystallization of the meta-tonalite. Selected grains show Th/U between 0.2 and 0.37.

3.5.1.5. Peraluminous Suite (PS): Sample AS-34

The sample was collected about 10 km southwest of Dianópolis. The studied rock is granodioritic in composition, medium- to coarse-grained, shows xenomorphic and equigranular textures, and is slightly foliated (Fig. 3.4E). Essential minerals are quartz, K-feldspar,

microcline, plagioclase (oligoclase) and biotite. Zircon is the accessory mineral, while white mica, sericite, carbonate and zoisite are the hydrothermal minerals.

The zircon is mainly represented by clear bipyramidal prisms with scarce fractures and some inclusions. They present strong oscillatory zoning and rare core. Their isotopic composition was determined by SIMS. Fourteen spots were investigated, but six were discarded due to high content of common lead (Tab. N). Six spots present similar $^{207}Pb/^{206}Pb$ apparent ages, five of them (Th/U between 0.21-0.31) are concordant and were used for de calculation of the Concordia Age of 2184 ± 5.1 Ma, associated with MSWD of 0.75 (Fig. 3.5E), interpreted as the crystallization age. Two inherited zircon analyses yielded older U-Pb ages of 2460 and 2480 Ma.

3.5.2. Whole-rock Geochemistry

The samples of the GTS have SiO_2 contents of 57.1–75 wt. % and show K-enrichment during magmatic differentiation, following the calc-alkaline trend (Tab. 3.2, Fig. 3.6a). In the diagram of Fig. 3.6b, the samples of the GTS have a dominant medium- to high-K calc-alkaline signature with only two samples (AS-209 and AS-366) plotting in the tholeitic series field. Samples of the PS have SiO_2 contents of 65.4–74.6 wt. % and define a trend parallel to the trondhjemitic line in Fig. 3.6a, belong to the medium-K calc-alkaline series (Fig. 3.6b). According to the classification of Shand (1943), rocks of the GTS are dominantly peraluminous (A/CNK > 1) with four samples (AS-208, AS-216, AS-246A and AS-366) being metaluminous (A/CNK ≤ 1) (Fig. 3.6c). Five samples of the GTS (AS-107, AS-109, AS-209A, AS-214 and AS-235B) have A/CNK ≥ 1.1 values. Most samples of the PS are peraluminous with A/CNK > 1.1 and two samples (AS-34 and AS-40) are weakly peraluminous.

According to the classification of Frost et al. (2001), rocks of the GTS and the PS are distributed in the calcic and calc-alkalic fields (Fig. 3.7a), with emphasis on the field of the Cordilleran granitoids (which are mostly representative of I-type granites). Some calc-alkalic samples fit in the post-tectonic Caledonian granitoids field. Rocks of the GTS are dominantly magnesian (Fig. 3.7b) and have <70 % of SiO_2, which are characteristics of Cordilleran batholiths. Only two samples (AS-109 and AS-217) with SiO_2 >70 %, weakly peraluminous and calc-alkalic are ferroan.

Unit/Rock	GTS/ Dior.	GTS/ Dior.	GTS/ Tonal.	GTS/ Tonal.	GTS/ Tonal.	GTS/ Tonal.	GTS/ Tonal.	GTS/ Granod.	GTS/ Granod.	GTS/ Granod.	GTS/ Granod.	GTS/ Granod.	GTS/ Granod.
Sample	AS-244	AS-246A	AS-17	AS-208	AS-209	AS-229	AS-366	AS-209A	AS-214	AS-214A	AS-216	AS-217	AS-221
SiO_2	57.1	57.2	68.1	64.3	63.8	62.9	68.6	65.4	67.8	72.8	62.5	70.5	69.2
TiO_2	0.74	0.77	0.45	0.77	0.76	0.6	0.38	0.34	0.35	0.2	0.67	0.24	0.28
Al_2O_3	17	16.6	15.8	15.6	15.9	16	16.5	17.1	15	14.8	15.7	14.6	14.7
Fe_2O_3t	7.92	8.35	4.49	6.88	7.09	6.29	3.54	4.9	4.19	2.77	7.26	3.26	2.92
MgO	4.29	4.6	1.31	1.96	2.14	3.06	0.87	1.61	1.37	0.82	3.21	0.42	0.81
CaO	5.33	5.13	3.33	5.2	4.36	4.69	4.14	4.23	2.04	3.27	4.7	2.22	2.39
Na_2O	3.11	3.88	4.35	3.2	3.97	3.28	4.95	3.24	3.03	3.39	2.92	3.24	3.26
K_2O	1.87	1.42	2.18	1.13	0.99	1.69	0.85	1.97	3.33	1.95	2.5	4	3.78
P_2O_5	0.16	0.18	0.2	0.2	0.22	0.17	0.11	0.12	0.06	0.03	0.21	0.07	0.1
MnO	0.11	0.14	0.07	0.09	0.1	0.1	0.04	0.07	0.04	0.05	0.13	0.08	0.06
LOI	2.35	2.06	1.18	1.53	1.53	1.05	0.56	1.6	0.99	0.89	1.23	0.84	1.02
SUM	99.98	100.33	101.46	100.86	100.86	99.83	100.54	100.58	98.2	100.97	101.03	99.47	98.52
Ni	51	50	6.1	29	30	43	10	20	19	10	29	2	10
Co	21.1	18.7	6.50	18.6	21.4	18.6	7.4	11.4	10.1	5.6	20.5	3.5	3.1
Ba	710	392	1575	274	239	615	222	652	648	370	705	759	886
Rb	61.2	44.7	48.1	44.9	37.2	48.6	21	60.2	114.1	64	101.9	169.1	93.2
Sr	793.3	466.4	795.7	313.6	294.4	537.2	342.4	303.5	283.5	376.2	439.8	193.2	468
Nb	4.09	3.38	10.77	7.46	6.57	2.67	2.65	1.91	5.85	2.12	5.77	3.38	3.35
Ta	0.31	0.18	2.31	0.36	0.41	0.07	0.13	0.09	0.33	0.21	0.34	0.53	0.23
Zr	149.3	144.3	241.6	239.7	230.6	132.3	162.5	135.8	165.3	116.2	170	127.9	146.5
Hf	3.27	3.31	5.54	5.42	5.39	2.74	3.83	3.14	3.91	3.04	3.84	3.3	3.4
Pb	1.6	1.8	2.4	1.6	1.6	2.6	0.9	1.5	36.1	5	3	18.6	18.8
Zn	65	69	53	90	96	75	48	55	55	24	77	30	24
Th	2.2	1.6	8.1	7.7	7.4	3.5	2.4	2.2	11.9	10.4	9.9	10.5	4.2
U	0.29	0.2	1.07	0.67	0.48	0.24	0.31	0.32	2.08	2.26	1.52	4.37	4.09
Ga	22.3	19	18.1	19.9	18.5	20.4	20.4	16.8	15	14.6	18.1	17.1	16.6
Cs	0.69	0.49	0.8	0.9	0.95	1.71	0.33	0.84	9.07	4.61	6.58	9.18	2.41
Y	19.02	15.38	18.25	8.28	8.91	8.75	5.21	7.56	7.45	7.33	17.43	18.42	8.06
La	24.7	22.9	65.9	48.7	30.6	24.6	11.3	21.2	35.5	43.1	36.5	30.1	34.7
Ce	50.2	41.2	128.3	102.8	67	45.1	20.3	22.9	67.7	80.4	70.8	68.6	35.2
Pr	6.4	4.96	14.54	10.49	7.14	5.2	2.2	2.68	8.01	8.61	8.11	7.41	4.4
Nd	23.2	17.2	49.1	38.9	26.2	17.4	8.5	7.5	28	29.5	29.9	24.8	14.2
Sm	5.2	3.7	7.4	6.3	5	3.2	1.9	1.9	5.5	5.1	5.6	4.8	3.3
Eu	1.2	1.19	1.75	1.29	1.32	1.1	0.6	0.94	1.42	1.31	1.41	0.64	0.89
Gd	4.24	3.23	5.05	4.3	4.05	2.55	1.86	1.68	3.48	3.31	4.27	3.92	2.95
Tb	0.61	0.47	0.69	0.46	0.47	0.31	0.25	0.2	0.41	0.41	0.59	0.57	0.36
Dy	3.49	2.75	2.90	1.9	2.04	1.7	1.28	1.17	1.68	1.9	3.2	3.18	1.77
Ho	0.71	0.54	0.64	0.3	0.32	0.33	0.19	0.26	0.24	0.26	0.62	0.68	0.28
Er	1.94	1.53	1.52	0.59	0.65	0.89	0.49	0.78	0.57	0.49	1.63	1.82	0.57
Tm	0.3	0.24	0.31	0.07	0.09	0.13	0.06	0.12	0.08	0.05	0.24	0.31	0.07
Yb	1.8	1.5	1.4	0.5	0.6	0.8	0.3	0.8	0.6	0.3	1.6	2	0.4
Lu	0.28	0.23	0.2	0.08	0.08	0.11	0.03	0.12	0.08	<0.05	0.24	0.28	0.05

Table 3.2 - Major and trace element data for the studied samples. Oxides (wt.%) and Trace elements (ppm). Abbreviations are: (GTS) Granodioritic to Tonalitic Suite, (PS) Peraluminous Suite, (Dior) Quartz-diorite and diorite, (Tonal.) Tonalite, (Granod.) Granodiorite, (Monz.) Monzogranite.

Unit/Rock	GTS/ Granod.	GTS/ Granod.	GTS/ Granod.	GTS/ Monz.	GTS/ Monz.	PS/ Tonal.	PS/ Granod.	PS/ Granod.	PS/ Granod.	PS/ Granod.	PS/ Granod.	PS/ Granod.	PS/ Granod.
Sample	AS-235B	AS-236	AS-340	AS-107	AS-109	AS-321A	AS-34	AS-40	AS-304	AS-304A	AS-308	AS-318	AS-325A
SiO_2	72.2	69.3	68	71.7	75	71.4	72.3	71	65.4	74.6	69.6	72.8	70.9
TiO_2	0.27	0.4	0.4	0.23	0.18	0.23	0.27	0.34	0.46	0.13	0.33	0.15	0.25
Al_2O_3t	14.7	15.5	15.2	14.4	13.2	15.1	14.8	15.5	15.3	14.6	15.4	15.1	16
Fe_2O_3	2.7	3.9	4.02	2.56	2.62	2.71	2.43	2.88	6.2	2.05	3.66	2.36	2.68
MgO	0.76	1.23	0.95	0.83	0.4	0.57	0.84	0.88	2.9	0.39	0.85	0.38	1.08
CaO	2.12	2.96	3.01	1.34	0.74	1.59	2.54	2.96	3.22	1.6	2.68	1.99	1.75
Na_2O	3.48	3.72	3.83	3.63	3.6	4.14	3.51	4.17	2.86	4.62	3.59	4.28	3.78
K_2O	2.87	2.69	2.7	3.34	4.42	2.74	3.06	2.56	2.55	2.11	2.45	2.26	2.84
P_2O_5	0.07	0.12	0.19	0.08	0.04	0.1	0.04	0.08	0.12	0.04	0.11	0.08	0.03
MnO	0.06	0.06	0.04	0.03	0.03	0.05	0.03	0.04	0.08	0.03	0.06	0.03	0.03
LOI	1.15	0.96	1.29	2.11	0.49	1.07	0.45	0.77	1.37	0.75	1.06	0.84	1.4
SUM	100.38	100.84	99.63	100.25	100.72	99.7	100.27	101.18	100.46	100.92	99.79	100.27	100.74
Ni	14	19	9	4.3	3	13	5.5	4.8	35.3	5	10	10	6
Co	3.1	10.4	6.8	1.8	1.6	3.6	4	4.2	20.9	2.1	6.5	3	4.3
Ba	900	459	1443	1172	985	594	1771	699	588	1042	809	687	813
Rb	91.1	118.6	47.4	53.3	98.4	70.1	67.1	79.5	104.8	50.3	79.9	60.2	64.6
Sr	435.4	438.1	770.2	272.9	320	359.5	546.6	368.8	369.5	365.1	474.2	430.4	628.2
Nb	2.28	5.13	5.04	6.27	10.49	2.60	4.27	12.71	7.65	2.83	5.87	3.17	3.71
Ta	0.16	0.54	0.85	0.66	0.98	0.15	1.04	2.14	1.07	0.03	0.95	0.63	0.54
Zr	151.6	132.4	174.6	145.1	181.5	68.7	141.2	133.4	94.1	46.2	144.7	80.7	66.1
Hf	3.57	3.21	4.48	3.64	5	1.91	3.36	3.76	3.2	1.41	4.11	2.4	2.04
Pb	16.5	11.1	5.5	4.2	8.5	8.5	10	7.7	5	11.2	20	16.1	7.4
Zn	34	63	35	8	17	28	36	49	96	28	42	20	18
Th	10.6	6.5	10.9	6.2	15.8	4.1	9.8	6.2	7.6	3	9.9	5.6	2.5
U	1.92	2.04	1.47	1.19	1.92	0.92	0.79	1.44	1.03	0.26	1.07	1.04	0.28
Ga	19	21.9	17.9	15.4	16.3	18	18.4	20.6	20.8	2	19.3	18.5	21.3
Cs	1.68	5.93	0.5	0.43	0.5	1.79	0.98	2.42	3.91	1.25	1.86	0.98	0.74
Y	11.47	7.12	10.82	11.93	13.88	4.34	1.66	5.12	11.65	3.56	10.18	4.99	1.35
La	90.8	27.5	68.7	39.8	49.2	19.1	31	17.9	18.5	24.9	40.5	23.7	12.3
Ce	109.8	53.9	132.2	75.4	100.2	32	54.3	34.1	36.8	37.7	79.5	39.9	22.2
Pr	14.06	6.02	14.36	8.63	9.84	3.7	5.54	3.92	3.75	4.38	7.92	3.79	2.42
Nd	47.2	21.4	49.2	28.8	34.4	13.2	19.9	13.6	16.3	15.5	31.6	15.1	8.1
Sm	6.3	3.6	6.9	3.8	5.3	2.1	2.7	2.4	2.6	2.3	4.3	2	1.4
Eu	1.53	0.96	1.62	0.98	1.02	0.57	1.29	0.86	0.95	0.5	1.28	0.81	0.82
Gd	3.8	2.42	4.48	2.55	4.18	1.58	1.64	2.12	2.11	1.57	3.01	1.3	0.92
Tb	0.38	0.29	0.53	0.31	0.43	0.2	0.11	0.31	0.51	0.18	0.5	0.23	0.15
Dy	1.55	1.37	2.31	2	2.29	0.93	0.42	1.27	1.98	0.72	1.75	0.73	0.33
Ho	0.29	0.27	0.46	0.39	0.49	0.16	0.05	0.25	0.54	0.12	0.41	0.22	0.09
Er	0.7	0.67	1.15	1.33	1.34	0.45	0.14	0.5	1.07	0.34	0.88	0.35	0.15
Tm	0.1	0.09	0.2	0.16	0.2	0.05	0.07	0.15	0.31	0.03	0.23	0.14	0.06
Yb	0.6	0.6	1	1	1.2	0.4	0.1	0.5	1	0.2	0.8	0.3	0.2
Lu	0.08	0.1	0.22	0.14	0.24	0.02	0.03	0.03	0.33	0.03	0.23	0.09	0.03

Table 3.2 - Continued.

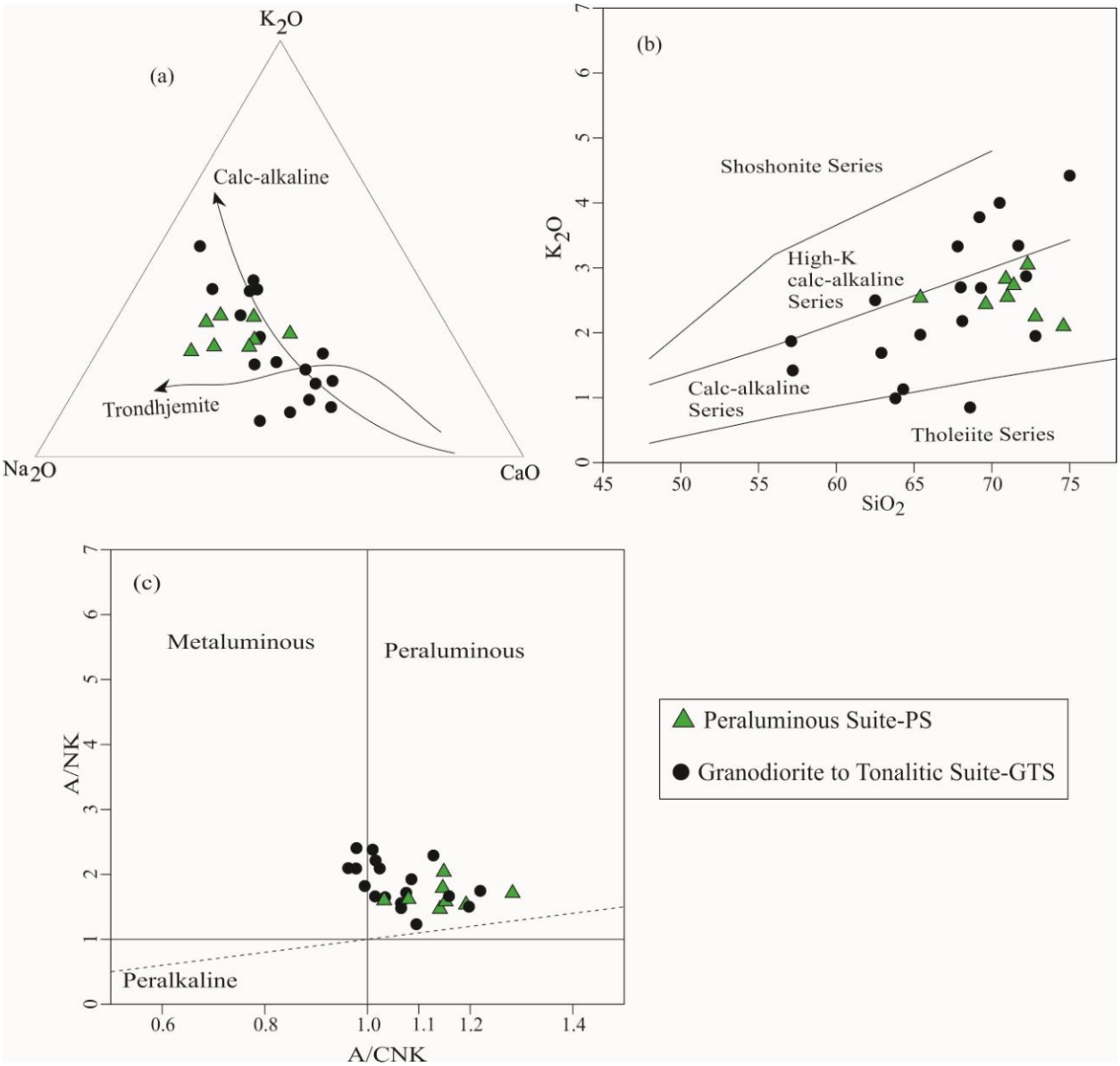

Figure 3.6 - (a) Ternary diagram K_2O-Na_2O-CaO (Barker and Arth, 1976). (b) Diagram SiO_2 vs. K_2O of Peccerillo and Taylor (1976). (c) Diagram A/CNK vs. A/NK of Shand (1943).

The rocks of the PS are magnesian and ferroan, with four samples (AS-304A, AS-308, AS-318 and AS-321A) more enriched in iron, peraluminous and calcic to calc-alkalic. Fig. 3.7c shows that the studied rocks do not correspond to highly fractionated granites, according to Whalen et al. (1987), and only the AS-109 sample of the GTS occupies the field of fractionated granites.

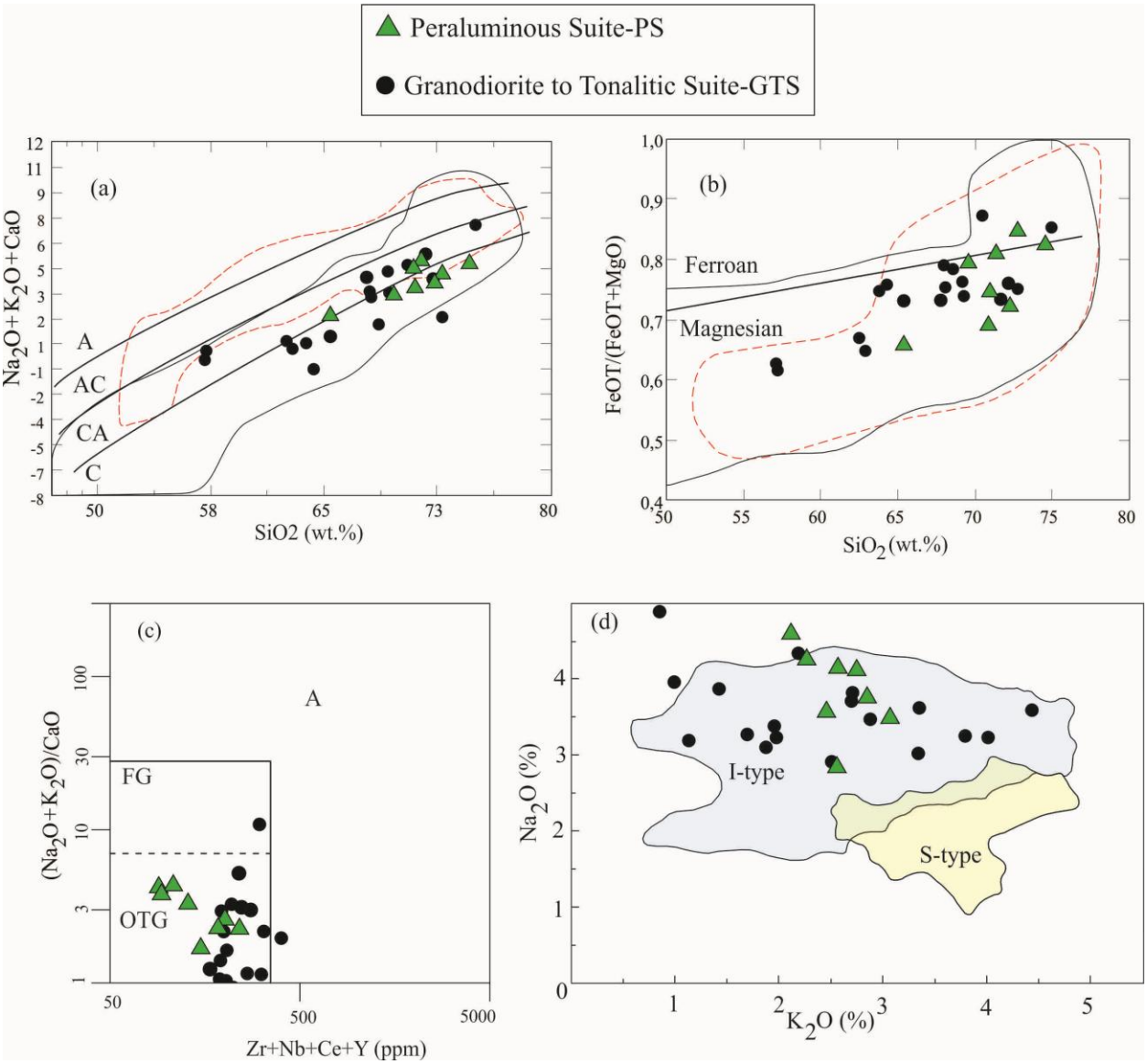

Figure 3.7 - (a) Diagram SiO_2 vs. Na_2O+K_2O-CaO of Frost et al. (2001). The field with continuous black line represents the Cordilleran granitoids and the dashed red line field represents the Caledonian plutons. Acronyms are: A (alkali), C (calcic), AC (alkali-calcic), CA (calc-alkalic). (b) Diagram SiO_2 vs. FeOt/(FeOt + MgO) of Frost et al. (2001). (c) Discriminant Diagram of Whalen et al. (1987), with the fields of Fractionated felsic granites (FG), unfractionated M-, I- and S-type granites (OTG) and (A) A-type granites. (d) Diagram Na_2O vs. K_2O (wt %), with the fields of I- and S-type granitoids of the Lachlan Fold Belt, according to White and Chappell (1983).

All the studied rocks plot in the field of I-type granites of the Lachlan Fold Belt in Fig. 3.7d, according to White and Chapell (1983), which shows the low K_2O/Na_2O ratios characteristic of these granitoids. According to White and Chappell (1983), S-type granites have high values of K_2O and K_2O/Na_2O and low contents of CaO compared to the I-type granites. So, with respect to the K_2O, K_2O/Na_2O and CaO values the GTS and PS samples are classified as I-type granitoids.

The GTS samples in the chrondrite normalized diagram (Boyton, 1984) (Fig. 3.8a and 3.8c), show the predominance of moderate to highly fractionated LREE vs. HREE patterns $(La/Yb)_N$ = 15.3 - 102 (Tab. 3.2). Only three samples have low $(La/Yb)_N$ values (<10.2). They also show weak to moderate negative Eu anomalies (Eu/Eu*= 0.45 – 1.18) and one sample (AS-209A) displays positive Eu anomaly (Eu/Eu*= 1.61), which indicate accumulation of plagioclase. The primitive mantle multi-element normalized diagram (Sun and McDonough, 1989) for this suite (Fig. 3.8b and 3.8d) is characterized by pronounced negative Nb, P and Ti anomalies for most samples. Six samples have strong positive Pb anomalies. In the chrondrite normalized diagram the PS samples (Fig. 3.8e and 3.8g) display moderate to highly fractionated $(La/Yb)_N$ = 24.1 – 83.9 patterns, and one sample (AS-34) has highly fractionated $(La/Yb)_N$ = 209 pattern. They show weak negative to significant positive Eu anomalies (Eu/Eu*= 0.8 – 2.2), which indicate a lesser or greater degree of importance of the fractionation of plagioclase in the genesis of these rocks, respectively. In the primitive mantle multi-element normalized diagram (Fig. 3.8f and 3.8h) these rocks show prominent negative Nb, P and Ti anomalies for most samples. All samples of this suite have strong positive Pb anomalies.

3.6. Discussion

3.6.1. Source and Tectonic Setting

Regarding granite classification, it is extremely important to identify the nature of the magma source (Chappell et al., 2012). The GTS and PS samples define different trends in Fig. 3.9a where the GTS compositions are similar to those of experimental melting of amphibolites and quartz-feldspathic (metagreywackes or orthogneisses) sources. The PS compositional trend is mainly related to experimental melts derived from quartz-feldspathic rocks, suggesting derivation from a more felsic crustal protolith.

On the diagrams of major elements elaborated by Patiño Douce (1999) in Fig. 3.9b and 3.9c, the GTS and PS samples plot clearly in the field corresponding to melts derived from amphibolites and meta-tonalites. Overlaps with the field of metagreywacke sources are observed to a limited extent. These characteristics may indicate a magma composed predominantly by sources of metaigneous origin with little or no interaction of metasediment-derived melts. The GTS and PS rocks follow the experimental curve of low pressure reactions (Fig. 3.9c) between melts of quartzo-feldspathic metamorphic rocks and high-Al basalts of Patiño-Douce (1995), that indicates shallow to medium depths (19 to ~30 km) in the crust for these reactions.

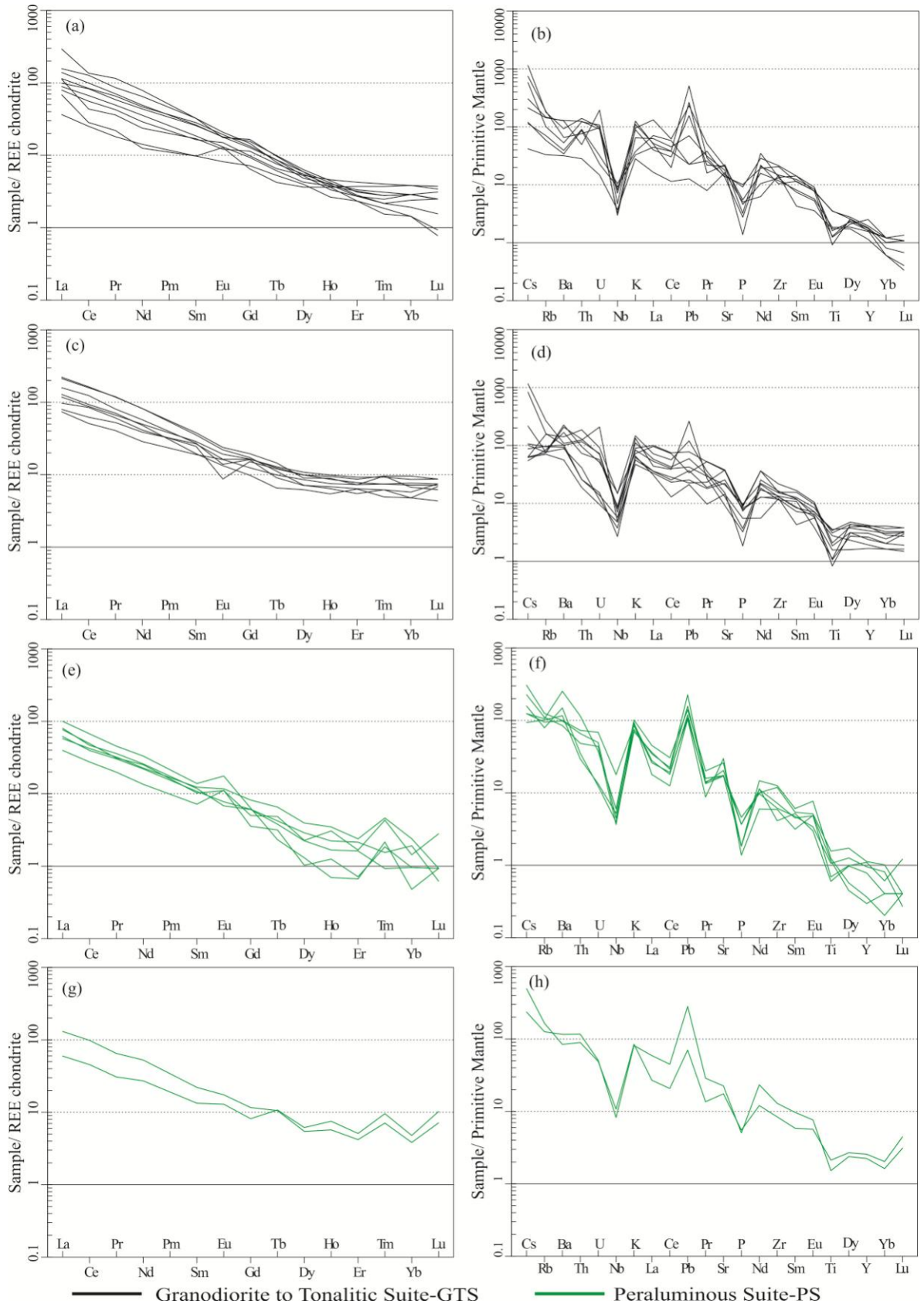

Figure 3.8 - (a) and (c) Chondrite normalized REE patterns (Boynton, 1984), and (b) and (d) Primitive mantle normalized multi-element (Sun and McDonough, 1989) patterns for the GTS samples. (e) and (g) Chondrite normalized REE patterns (Boynton, 1984), and (f) and (h) Primitive mantle normalized multi-element (Sun and McDonough, 1989) patterns for the PS samples.

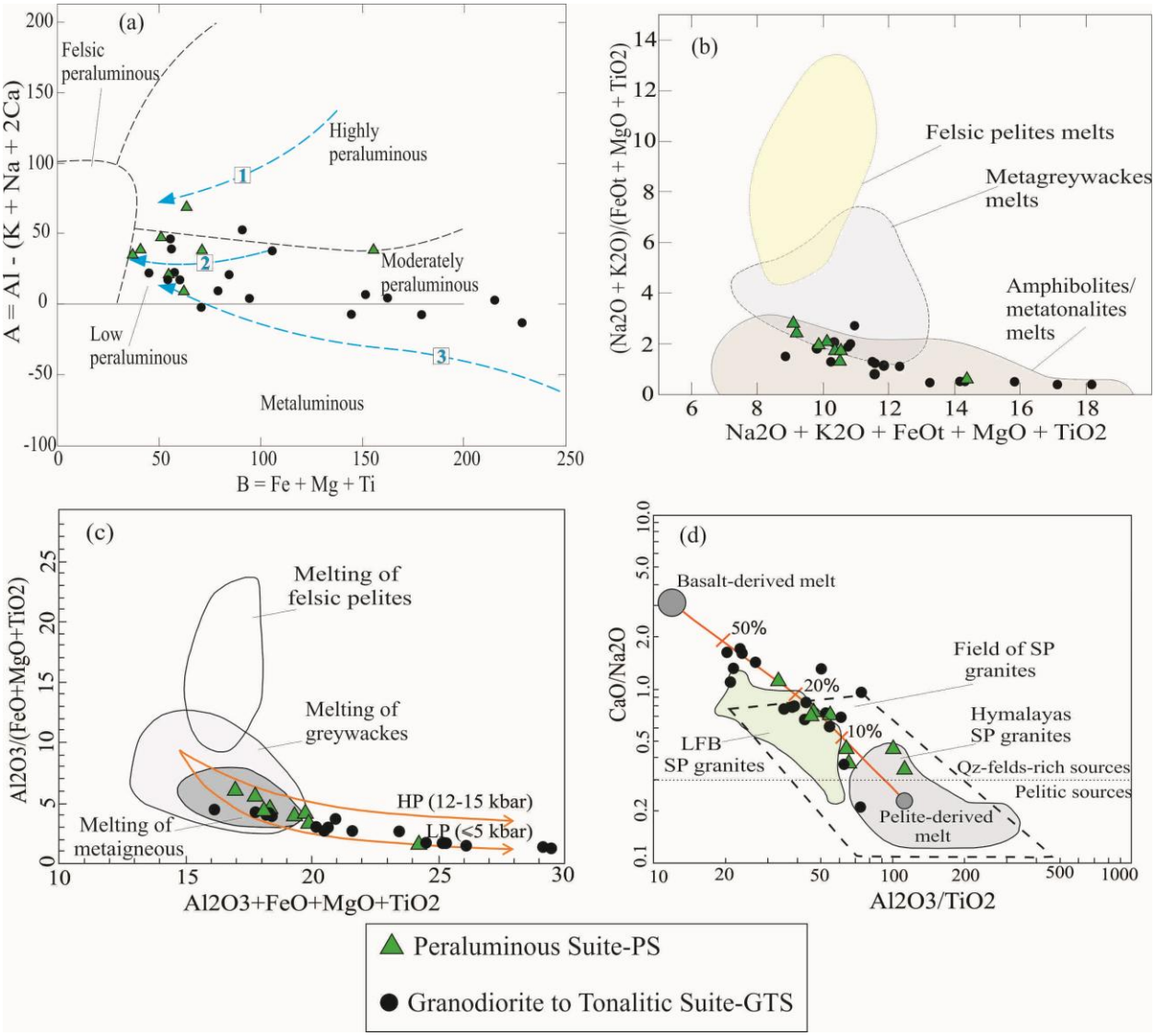

Figure 3.9 - (a) A-B diagram of Debon and LeFort (1983) modified by Villaseca et al. (1998). Dashed blue arrows are trends of experimental melts from different protoliths according to Grosse et al. (2011; and references therein): 1 - pelite-derived melt (Vielzeuf and Holloway, 1988); 2 - greywacke-derived melt (Conrad et al., 1988); 3 - amphibolite-derived melt (Beard and Lofgren, 1991). (b) and (c) are major element diagrams of Patiño Douce (1999) with the studied rocks. Fields are compositions of experimental dehydration-melting of different rock types. HP – high pressure and LP – low pressure are reaction curves between the indicated sources and high-Al basalts (Patiño-Douce, 1995). (d) CaO/Na_2O versus Al_2O_3/TiO_2 (Sylvester, 1998). LFB - Lachlan Fold Belt; SP – strongly peraluminous; Qz-felds – quartz-feldspathic.

The diagram in Fig. 3.9d (Sylvester, 1998) shows that the GTS and PS samples have high CaO/Na_2O ratios and suggests quartz-feldspathic-rich sources such as tonalites/granodiorites. Also in Fig. 3.9d, most of the PS samples occupy the strong peraluminous granites field and the majority of the GTS samples plot in or near the Lachlan Fold Belt strong peraluminous granites field.

According to the multicationic diagram of Fig. 3.10a (Batchelor and Bowden, 1985), the

studied rocks show compositions that allow them to be related to the subduction (pre-plate collision) and syn-tectonic (syn-collisional) settings. It is noteworthy that most samples of the PS are near or in the field of the syn-tectonic setting. On the tectonic discrimination diagrams (Fig. 3.10b-c) of Yb vs. Ta and Hf-Rb/10-Ta*3 (Pearce et al., 1984; Harris et al., 1986) the GTS samples dominantly plot in the volcanic arc granite field, which is related to the subduction setting and most samples of the PS plot on or near the syn-tectonic (syn-collisional) field.

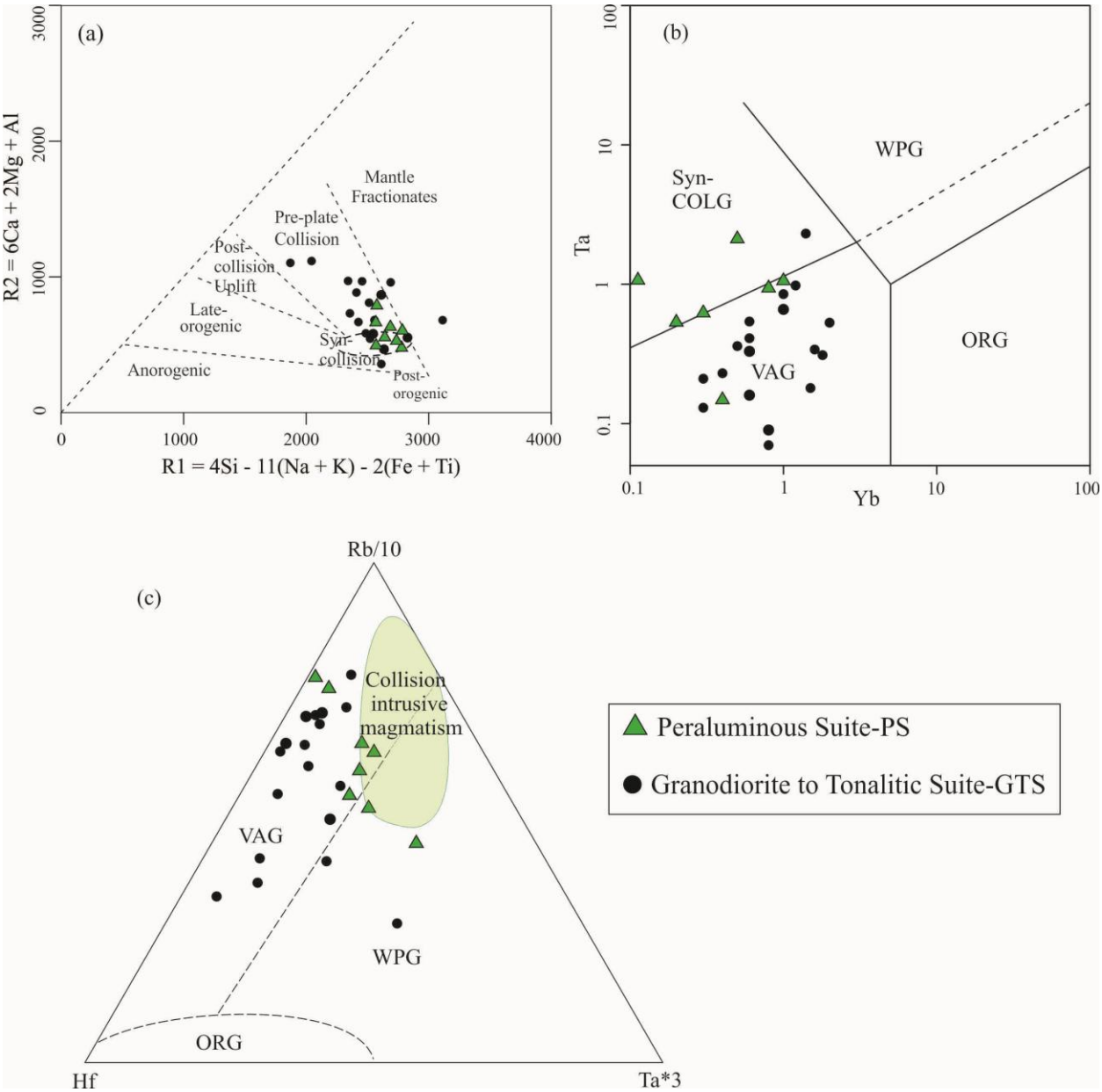

Figure 3.10 - (a) Multicationic diagram R1-R2 according to Batchelor and Bowden (1985). (b) Tectonic discrimination diagram of Pearce et al. (1984). (c) Tectonic discrimination diagram of Harris et al. (1986).

3.6.2. Ages, Geochemical Signatures and Tectonic Implications

The well-defined U-Pb ages in this work better constrain the timing of the Almas-Conceição do Tocantins Domain during the Rhyacian period and indicate a magmatic evolution around at least 2.29 to 2.18 Ga. The older $^{207}Pb/^{206}Pb$ apparent ages (sections 3.5.1.3 and 3.5.1.5) obtained in inherited zircon crystals from AS-217 (2497 and 2475 Ma) and AS-34 (2480 and 2460 Ma) samples are very similar to those found in the older metagranitoids basement unit in the studied region (the Ribeirão das Areias Complex of Cruz et al., 2003), which may have contributed as a source of the GTS and PS magmatism.

As seen in section 3.6.1 the GTS granitoids were dominantly derived from partial melting of metamafic rocks and older rocks of the basement (meta-tonalites and meta-granodiorites), with little or no participation of metasedimentary sources material. We can infer that the GTS represents I-type granites suites that extend from metaluminous to peraluminous compositions as the Moonbi Suite of southeastern Australia (Chappell et al., 2012). The PS granitoids included melts mostly derived from a felsic continental crust such as tonalitic-granodioritic orthogneisses, meaning a less mafic source compared to the GTS. We can deduce that the PS represents peraluminous I-type granitoids.

Most of the studied samples are characterized by enrichment in Large Ion Lithophile elements (LILEs) and Light Rare Earth Elements (LREE), but with negative anomalies and depleted in High Field Strenght Elements (HFSE; e.g. Nb, Ta, Ti), which are geochemical features of magmas produced in subduction zones (Pearce and Peate, 1995; Pearce, 1996). The GTS samples are concentrated into the volcanic arc field and the PS samples mainly plot in the syn-tectonic field (Fig. 3.10). We propose that the studied granitoids were generated in a continental arc (Cordilleran type) where the GTS rocks were generated in a subduction (pre-plate collision) setting. The tectonic scenario of this accretionary orogen probably evolved to allow the PS magmatism to form in the transition from initial subduction to syn-tectonic stages.

The spatial zonation and diachronism between the different types of granitoids in subduction settings have been described in other regions of the world: e.g., in western North America (Miller and Bradfish, 1980); Lachlan Fold Belt in Eastern Australia (Collins and Richards, 2008); Sierras Pampeanas of northwestern Argentina (Grosse et al., 2011); Central Brazil (Cuadros et al., 2017b); Peninsular Malaysia in southeast Asia (Ghani et al., 2013); and the Pan-African Belt in south Morocco (El Baghdadi et al, 2003). Our data along with data compiled from the literature allow us to infer a plate-tectonic framework with spatial and temporal zonation for the studied metagranitoids in a continuous evolution of a continental-arc magmatism (Fig. 3.11), where: (i) metagranitoids of the GTS have larger area of occurrence in

the mapped area, and predominate toward the western portion (continental margin or outboard region) of the Almas- Conceição do Tocantins Domain. They represent major contributions of peraluminous melts with subordinately metaluminous melts from metamafic and metafelsic (orthogneisses) sources. (ii) metagranitoids of the PS are more concentrated in the eastern portion of the studied area, towards the continental interior/inboard region, and represent contribution of peraluminous melts from more metafelsic crustal sources in relation to the GTS. In this inboard setting, crustal thickening occurred by eastward subduction advancing movements similarly to the concept of advancing orogen detailed by Cawood et al. (2009) and Ducea et al. (2015), which allowed the heat flow and consequently emplacement of peraluminous I-type magmas. Barbarin (1999) also indicated that peraluminous granitoids are placed at crustal thickening sites and some types are concentrated along shear zones that cut the thickened crust.

3.6.3. Regional Implications

The geochronological data of the literature show that magmatism around 2.26 to 2.18 Ga is the most widespread in the Almas-Conceição do Tocantins Domain. This magmatism is dominantly felsic and shows negative εNdT suggestive of a continental arc that might have started at 2.4 Ga (Cruz et al., 2003; Sousa et al., 2016; Fuck et al., 2014). New ages of 2296 Ma for the Monzogranite Unit and 2280 Ma for the Quartz-dioritic Suite and the 2.26 Ga early ages of the GTS in the literature (see Tab. 3.1) suggest that although larger volumes of magmatism are concentrated around 2.4-2.3 Ga and around 2.2 Ga, magmatic activity did not cease within these 100 Ma interval. We interpret that these intrusions represent the first Rhyacian magmatic stages of a long-lived orogenic system. These 2.29-2.28 Ga granitic-dioritic intrusions may be related to post-collisional extension after the Siderian (2.47-2.3 Ga) TTG rock-forming events. However, more specific studies are needed to detail these magmatic stages.

The youngest crystallization age in this study for the Almas-Conceição do Tocantins Domain relates to the PS (2184 Ma) and corresponds to a compressional phase with formation of peraluminous I-type granitoids of this continental arc (section 3.6.2). This age around 2.18 Ga overlaps other ages found in units mapped and understood in this work within the Almas-Conceição do Tocantins Domain (Tab. 3.1). This finding is consistent with our geotectonic model (Fig. 3.11), whereby metaluminous to peraluminous magmas of the GTS represent the dominant phases of the continental arc (~2.26-2.2 Ga). The evolution of the compressional dynamics of this arc allowed phases of diachronism in the generation of the GTS and PS magmas and a suggestion of zonation, where PS peraluminous magmas emplaced in the inboard

regions and younger granitoids of the GPS are emplaced in the outboard regions of the arc.

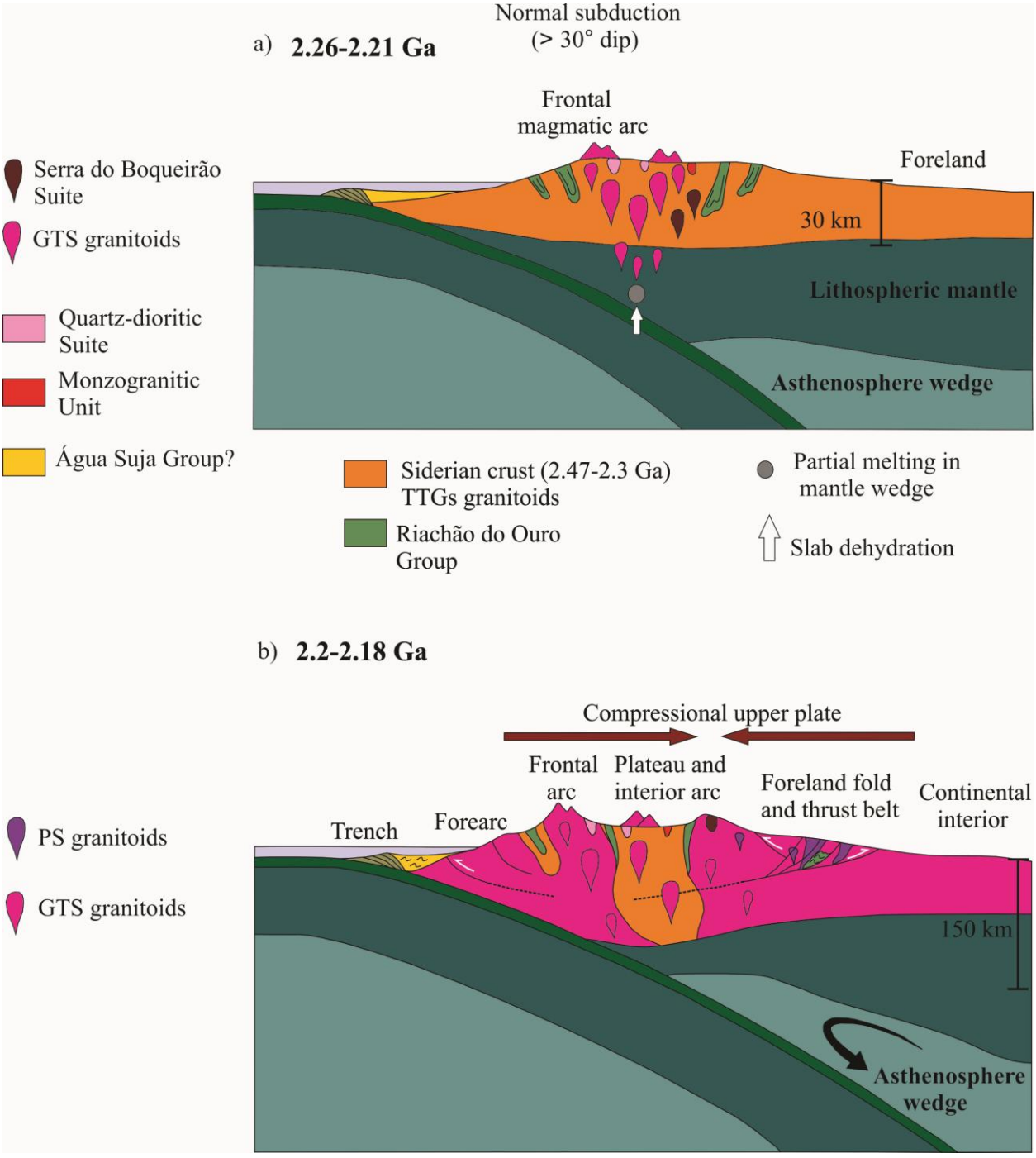

Figure 3.11 - Schematic model of the tectonic evolution of the studied rocks: (a) Normal subduction with intrusions of the GTS granitoids and Serra do Boqueirão Suite. (b) Compressional orogeny with formation of PS magmatism in the inboard regions and GTS granitoids along the arc. Schematic figures based on Gutscher et al. (2000) and Ducea et al. (2015).

Recurrent events of magmatism in the period between 2.45 to 2.18 Ga proposed in this work has also been proposed in previous studies (eg. Cruz et al., 2003; Fuck et al., 2014; Sousa

et al., 2016). These two last authors also included the Aurumina Suite in this context of long-lived Paleoproterozoic magmatic events. Sousa et al. (2016) concluded that during the period between 2.17 to 2.15 Ga, there was a collisional event of the continental arc with another crustal block for the generation of the syn-collisional granites of the Aurumina Suite (2.16-2.12 Ga). Cuadros et al. (2017b), on the other hand propose a hinterland setting for the magmatism of the Aurumina Suite between 2.16 to 2.11 Ga. Additionally, the Aurumina Suite magmatism is coeval with that of the Campinorte Arc, which initially took place as an intraoceanic island arc (Cordeiro et al., 2014). These interpretations leave open the question whether the accretionary orogen addressed in this study evolved into an accretionary-collisional orogen.

Other terranes of the São Francisco Craton and pericraton recorded Rhyacian (~2.3-2.1 Ga) magmatic events and an attempt of regional geologic-tectonic correlation and evolution can be made: (i) In the Mineiro Belt, situated in the southern part of São Francisco Craton (Fig. 3.12), the Minas Orogen represents a long-lived accretionary system (2.47-2.1 Ga) of oceanic and continental arcs, which developed on the continental margin of the Archean core (Heilbron et al., 2017). The oldest TTGs oceanic arcs, called Cassiterita-Resende Costa-Lagoa Dourada (~2.47-2.35 Ga) can be correlated with the arc-related rocks of Siderian ages (2.45-2.34 Ga) of the Almas-Conceição do Tocantins Domain (Barbosa et al., 2018; Cruz et al., 2003; Lima, 2014; Fuck et al., 2014; Sousa et al., 2016).

The Serrinha-Tiradentes oceanic arcs (2.23-2.2 Ga) and the Ritápolis continental arc (2.17-2.12 Ga) (Ávila et al., 2010, 2014; Barbosa et al., 2015; Cardoso et al., 2019) are correlated with the continental arc rocks of this work. (ii) In the southern Gavião Block (Fig. 3.12), Cruz et al. (2016) based on robust integration of geochronological and geochemical data suggested that between 2.38 and 2.11 Ga a continental magmatic arc (Western Bahia Magmatic Arc) was installed on the eastern continental margin of the Gavião Paleoplate and a subduction zone also developed to the west. These calcic to calc-alkalic arc rocks were generated before the 2.1 to 2.09 Ga collision event between the Gavião and Jequié paleoplates. They also did a correlation of this Western Bahia Magmatic Arc with the Mineiro Belt, Mantiqueira Complex, Serrinha and Congo Paleoplates, and this regional correlation is shown in Fig 3.12. It has also been indicated that these four arc systems evolve to an accretionary-collisional orogen.

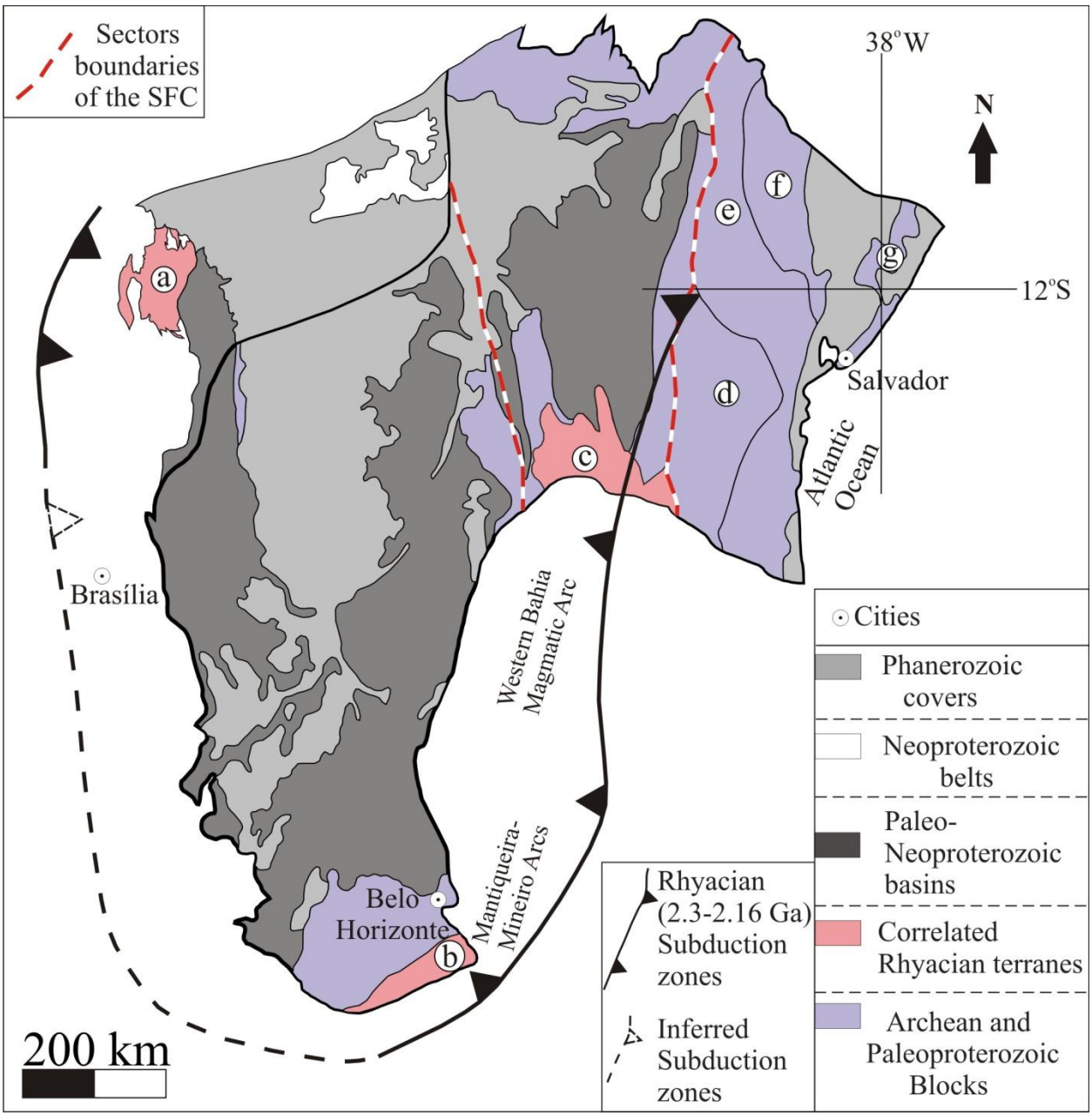

Figure 3.12 - The São Francisco Craton (CFS) and the correlation of the terranes, which contain units of Rhyacian age rocks (2.3 to 2.16 Ga). The subduction zone continuity between the Western Bahia Magmatic Arc and the Mantiqueira and Mineiro arcs is according to Cruz et al. (2016). Legend: (a) Almas-Conceição do Tocantins Domain, (b) Mineiro Belt, (c) Southern Gavião, (d) Jequié Block, (e) Itabuna–Salvador–Curaçá Belt, (f) Serrinha Block, (g) Salvador-Esplanada-Boquim Belt. Modified from Hasui et al. (2012).

The Siderian Rio do Paulo/Aracatu Suites (2.38 to 2.32 Ga) can be correlated again with the arc-related rocks of Siderian ages (2.45-2.34 Ga) of the Almas-Conceição do Tocantins Domain. The Rhyacian granitoids of group 1 (2.2- 2.1 Ga) are considered to represent continental arcs (Cruz et al., 2016) and are correlated with the continental arc rocks of this work. This regional geotectonic correlation of Siderian-Rhyacian (~2.3-2.1 Ga) magmatic units in the São Francisco Craton shown in Fig. 3.12, allows checking the diachronic character of these orogens as

proposed by Cruz et al. (2016).

Finally, our data are consistent with magmatic events related to a convergent margin attributed to a long-lived orogenic system. The correlation of this orogen hosted within the Almas-Conceição do Tocantins Domain with equivalents in the Mineiro Belt, Mantiqueira Complex and the Western Bahia Magmatic Arc imply that different building blocks of the São Francisco paleocontinent share at least three synchronous orogeny-related events.

3.7. Conclusions

The U-Pb ages indicate that the Pau Ramalhudo Body of the Monzogranitic Unit (2.29 Ga) and the Quartz-dioritic Suite (2.28 Ga) correspond to the earliest Rhyacian magmatic stages within the Almas-Conceição do Tocantins Domain. A later magmatic event around 2.2 Ga represents the development of a continental magmatic arc and the emplacement of the Granodioritic to Tonalic Suite-GTS and the Serra do Boqueirão Suite. The GTS is composed of metaluminous to peraluminous I-type granites likely generated by partial melting of metamafic rocks and orthogneisses rocks of the continental crust. Later development of the arc around 2.18 Ga gave origin to peraluminous I-type granites essentially generated by a less metamafic crustal source.

Other terrains in the São Francisco Craton exhibit similar and synchronous Rhyacian evolution and correlations can be established with the Mineiro Belt, Mantiqueira Complex and Western Bahia Magmatic Arc. The studied orogen and the other correlates in the São Francisco Craton are representative of magmatic events to form the building blocks of the Columbia Supercontinent.

Acknowledgements

We thank the Institute of Geosciences of the University of Brasilia (IG/UnB) and the Geological Survey of Brazil (CPRM) for the field work support and the laboratory analysis. The CNPq (Conselho Nacional de Desenvolvimento Científico e Tecnológico) is acknowledged for grants provided to CGO (process number 305769/2019-7). We are grateful to Dr. Natalia Hauser, Dr. Andres Folguera and Dr. Reinhardt Fuck for handling this paper and to the three anonymous reviewers for the valuable suggestions and corrections that helped improve the article. This study was financed in part by the Coordenação de Aperfeiçoamento de Pessoal de Nível Superior - Brasil (CAPES) - Finance Code 001 and the INCT Estudos Tectônicos.

Capítulo 4

4. CONCLUSÕES E CONSIDERAÇÕES FINAIS

Esta pesquisa determinou idades de cristalização, informações de petrogênese e tectônicas das rochas plutônicas relacionadas à evolução do Domínio Almas-Conceição do Tocantins (DACT). Para isso, foram utilizados dados de mapeamento geológico, geocronológicos U-Pb em zircão (SHRIMP e LA-ICP-MS) e geoquímicos (rocha total-elementos maiores e traços).

Com base nos resultados obtidos, seguem as conclusões, além das conclusões já descritas nos capíulos 2 e 3, considerações, recomendações e contribuições científicas da Tese:

- Uma proposta de melhor definição dos limites cartográficos do DACT foi apresentada. Esta sugestão cartográfica foi baseada na classificação litoestratigráfica do Complexo Almas-Cavalcante (PP12γac) utilizada pelo Serviço Geológico do Brasil (SGB-CPRM). Esta classificação foi usada para organizar as diversas unidades litológicas e suas relações estratigráficas dentro da hierarquia formal de Complexo. Contudo, o termo Domínio definido por Fuck *et al.*, (2014) caracterizou de forma mais precisa as associações de rochas da área deste trabalho, além de já estar consagrado na literatura científica da região. Com o intuito de avançar no conhecimento geológico e de evitar o excesso de nomenclaturas, adotou-se o termo Domínio Almas-Conceição do Tocantins para agrupar o conjunto das unidades litoestratigráficas deste estudo.
- Esta pesquisa possibilitou o incremento da caracterização geológica e do entendimento geotectônico durante o período Sideriano das associações de trondhjemitos-tonalitos-granodioritos relacionadas ao Complexo Ribeirão das Areias (2,47-2,45 Ga) de Cruz *et al.*, (2003) e da Suíte Ribeirão Itaboca (2,3 Ga) aqui definida. Quanto aos elementos maiores e menores estas rochas são classificadas como TTGs peraluminosos gerados em ambiente tectônico relacionado com subducção, possivelmente a partir da fusão da crosta oceânica máfica subductada em profundidades de média a alta pressão. O conjunto de dados obtidos permitiu caracterizar eventos de formação de rochas TTGs de pelo menos 170 Ma. Também foram caracterizadas rochas graníticas da série cálcialcalina de alto-K que ocorrem de forma restrita nos corpos de rochas TTG, e que provavelmente se formaram após o magmatismo TTG.
- Martins-Ferreira *et al.*, (2020) identificaram 4 unidades de metagranitoides de idade Sideriana: Batólito Porto Alegre (2.47 Ga), Batólito Rio do Peixe (2.47 Ga), Granodiorito

Ribeirão das Areias (2.46 Ga), e Batólito Serra do Pilão (2.39 Ga). Assim sendo, estudos específicos posteriores devem ser realizados para integrar e detalhar estes novos resultados e os da presente pesquisa, com o propósito de progredir no conhecimento das unidades de rochas e dos eventos magmáticos ocorridos durante o Sideriano.

- Os dados de Lu-Hf de Martins-Ferreira *et al*., (2020) preenchem uma lacuna importante a respeito da carência do uso desta metodologia na área estudada. Logo, o conjunto dos dados isotópicos (Sm-Nd, Lu-Hf e U-Pb) para os **metagranitoides de idade sideriana**, disponíveis na literatura e nesta tese são indicativos de cenários magmáticos de formação de crosta continental, em que: (i) O período entre 2,47 e 2,45 Ga, apresenta valores positivos de εNd(t)=+0,58 e de εHf(t)=+6,36 a +0,57, e caracteriza evento de acreção juvenil (Cruz *et al*., 2003; Martins-Ferreira *et al*., 2020); (ii) O período entre 2,39 e 2,34 Ga, possui decréscimo dos valores positivos de εHf(t)=+4,3 a +0,1 e valor negativo de εNd(t)=-3,10, e determina evento de retrabalhamento de crosta mais antiga e subordinada adição de crosta juvenil (Fuck *et al*., 2014; Martins-Ferreira *et al*., 2020). (iii) O evento de 2,3 Ga, possui zircão herdados com idades aparentes $^{207}Pb/^{206}Pb$ entre 2,34 a 2,52 Ga, e sugere contaminação/assimilação de crosta mais antiga (Saboia *et al*., 2020a).
- Um considerável volume de rochas TTG Siderianas foi caracterizado neste trabalho e que em conjunto com os dados isotópicos da literatura (tópico acima) mostram importantes eventos magmáticos gerados tanto a partir da fusão mantélica (juvenil) quanto a partir da fusão crustal (retrabalhado) neste período. A significante formação de crosta juvenil no Sideriano mostra um panaroma mais amplo no registro do início do Paleoproterozoico na história da Terra.
- Este estudo caracterizou um magmatismo ácido e intermediário entre 2,29-2,28 Ga relacionado com a unidade Monzogranítica e a Suíte Quatzo-Diorítica, respectivamente. O termo informal unidade Monzogranítica (PP2γacsm) foi utilizado de acordo com os mapeamentos geológicos da Folha Arraias (Abdallah & Meneghini, 2017) e Dianópolis (Saboia & Meneghini, 2019), já o termo formal Suíte Quartzo-Diorítica foi definida com base na nomenclatura informal de unidade/fácies que constam nestes trabalhos citados.
- Esta tese usou a definição da Suíte Serra do Boqueirão (PP2γacsb) de acordo com o GIS Brasil do SGB-CPRM (Vasconcelos *et al*., 2004) somente para os corpos tonalíticos Corrente e Cantu descritos por Correia Filho & Sá (1980). Esta concepção foi apresentada no mapeamento geológico da Folha Dianópolis e deve-se pelo fato de que os corpos Corrente e Cantu são representados principalmente por ±bt-hbl metatonalitos, enquanto que os outros corpos (Serra do Boqueirão, Serra Nova, Garrafas e Pau Ramalhudo) correspondem principalmente tonalitos-leucotonalitos-granodioritos-granitos

com biotita. Embora nesta pesquisa tenha sido apresentado um corpo como representante desta unidade, o termo suíte foi utilizado pelos motivos de que podem existir dois corpos (Corrente e Cantu) e para evitar a multiplicação de nomenclaturas.

- A presente tese utilizou as nomenclaturas de Suíte Granodiorítica a Tonalítica (GTS-2,2 Ga) e de Suíte Peraluminosa (PS-2,18 Ga) para agrupar/organizar a maior parte das rochas definidas como Suítes 1 e 2 (2,2 Ga) por Cruz *et al*. (2003). Esta nova proposta foi baseada na classificação litoestratigráfica adotada nos mapeamentos geológicos da Folha Arraias e Dianópolis.
- Em relação a Suíte Almas-Conceição do Tocantins (2,3-2,16 Ga) definida por Sousa *et al*. (2016), este trabalhou optou por não aplicar esta proposta de classificação litoestratigráfica. O principal motivo é que, no presente entendimento, a respectiva suíte engloba um conjunto de diferentes suítes e unidades litoestratigráficas, e por dedução esta classificação hierárquica não corresponde ao agrupamento destas rochas.
- Em relação à proposta de definição das unidades de metagranitoides com idades Riacianas de Martins-Ferreira *et al*. (2020), tem-se que: (1) a Suíte Serra do Boqueirão desta tese corresponde a fácies SBS3 da Suíte Serra do Boqueirão do respectivo trabalho. As idades obtidas entre 2.214 ± 13 e 2.202 ± 5 Ma são coerentes, dentro do erro associado. (2) Existem diferenças nas duas propostas em questão sobre as definições das demais unidades deste período, desta forma, estudos futuros de mapeamento geológico e de geocronologia são necessários para evolução do conhecimento destas rochas.
- Segundo Ducea & Barton (2007) episódios de encurtamento e espessamento crustal são responsáveis por períodos de fluxos magmáticos intensos (*flare-ups*) em arcos continentais, a exemplo dos arcos cordilheirianos da América do Norte. Neste contexto, o modelo geotectônico desta tese de uma fase compressional entre ~2,2 e 2,18 Ga (cerca de 20 Ma) para geração conjunta das Suítes Granodiorítica a Tonalítica e Peraluminosa corresponde episódio de alto fluxo magmático (*flare-up*). Esta concepção vai, em parte, de acordo com o trabalho de Martins-Ferreira *et al*., (2020) de que pelo menos um episódio de *flare-up* ocorreu entre 2.235 ± 26 a 2.201 ± 5 Ma.
- Esta tese apresenta compilação de referências e descrições em mapa de diversas unidades de rocha de idades Siderianas, que ocorrem no contexto do Maciço de Goiás e do Cráton São Francisco e suas regiões pericratônicas. Como consideração, adiciona-se o enxame de diques do Terreno Crixás-Goiás (Girardi *et al*., 2013; Jost *et al*., 2019) nesta correlação regional. Segundo estes autores, diques e *stocks* máficos apresentam idades K/Ar de 2,4 Ga e $^{40}Ar/^{39}Ar$ de 2.490 ± 40 Ma, e teriam sua gênese relacionada ao período Sideriano.

5.REFERÊNCIAS BIBLIOGRÁFICAS

Abdallah, S., Meneghini, P. F. V. B., 2017. Geologia e recursos minerais da folha Arraias, SD. 23-VA, estado do Tocantins. CPRM (in portuguese).

Albarède, F., Telouk, P., Blichert-Toft, J., Boyet, M., Agranier, A., Nelson, B. 2004. Precise and accurate isotopic measurements using multi-collector ICPMS. Geochimica et Cosmochimica Acta, 68:2725-2744. doi:10.1016/j.gca.2003.11.024.

Alkmim, F. F., & Teixeira, W. (2017). The Paleoproterozoic Mineiro Belt and the Quadrilátero Ferrífero. In São Francisco Craton, Eastern Brazil, pp. 71-94. Springer, Cham.

Almeida, F.F.M., Hasui, Y., Brito-Neves, B.B., Fuck, R.A., 1981. Brazilian structural provinces: an introduction. Earth-Science Reviews 17, 1–29.

Alvarenga, C.J.S., Dardenne, M.A., Botelho, N.F., Lima, O.N.B., Machado, M.A., Almeida, T., 2007. Nota Explicativa das folhas SD.23-V-C-III Monte Alegre de Goiás, SD.23-V-C-V Cavalcante, SD.23-V-C-VI Nova Roma. CPRM, Brasília, p. 65 (in portuguese).

Ávila, C. A., Teixeira, W., Cordani, U. G., Moura, C. A. V., & Pereira, R. M., 2010. Rhyacian (2.23–2.20 Ga) juvenile accretion in the southern São Francisco craton, Brazil: Geochemical and isotopic evidence from the Serrinha magmatic suite, Mineiro belt. Journal of South American Earth Sciences, 29, 464-482.

Ávila, C. A., Teixeira, W., Bongiolo, E. M., Dussin, I. A., Vieira, T. A. T., 2014. Rhyacian evolution of subvolcanic and metasedimentary rocks of the southern segment of the Mineiro belt, São Francisco Craton, Brazil. Precambrian Research, 243, 221-251.

Barbarin, B., 1999. A review of the relationships between granitoid types, their origins and their geodynamic environments. Lithos, 46, 605-626.

Barbosa, N.S., 2015. Evolução Paleoproterozoica do Cinturão Mineiro: Geocronologia U-Pb, isótopos de Nd-Hf-Sr e geoquímica de rochas plutônicas. PhD Thesis. Universidade de São Paulo, p. 229 (in portuguese).

Barbosa, N. S., Teixeira, W., Ávila, C. A., Montecinos, P. M., Bongiolo, E. M., 2015. 2.17–2.10 Ga plutonic episodes in the Mineiro belt, São Francisco Craton, Brazil: U-Pb ages, geochemical constraints and tectonics. Precambrian Research, 270, 204-225.

Barbosa, J. S. F., Barbosa, R. G., 2017. The paleoproterozoic eastern bahia orogenic domain. In São Francisco Craton, Eastern Brazil, p. 57-69. Springer, Cham.

Barbosa, J.S.F., Sabaté, P., 2004. Archean and paleoproterozoic crust of the São Francisco Cráton, Bahia, Brazil: geodynamic features. Precambrian Research 133, 1-27.

Barbosa, N., Teixeira, W., Ávila, C. A., Montecinos, P. M., Bongiolo, E. M., Vasconcelos, F. F., 2019. U-Pb geochronology and coupled Hf-Nd-Sr isotopic-chemical constraints of the Cassiterita Orthogneiss (2.47–2.41-Ga) in the Mineiro belt, São Francisco craton: Geodynamic fingerprints beyond the Archean-Paleoproterozoic transition. Precambrian Research, 326, 399-416.

Barbosa, J. S. F., Cruz, S. C. P., Souza, J. D., 2012. Terrenos metamórficos do embasamento. Geologia da Bahia: pesquisa e atualização, CBPM 1, 101-201 (in portuguese).

Barbosa, J. S. F., Marinho, M. M., de Menezes Leal, A. B., de Oliveira, E. M., de Souza-Oliveira, J. S., de Argollo, R. M., Santos, L. T. L., 2018. As raízes granulíticas do cinturão Salvador-Esplanada-Boquim, Cráton do São Francisco, Bahia-Sergipe, Brasil. Geologia USP. Série Científica 18(2), 103-128 (in portuguese).

Barker, F., Arth, J.G., 1976. Generation of Trondhjemite -Tonalite liquids and Archaean bimodal Trondhjemite-basalt suites. Geology 4, 596-600.

Batchelor, R.A., Bowden, P., 1985. Petrogenetic interpretation of granitoid rocks series using multicationic parameters. Chemical Geology 48, 43-55.

Beard, J.S., Lofgren, G.E., 1991. Dehydration melting and water-saturated melting of basaltic and andesitic greenstones and amphibolites at 1, 3, and 6.9 kbar. Journal of Petrology, 32, 365-401.

Berman, R. G., Pehrsson, S., Davis, W. J., Ryan, J. J., Qui, H., Ashton, K. E., 2013. The Arrowsmith orogeny: Geochronological and thermobarometric constraints on its extent and tectonic setting in the Rae craton, with implications for pre-Nuna supercontinent reconstruction. Precambrian Research 232, 44-69.

Bevington, P.R., Robinson, D.K. 2003. Data reduction and error analysis for the physical sciences. 3. Ed. McGraw-Hill Science/Engineering/Math. 336 p. ISBN-13: 978-0072472271.

Bizzi, L.A., Schobbenhaus, C., Vidotti, R.M., Gonçalves, J.H., (Orgs), 2003. Geologia, Tectônica e Recursos Minerais do Brasil: texto, mapas e SIG. CPRM (in portuguese).

Black, L.P., Kamo, S.L., Allen, C.M., Aleinikoff, J.N., Davis, D.W., Korsch, R.J., Foudoulis, C., 2003. TEMORA 1: a new zircon standard for Phanerozoic U-Pb geochronology. Chemical Geology 200 (1–2), 155–170.

Borges, M. S., Costa, J. B. S., Hasui, Y., 1998. Lito-estratigrafia da sequência metavulcano-sedimentar de Dianópolis-Almas, sudeste do Tocantins. Geociências17(1), 61-79 (in portuguese).

Borges, M. S., Costa, J. B. S., Hasui, Y., 1999. A Estruturação da Sequencia Metavulcano-sedimentar de Almas-Dianopolis, Sudeste de Tocantins. Anais da Academia Brasileira de Ciências 71(4 PART 1), 697-716 (in portuguese).

Boynton, W.V., 1984. Geochemistry of the rare earth elements: meteorite studies. In: Henderson P. (Eds.). Rare earth element geochemistry. Elsevier, 63-114.

Bühn, B., Pimentel, M. M., Matteini, M., Dantas, E. L., 2009. High spatial resolution analysis of Pb and U isotopes for geochronology by laser ablation multi-collector inductively coupled plasma mass spectrometry (LA-MC-ICP-MS). Anais da Academia Brasileira de Ciências 81(1), 99-114.

Brito Neves de, B. B., 2011. The Paleoproterozoic in the South-American continent: Diversity in the geologic time. Journal of South American Earth Sciences, 32(4), 270-286.

Brito Neves, B. B., Fuck, R. A., Campanha, G. A. C., 2021. Basement inliers of the brasiliano structural provinces of South America. Journal of South American Earth Sciences, 110, 103392.

Brown, G.C., Thorpe, R.S., Webb, P.C., 1984. The geochemical characteristics of granitoids in contrasting arcs and comments on magma sources. Journal of the Geological Society, 141(3), 413-426.

Bruno, H., Elizeu, V., Heilbron, M., Morisson Valeriano, C., Strachan, R., Fowler, M., Bersan, S., Moreira, H., Dussin, I., Silva, L.G.E., Tupinambá, M., Almeida, J., Neto C., Storey, C., 2020. Neoarchean and Rhyacian TTG-Sanukitoid suites in the southern São Francisco Paleocontinent, Brazil: evidence for diachronous change towards modern tectonics. Geoscience Frontiers, 11 (5), 1763-1787.

Cardoso, C. D., Ávila, C. A., Neumann, R., Oliveira, E. P., de Morisson Valeriano, C., Dussin, I. A., 2019. A Rhyacian continental arc during the evolution of the Mineiro belt, Brazil: Constraints from the Rio Grande and Brumado metadiorites. Lithos, 326, 246-264.

Castillo, P. R., Rigby, S. J., Solidum, R. U., 2007. Origin of high field strength element enrichment in volcanic arcs: geochemical evidence from the Sulu Arc, southern Philippines. Lithos 97(3-4), 271-288.

Castro, D. L., Fuck, R. A., Phillips, J. D., Vidotti, R. M., Bezerra, F. H., Dantas, E. L., 2013. Crustal structure beneath the Paleozoic Parnaíba Basin revealed by airborne gravity and magnetic data, Brazil. Tectonophysics, 614, 128-145.

Cawood, P. A., Kröner, A., Collins, W. J., Kusky, T. M., Mooney, W. D., Windley, B. F., 2009. Accretionary orogens through Earth history. Geological Society of London, Special Publications, 318, 1-36.

Cawood, P.A., Hawkesworth, C.J. and Dhuime, B., 2013. The continental record and the generation of continental crust. GSA Bulletin, 125; 14-32.

Chappell, B. W., Bryant, C. J., Wyborn, D., 2012. Peraluminous I-type granites. Lithos, 153, 142-153.

Chappell, B.W., White, A.J.R., 1992. I-and S-type granites in the Lachlan Fold Belt. Earth and Environmental Science Transactions of the Royal Society of Edinburgh, 83(1-2), 1-26.

Clemens, J. D., Stevens, G., 2012. What controls chemical variation in granitic magmas? Lithos, 134, 317-329.

Cohen, K.M., Finney, S.C., Gibbard, P.L., Fan, J.X., 2013. The ICS international chronostratigraphic chart. Episodes, 36(3), 199-204.

Collins, W. J., Richards, S. W., 2008. Geodynamic significance of S-type granites in circum-Pacific orogens. Geology, 36, 559-562.

Condie, K.C., 2007. Accretionary orogens in space and time. Memoirs-Geological Society of America, 200, 145.

Condie, K.C., 2008. Did the character of subduction change at the end of the Archean? Constraints from convergent-margin granitoids. Geology 36 (8), 611–614.

Condie, K. C., 2014. How to make a continent: thirty-five years of TTG research. In Evolution of archean crust and early life (pp. 179-193). Springer, Dordrecht, 179-193.

Condie, K. C., Aster, R. C., 2010. Episodic zircon age spectra of orogenic granitoids: the supercontinent connection and continental growth. Precambrian Research 180(3-4), 227-236.

Condie, K. C., Kröner, A., 2008. When did plate tectonics begin? Evidence from the geologic record. In: When did plate tectonics begin on planet Earth. Geological Society of America Special PapersVol. 440, 281-294.

Condie, K.C., Kröner, A., 2013. The building blocks of continental crust: evidence for a major change in the tectonic setting of continental growth at the end of the Archean. Gondwana Research 23(2), 394-402.

Condie, K.C., O'Neill, C., 2010. The Archean-Proterozoic boundary: 500 My of tectonic transition in Earth history. American Journal of Science 310(9), 775-790.

Condie, K.C., O'Neill, C.O., Aster, R.C., 2009. Evidence and implications for a widespread magmatic shut-down for 250 My on Earth. Earth and Planetary Science Letters 282, 294–298.

Condie, K.C., 2013. Preservation and recycling of crust during accretionary and collisional phases of Proterozoic orogens: A bumpy road from Nuna to Rodinia. Geosciences, 3 (2), 240-261.

Condie, K.C., Bickford, M.E., Aster, R.C., Belousova, E., Scholl, D.W., 2011. Episodic zircon ages, Hf isotopic composition, and the preservation rate of continental crust. Bulletin 123(5-6), 951-957.

Conrad, W.K., Nicholls, I.A., Wall, V.J., 1988. Water-saturated and undersaturated melting of metaluminous and peraluminous crustal composition at 10 kb: evidence for the origin of silicic magmas in the Taupo Volcanic Zone, New Zealand, and other occurrences. Journal of Petrology 29, 765-803.

Cordani, U.G., V. A. Ramos, L. M. Fraga, M. Cegarra, I. Delgado, K.G. de Souza, F. E. M. Gomes, C. Schobbenhaus, Tectonic Map of South America at 1:5.9 M, CGMW-CPRM-SEGEMAR, 2016.

Cordeiro, P. F. O., Oliveira, C. G., Della Giustina, M. E. S., Dantas, E. L., Santos, R. V., 2014. The Paleoproterozoic Campinorte Arc: Tectonic Evolution of a Central Brazil pre-Columbia Orogeny. Precambrian Research, 251, 49-61.

Cordeiro, P. F. O., Oliveira, C. G. (2017). The Goiás Massif: Implications for a pre-Columbia 2.2–2.0 Ga continent-wide amalgamation cycle in central Brazil. Precambrian Research, 298, 403-420.

Corrêa, R. S.; Oliveira, C. G.; Vidotti R. M. V., Souza V. S. 2015. Regional-scale pressure shadow-controlled mineralization in the Príncipe Orogenic Gold Deposit, Central Brazil. Ore Geology Reviews 71, 273–304.

Correia Filho, F.C.L. Sá, A.M., 1980. Projeto Natividade. Goiânia, DNPM/CPRM. Relatório técnico, p. 120 (in portuguese).

Costa, J. B.S., 1985. Aspectos Lito-Estruturais e Evolução Crustal da Região Centro-Norte de Goiás. Unpublished PhD. Thesys. Belém, UFPA. Centro de Geociências, p. 209 (in portuguese).

CPRM - SERVIÇO GEOLÓGICO DO BRASIL. Geologia e resultados prospectivos da área Barra da Gameleira, Tocantins. Escala 1:50.000. Goiânia: CPRM, 2000. Informe de Recursos Minerais. Série Metais do Grupo da Platina e Associados, 14 (in portuguese).

Cruz, E.L.C.C.; Kuyumjian R.M., 1998. The geology and tectonic evolution of the Tocantins granite-greenstone terrane, Almas-Dianópolis region, Tocantins State, Central Brasil. Revista Brasileira de Geociências 28(2), 173-182.

Cruz, E.L.C.C.; Kuyumjian R.M. 1999. Mineralizações auríferas filoneanas do terreno granito-greenstone do Tocantins. Rev. Bras. Geoc., 29(3), 291-298 (in portuguese).

Cruz, E. L. C. C; Kuyumjian, R. M; Boa Ventura, G. R. 2003. low-k calc-alkaline granitic series of southeastern tocantins state: chemical evidence for two sources for the granite gneissic complexes in the paleoproterozoic Almas-Dianópolis. Revista Brasileira de Geociências 33(2):125-136.

Cruz, S. C. P., Barbosa, J. S. F., Pinto, M. S., Peucat, J. J., Paquette, J. L., de Souza, J. S., Carneiro, M. A., 2016. The Siderian-Orosirian magmatism in the Gavião Paleoplate, Brazil: U–Pb geochronology, geochemistry and tectonic implications. Journal of South American Earth Sciences 69, 43-79.

Cruz Filho, B.E., Martins, A.A.M., 2013. Mapa Geológico Folha Rio de Contas (1:100.000). Serviço Geológico do Brasil (in portuguese).

Cuadros, F. A., Botelho, N. F., Fuck, R. A., Dantas, E. L., 2017a. The Ticunzal Formation in central Brazil: Record of Rhyacian sedimentation and metamorphism in the western border of the São Francisco Craton. Journal of South American Earth Sciences 79, 307-325.

Cuadros, F. A., Botelho, N. F., Fuck, R. A., Dantas, E. L., 2017b. The peraluminous Aurumina Granite Suite in central Brazil: An example of mantle-continental crust interaction in a Paleoproterozoic cordilleran hinterland setting? Precambrian Research 299, 75-100.

Cutts, K.C., Lana, C., Moreira, H., Alkmim, F., Peres, G.G., 2019. Zircon U-Pb and Lu-Hf record from high-grade complexes within the Mantiqueira Complex: First evidence of juvenile crustal input at 2.4–2.2 Ga and implications for the Palaeoproterozoic evolution of the São Francisco Craton. Precambrian Research, 338:105567.

Cutts, K., Lana, C., Alkmim, F., Peres, G.G., 2018. Metamorphic imprints on units of the southern Araçuaí belt, SE Brazil: The history of superimposed Transamazonian and Brasiliano orogenesis, 58, 211-234.

Dardenne M.A. 2000. The Brasília fold belt. In: Cordani, U.G., Milani, E.J., Thomaz Filho, A., Campos, D.A (eds.), Tectonic Evolution of South America, Brazil 2000, 31th International. Geological Congress, Rio de Janeiro, 231-263.

Dardenne, M.A., Saboia, A.M. Litoestratigrafia do Grupo Natividade na região de Natividade-Pindorama, Tocantins. In: Horbe, A.M.C., Souza, V.S. (Org.). Contribuições à Geologia da Amazônia. Belém: Sociedade Brasileira de Geologia,, v. 5, 29–38, 2007(in portuguese).

Dardenne, M.A., Giustina, M.E.S.D., Saboia, A.M., Bogossian, J., 2009. Datação Geocronológica U–Pb da Sequência Vulcânica de Almas, Tocantins. In: SBG, Simp.Geol. Centro-Oeste, 11, Anais, 1 CD-Rom (in portuguese).

Debon F., Le Fort P., 1983. A chemical-mineralogical classification of common plutonic rocks and associations. Earth and Environmental Science Transactions of the Royal Society of Edinburgh, 73, 135-149.

Delgado, I.M., Souza, J.D., Silva, L.C., Silveira Filho, N.C., Santos, R.A., Pedreira, A.J., Guimarães, J.T., Angelim, L.A., Vasconscelos, A.M., Gomes, I.P., Lacerda Filho, J.V., Valente C.R., Perrotta, M.M., Heinick, C.A., 2003. Província Tocantins. In: Bizzi, L.A., Schobbenhaus, C., Vidotti, R.M., Gonçalves, J.H., (Ed.). Geologia, Tectônica e Recursos Minerais do Brasil. Rio de Janeiro: CPRM. p. 281-292.

Diwu, C., Sun, Y., Zhao, Y., Lai, S., 2014. Early Paleoproterozoic (2.45–2.20 Ga) magmatic activity during the period of global magmatic shutdown: Implications for the crustal evolution of the southern North China Craton. Precambrian Research, 255, 627-640.

Drummond, M.S., Defant, M.J., 1990. A model for trondhjemite-tonalite-dacite genesis and crustal growth via slab melting: Archaean to modern comparisons. Journal of Geophysical Research. 95, 21503-21521.

Ducea, M.N., Barton, M.D., 2007. Igniting flare-up events in Cordilleran arcs. Geology, 35(11), 1047-1050.

Ducea, M.N., Paterson, S.R., DeCelles, P.G., 2015. High-volume magmatic events in subduction systems. Elements 11 (2), 99–104.

Ducea, M. N., Saleeby, J. B., Bergantz, G., 2015. The architecture, chemistry, and evolution of continental magmatic arcs. Annual Review of Earth and Planetary Sciences, 43, 299-331.

El Baghdadi, M., El Boukhari, A., Jouider, A., Benyoucef, A., Nadem, S., 2003. Calc-alkaline arc I-type granitoid associated with S-type granite in the Pan-African Belt of Eastern Anti-Atlas (Saghro and Ougnat, South Morocco). Gondwana Research, 6, 557-572.

Eriksson, P.G., Condie, K.C., 2014. Cratonic sedimentation regimes in the ca. 2450–2000 Ma period: relationship to a possible widespread magmatic slowdown on Earth?. Gondwana Research, 25(1), 30-47.

Foley, S.F., Tiepolo, M., Vannucci, R., 2002. Growth of early continental crust controlled by melting of amphibolite in subduction zones. Nature 417, 637–640.

Frasca, A.A.S., Lima, H. A., Moraes, L. L. D., Ribeiro, P. S. E., 2010. Geologia e recursos minerais da folha Gurupi SC. 22-ZD (in portuguese).

Frasca, A.A.S., Ribeiro, P.S.E., Lacerda Filho, J.V.D., Meneghini, P.F.V.B., Moraes, L. L.D., Lima, H.A.F., 2018. Geologia e recursos minerais da folha Alvorada SD. 22-XB: estado do Tocantins. CPRM (in portuguese).

Frost, B.R., Barnes, C.G., Collins, W.J., Arculus, R.J., Ellis, D.J., Frost, C.D., 2001. A geochemical classification for granitic rocks. Journal of Petrology 42, 2033-2048.

Fuck, R.A., Pimentel, M.M., Alvarenga, C.J., Dantas, E.L., 2017. The northern Brasília belt. In São Francisco Craton, Eastern Brazil , 205-220. Springer Cham.

Fuck, R.A., Dantas, E.L., Pimentel, M.M., Botelho, N.F., Armstrong, R., Laux, J.H., Junges, S.L., Soares, J.E., Praxedes, I.F., 2014. Paleoproterozoic crust-formation and reworking events in the Tocantins Province, central Brazil: A contribution for Atlantica supercontinent reconstruction. Precambrian Research 244, 53-74.

Ghani, A. A., Searle, M., Robb, L., Chung, S. L., 2013. Transitional I-S type characteristic in the Main Range Granite, Peninsular Malaysia. Journal of Asian Earth Sciences, 76, 225-240.

Girardi, V.A.V., Teixeira, W., Mazzucchelli, M., da Costa, P.C., 2013. Sr–Nd constraints and trace-elements geochemistry of selected Paleo and Mesoproterozoic mafic dikes and related intrusions from the South American Platform: Insights into their mantle sources and geodynamic implications. Journal of South American Earth Sciences, 41, 65-82.

Grosse, P., Bellos, L. I., Camilo, R., Larrovere, M. A., Rossi, J. N., Toselli, A. J., 2011. Across-arc variation of the Famatinian magmatic arc (NW Argentina) exemplified by I-, S-and transitional I/S-type Early Ordovician granitoids of the Sierra de Velasco. Journal of South American Earth Sciences, 32, 110-126.

Gutscher, M. A., Maury, R., Eissen, J. P., Bourdon, E., 2000. Can slab melting be caused by flat subduction? Geology 28(6), 535-538.

Halla, J., van Hunen, J., Heilimo, E., Hölttä, P., 2009. Geochemical and numerical constraints on Neoarchean plate tectonics. Precambrian Research 174(1-2), 155-162.

Halla, J., Whitehouse, M. J., Ahmad, T., Bagai, Z., 2017. Archaean granitoids: an overview and significance from a tectonic perspective. Geological Society, London, Special Publications 449(1), 1-18.

Harris, N.B.W.; Pearce, J.A.; Tindle, A.G., 1986. Geochemical characteristics of collision-zone magmatism. In: M.P. Coward and A.C. Ries (eds.) Collision Tectonics. Geological Society of London, Special Paper 19,115-158.

Hasui, Y., Costa, J., Saad, A.R., Campanha, V.A., 1990. O Grupo Natividade e sua correlação com o Grupo Bambuí. Geociências, 299-316 (in portuguese).

Hasui, Y.; Carneiro, C. D. R. (Org.) ; Almeida, F. F. M. (Org.) ; Bartorelli, A. (Org.), 2012. Geologia do Brasil. 1. ed. São Paulo: Editora Beca, v. 1. p.900 (in portuguese).

Heilbron, M., Cordani, U. G., Alkmim, F. F., (Eds.), 2017. São Francisco Craton, Eastern Brazil: Tectonic Genealogy of a Miniature Continent, (pp. 321-331). Springer, Cham.

Heilbron, M., Cordani, U. G., & Alkmim, F. F. (2017b). The São Francisco craton and its margins. In São Francisco Craton, Eastern Brazil (pp. 3-13). Springer, Cham.

Horstwood, M.S.A., Kosler, J. Gehersl, G., Jackson, S.E. McLean, N.M., Paton, C., Pearson, N.J., Sircombe, K., Sylvester, P., Vermeesh, P., Bowring, J.F., Condon, D.J., Schoene, B., 2016. Community-derived standards for LA-ICP-MS U-(Th-)Pb geochronology – uncertainty propagation, age interpretation and data reporting. Geostand. Geoanal. Res. 40 (3), 311–332.

Kröner, A., Wan, Y., Liu, X., Liu, D., 2014. Dating of zircon from high-grade rocks: Which is the most reliablemethod? Geoscience Frontiers, 5 (2014) 515-523.

Kuyumjian, R. M., Araújo Filho, J. D. (2005). Depósitos e ocorrências de ouro no terreno arqueanopaleoproterozóico de Almas-Dianópolis (TO): evidências da importância metalogenética do evento Brasiliano. Revista Brasileira de Geociências 35(4), 611-614 (in portuguese).

Kuyumjian, R. M., Cruz, E. L. C. C., de Araújo Filho, J. O., Moura, M. A., Guimarães, E. M., & da Silva Pereira, K. M. (2012). Geologia e ocorrências de ouro do Terreno Granito-Greenstone do Tocantins, TO: síntese do conhecimento e parâmetros para exploração mineral. Revista Brasileira de Geociências 42(1), 213-228 (in portuguese).

Jackson, S.E., Pearson, N.J., Griffin, W.L., Belousova, E.A. 2004 The application of laser ablation-inductively coupled plasma-mass spectrometry to in situ U–Pb zircon geochronology. Chemical Geology, 211:47–69.

Janousek, V., Farrow, C. M. & Erban, V. 2006. Interpretation of whole-rock geochemical data in igneous geochemistry: introducing Geochemical Data Toolkit (GCDkit). Journal of Petrology 47, 1255-1259.

Jost, H., Apollo, J.F.H., Weber, W., dos Reis Salles, R., Marques, J.C., Massucatto, A.J., Costa, D.A., dos Santos, B.A., 2019. Stratigraphic update, paleotectonic, paleogeographic, and depositional environments of the Crixás Greenstone Belt, Central Brazil. Journal of South American Earth Sciences, 96, 102329.

Košler, J., Fonneland, H., Sylvester, P., Tubrett, M., Pedersen, R.B. 2002. U–Pb dating of detrital zircons for sediment provenance studies—a comparison of laser ablation ICPMS and SIMS techniques. Chemical Geology, 182:605–618.

Laurent, O., Martin, H., Moyen, J.F., Doucelance, R., 2014. The diversity and evolution of late-Archean granitoids: Evidence for the onset of "modern-style" plate tectonics between 3.0 and 2.5 Ga. Lithos 205, 208-235.

Lima, E.A.M. 2014. Petrografia, química mineral e geocronologia U-Pb LA-ICPMS de minerais acessórios da localidade de Príncipe, Bloco Natividade-Cavalcante, Tocantins. Unpublished Msc. dissertation. Instituto de Geociências, Universidade de Brasília. p.86 (in portuguese).

Ludwig, K., 2002. SQUID, Version 1.02, A User´s Manual: Berkley Geochronological Center Special Publication 2, 17p.

Ludwig, K., 2012. User's manual for Isoplot version 3.75-4.15: a geochronological toolkit for Microsoft Excel: Berkley Geochronological Center Special Publication, (5).

Martin, H., 1986. Effect of steeper Archean geothermal gradient on geochemistry of subduction-zone magmas. Geology 14(9), 753-756.

Martin, H., Chauvel, C., Jahn, B.M., 1983. Major and trace elemento geochemistry and crustal evolution of granodioritic Archaean rocks from eastern Finland. Precambrian Research 21 159-180.

Martin, H., Smithies, R. H., Rapp, R., Moyen, J. F., Champion, D., 2005. An overview of adakite, tonalite–trondhjemite–granodiorite (TTG), and sanukitoid: relationships and some implications for crustal evolution. Lithos 79(1), 1-24.

Martin, H., Moyen, J. F., Guitreau, M., Blichert-Toft, J., Le Pennec, J. L., 2014. Why Archaean TTG cannot be generated by MORB melting in subduction zones. Lithos 198, 1-13.

Martins-Ferreira, M. A. C., da Silva, H. C. D. M., & Rodrigues, E. N. Idade Mínima de Deposição do Greenstone Belt de Almas Indicada por Xenólitos Máficos e Sedimentares no Batólito Ribeirão das Areias. 2017. XV Simpósio de Geologia do Centro-Oeste. Goiânia. Resumos Expandidos (in portuguese).

Martins-Ferreira, M.C., Dias, A.N.C., Chemale Jr, F., Campos, J.E.G., Seraine, M., Rodrigues, E.N., 2020. Multi-stage crustal accretion by magmatic flare-up and quiescence intervals in the western margin of the São Francisco Craton: U-Pb-Hf and geochemical constraints from the Almas Terrane. Gondwana Research 85, 32–54.

Masuda, A., Nakamura, N., Tanaka, T., 1973. Fine structures of mutually normalized rare-earth patterns of chondrites. Geochimica Et Cosmochimica Acta 37, 239–244.

Miller, C. F., Bradfish, L. J., 1980. An inner Cordilleran belt of muscovite-bearing plutons. Geology, 8, 412-416.

Moreira, H., Seixas, L., Storey, C., Fowler, M., Lasalle, S., Stevenson, R., Lana, C. 2018. Evolution of siderian juvenile crust to rhyacian high Ba-Sr magmatism in the Mineiro Belt, southern São Francisco Craton. Geoscience Frontiers 9(4), 977-995.

Moyen, J. F., Martin, H., 2012. Forty years of TTG research. Lithos 148, 312-336.

Moyen, J.F., Martin, H., Jayananda, M., Auvray B., 2003. Late Archaean granites: a typology based on the Dharwar Craton (India). Precambrian Research 127, 103-123.

Moyen, J. F., Laurent, O., Chelle-Michou, C., Couzinié, S., Vanderhaeghe, O., Zeh, A., Gardien, V. (2016). Collision vs. subduction-related magmatism: two contrasting ways of granite formation and implications for crustal growth. Lithos, 277, 154-177.

Moyen, J. F., Laurent, O., 2018. Archaean tectonic systems: a view from igneous rocks. Lithos 302, 99-125.

Moyen, J. F. (2019). Archean granitoids: classification, petrology, geochemistry and origin. Geological Society, London, Special Publications, 489, SP489-2018.

O'Connor, J.T., 1965. A classification for quartz-rich igneous rocks based on feldspar ratios. US Geological Survey Professional Paper 525,79-84.

Oliveira, F.V. 2010. Chronus: Um novo suplemento para a redução de dados U-Pb obtidas por LA-MC-ICPMS. Dissertação de Mestrado. Instituto de Geociências - Universidade de Brasília, 85p.

Oliveira, Felipe Valença de., 2015. Chronus: um novo suplemento para a redução de dados U-Pb obtidos por LA-MC-ICPMS. 91p. MSc Thesis - Universidade de Brasília, Insituto de Geociências. Brasília, Brazil.

Partin, C.A., Bekker, A., Sylvester, P.J., Wodicka, N., Stern, R.A., Chacko, T., Heaman, L.M., 2014. Filling in the juvenile magmatic gap: Evidence for uninterrupted Paleoproterozoic plate tectonics. Earth and Planetary Science Letters 388, 123-133.

Patiño-Douce, A.E., 1995. Experimental generation of hybrid silicic melts by reaction of high-Al basalt with metamorphic rocks. J. Geophys. Res. 100 (B8), 15623–15639.

Patiño Douce, A.E., 1999. What do experiments tell us about the relative contributions of crust and mantle to the origin of granitic magmas? Geological Society, London, Special Publications 168, 55-75.

Pearce, J. A., Harris, N. B., Tindle, A. G., 1984. Trace element discrimination diagrams for the tectonic interpretation of granitic rocks. Journal of petrology, 25, 956-983.

Pearce, J. A., Peate, D. W., 1995. Tectonic implications of the composition of volcanic arc magmas. Annual Review of Earth and Planetary Sciences, 23, 251-285.

Pearce, J.,1996. Sources and settings of granitic rocks. Episodes, 19, 120-125.

Pehrsson, S. J., Buchan, K. L., Eglington, B. M., Berman, R. M., & Rainbird, R. H. (2014). Did plate tectonics shutdown in the Palaeoproterozoic? A view from the Siderian geologic record. Gondwana Research, 26(3-4), 803-815.

Peccerillo, A., Taylor, S.R., 1976. Geochemistry of Eocene calc-alkaline volcanic rocks from the Kastamonu area, Northern Turkey. Contributions to Mineralogy and Petrology 58, 63-81.

Pereira, R.S., Fuck, R.A., 2005. Archean Nucleii and the distribution of kimberlite and related rocks in the São Francisco Craton, Brazil. Revista Brasileira de Geociências 35, 93-104.

Queiroz, J.P.R., 2001. Geologia e mineralização aurífera da área de Chapada, Tocantins. Unpublished Msc. Dissertation Universidade Federal do Pará, Belém, 114pp (in portuguese).

Ribeiro, P.S.E., Alves, C.L., 2017. Geologia e recursos minerais da região de Palmas-folhas Miracema do Norte SC. 22-XD, Porto Nacional SC. 22-ZB e Santa Teresinha SC. 22-ZA. Estado do Tocantins. CPRM (in portuguese).

Rios, D. C., Davis, D. W., Conceicão, H., Davis, W. J., Rosa, M. D. L. D. S., Dickin, A. P., 2009. Geologic evolution of the Serrinha nucleus granite–greenstone terrane (NE Bahia, Brazil) constrained by U–Pb single zircon geochronology. Precambrian Research 170(3-4), 175-201.

Rogers, J. J., Santosh, M., 2009. Tectonics and surface effects of the supercontinent Columbia. Gondwana Research, 15 (3-4), 373-380.

Saboia, A.M., de Oliveira, C.G., Dantas, E.L., Cordeiro, P., Scandolara, J.E., Rodrigues, J.B., Sousa, I.M. C., 2020a. The Siderian crust (2.47–2.3 Ga) of the Goiás Massif and its role as a building block of the São Francisco paleocontinent. Precambrian Research, 350, 105901.

Saboia, A.M., de Oliveira, C.G., Dantas, E.L., Scandolara, J.E., Cordeiro, P., Rodrigues, J.B., Sousa, I.M.C., 2020b. The 2.26 to 2.18 Ga Arc-Related Magmatism of the Almas-Conceição do Tocantins Domain: An Early Stage of the São Francisco Paleocontinent Assembly in Central Brazil. Journal of South American Earth Sciences, 104, 102757.

Saboia, A.M., 2009. O vulcanismo em Monte do Carmo e Litoestratigrafia do Grupo Natividade, estado de Tocantins. Unpublished Msc. Dissertation. Instituto de Geociências, Universidade de Brasília, Brasília, p.96. (in portuguese)

Saboia, A.M., Meneghini, P.F.V.B., Gonçalves,G. D. F., Lacerda Filho, J.V.D., 2014. Carta geológica: folha Dianópolis-SC. 23-YC. (in portuguese)

Saboia, A.M., Meneghini, P.F.V.B., 2019. Geologia e Recursos Minerais da Folha Dianópolis - SC.23-Y-C: Escala 1:250.000, Projeto Sudeste do Tocantins, estado do Tocantins – Goiânia: CPRM, 193 p. (in portuguese)

Sawyer, E.W., 2008. Atlas of migmatites. Canadian Mineral. P.371.

Sakyi, P. A., Addae, R. A., Su, B. X., Dampare, S. B., Abitty, E., Su, B. C., Liu, B., Asiedu, D. K. (2020). Petrology and geochemistry of TTG and K-rich Paleoproterozoic Birimian granitoids of the West African Craton (Ghana): Petrogenesis and tectonic implications. Precambrian Research, 336, 105492.

Seixas, L. A. R., David, J., Stevenson, R., 2012. Geochemistry, Nd isotopes and U–Pb geochronology of a 2350 Ma TTG suite, Minas Gerais, Brazil: implications for the crustal evolution of the southern São Francisco craton. Precambrian Research, 196, 61-80.

Shand, S.J., 1947. The Eruptive Rocks. 3rd. New York: John Wiley, 444 pp.

Silva E. R. P. 1987. Estudos das ocorrências Aurífera da área de Natividade-GO. Unpublished Msc. Dissertation. Universidade Federal do Pará, Belém. 125p (in portuguese).

Souza, J. D., Kosin, M., Melo, R. C., Santos, R. A., Teixeira, L. R., Sampaio, A. R., Arcanjo, J. B., 2003. Mapa geológico do estado da Bahia–Escala 1: 1.000. 000. Salvador: CPRM (in portuguese).

Souza J.D., Kosin M., Teixeira L.R., Martins A.A.M., Bento R.V., Borges V.P., Leite C.A., Arcanjo J.B., Loureiro H.S.C., Santos R.A., Neves J.P., Carvalho L.M., Pereira L.H.M., Netto C., Paes V.J.C., 2004b. Folha Salvador SD-24. In: C. Schobbenhaus, J.H. Gonçalves, J.O.S. Santos, M.B. Abram, R. Leão Neto, G.M.M. Matos. R.M. Vidotti, M.A.B. Ramos, J.D.A. Jesus. (Coords.). Carta Geológica do Brasil ao Milionésimo, Sistema de Informações Geográficas, Programa Geologia do Brasil, CPRM (in portuguese).

Sousa, I.M.C., Giustina, M.E.S.D., Oliveira, C.G., 2016. Crustal evolution of the northern Brasília Belt basement, central Brazil: A Rhyacian orogeny coeval with a pre-Rodinia supercontinent assembly. Precambrian Research, 273,129-150.

Streckeisen, A.L., 1976. To each plutonic rock its proper name. Earth Sci. Rev. 12,1–33.

Sun, S.S., McDonough, W.F., 1989. Chemical and isotopic systematics of oceanic basalts: implications for mantle composition and processes. In: Saunders, A.D., Norry, M.J. (Eds.). Magmatism in the Ocean Basins. Geological Society London Special Publication 42, 313-345.

Sylvester, P.J., 1998. Post-collisional strongly peraluminous granites. Lithos 45, 29–44.

Teixeira, W., Ávila, C. A., Dussin, I. A., Neto, A. C., Bongiolo, E. M., Santos, J. O., Barbosa, N. S., 2015. A juvenile accretion episode (2.35–2.32 Ga) in the Mineiro belt and its role to the Minas accretionary orogeny: Zircon U–Pb–Hf and geochemical evidences. Precambrian Research 256, 148-169.

Teixeira, W., Oliveira, E.P., Marques, L., 2017a. São Francisco Craton, Eastern Brazil. Tectonic Genealogy of a Miniature Continent. Chapter 3 'Nature and Evolution of the Archean crust of the São Francisco Craton'. 1st. ed. Berlin: Springer Verlag, 2016. pp. 29-56.

Teixeira, W., Oliveira, E. P., Peng, P., Dantas, E. L., & Hollanda, M. H., 2017b. U-Pb geochronology of the 2.0 Ga Itapecerica graphite-rich supracrustal succession in the São Francisco Craton: Tectonic matches with the North China Craton and paleogeographic inferences. Precambrian Research, 293, 91-111.

Terentiev, R.A., Santosh, M., 2020. Baltica (East European Craton) and Atlantica (Amazonian and West African Cratons) in the Proterozoic: The pre-Columbia connection. Earth-Science Reviews, 103378.

Van Hunen, J., van Keken, P. E., Hynes, A., Davies, G. F., Condie, K. C., Pease, V., 2008. Tectonics of early Earth: Some geodynamic considerations. When did plate tectonics begin on planet Earth, 157-171.

Vasconcelos, A.M., Kosin, M., Souza, J.D. de, Valente, C.R., Neves, J.P., Heineck, C.A.,Lacerda Filho, J.V., Teixeira, L.R., Borges, V.P., Bento, R.V., Guimarães, J.T., Neves, J.P., Oliveira, I.W.B., Gomes, I.P., Malouf, R.F., Carvalho, L.M. de, Abreu Filho, W., 2004. Folha SC.23 - Rio São Francisco. In: Schobbenhaus, C., Gonçalves, J.H., Santos, J.O.S., Abram, M.B.,

Leão Neto, R., Matos, G.M.M., Vidotti, R.M., Ramos, M.A.B., Jesus, J.D.A.de. (eds.), Carta Geológica do Brasil ao Milionésimo, Sistema de Informações Geográficas. Programa Geologia do Brasil, CPRM, Brasília. CD-ROM.

Vielzeuf, D., Holloway, J.R., 1988. Experimental determination of the fluid-absent melting relations in the pelitic system. Consequences for crustal differentiation. Contributions to Mineralogy and Petrology 98, 257-276.

Villaseca, C., Barbero, L., & Herreros, V., 1998. A re-examination of the typology of peraluminous granite types in intracontinental orogenic belts. Earth and Environmental Science Transactions of The Royal Society of Edinburgh, 89, 113-119.

Whalen, J.B., Currie, K.L., Chappell, B.W., 1987. A-type granite: geochemical characteristics. discrimination and petrogenesis. Contributions to Mineralogy and Petrology 95, 407- 419.

White, A. J. R., Chappell, B. W., 1983. Granitoid types and their distribution in the Lachlan Fold Belt, southeastern Australia. Geological Society of America Memoir, 159(12), 21-34.

Wiendenbeck, M., Allé, P., Corfu, F., Griffin, W.L., Meier, M., Orbeli, F., von Quadt, A., Roddick, J.C., and Spiegel, W., 1995. Three natural zircon standards for U-Th-Pb, Lu-Hf, trace element and REE analyses. Geostandards Newsletter 19, 1-23.

Williams, I.S., 1998. U-Th-Pb geochronology by ion microprobe. In: McKibben, M.A., Shanks III, W.C. (Eds.), Applications of Microanalytical Techniques to Understanding Mineralizing Processes. Reviews in Economic Geology, vol. 7. Society of Economic Geologists, 1–46.

Williams, I.S., Meyer, C., 1998. U–Pb geochronology of zircons from lunar breccia 73217 using a sensitive high mass-resolution ion microprobe. Journal Geophysical Research 89, B525–B534.

Wosniak, R., A. A. M. M, Oliveira, R.L.M., 2013. Mapa Geológico Folha Brumado (1: 100.000). Serviço Geológico do Brasil (in portuguese).

Wood, D. A. 1979. A variably veined suboceanic upper mantle - genetic significance for mid-ocean ridge hasalts from geochemical evidence. Geology 7, 499 503.

Yang, Q. Y., & Santosh, M. (2015). Paleoproterozoic arc magmatism in the North China Craton: no Siderian global plate tectonic shutdown. Gondwana Research, 28(1), 82-105.

Zhao, G., Sun, M., Wilde, S. A., Li, S., 2004. A Paleo-Mesoproterozoic supercontinent: assembly, growth and breakup. Earth-Science Reviews, 67, 91-123.

Anexos (materiais suplementares)

TABELA A: Dados U-Pb da amostra AS-1 (SHRIMP II)

				Ratios*					Ages (Ma)*					
Spot	**Th**	**207Pb**	**err (%)**	**207Pb**	**err (%)**	**206Pb**	**err (%)**	**Rho**	**207Pb**		**206Pb**			**Remarks**
Name	**U**	**206Pb**	**1sigma**	**235U**	**1sigma**	**238U**	**1sigma**		**206Pb**	**2s**	**238U**	**2s**	**Conc.(%)**	
1.1	0.408	0.160824	0.95	10,491	1.68	0.473156	1.38	0.82	2464	32	2497	58	101.34	1
2.1	0.828	0.164108	0.88	10,989	3.15	0.485693	3.03	0.96	2498	30	2552	128	102.14	2
3.1	0.586	0.158656	1.31	9,867	1.92	0.45105	1.37	0.71	2441	46	2400	54	98.29	2
4.1	0.579	0.160036	1.78	9,889	3.55	0.448175	3.06	0.86	2456	62	2387	122	97.19	2
5.1	0.581	0.162006	1.35	10,560	2.05	0.472763	1.53	0.74	2477	46	2496	64	100.76	1
6.1	0.646	0.163474	0.88	10,797	1.64	0.479032	1.38	0.84	2492	30	2523	58	101.24	1
7.1	0.375	0.164302	1.04	10,687	2.19	0.471778	1.92	0.87	2500	36	2491	80	99.63	1
8.1	0.776	0.162716	0.91	10,437	1.62	0.465229	1.33	0.82	2484	32	2463	54	99.13	1
9.1	0.586	0.161776	1.41	10,209	1.97	0.457671	1.33	0.67	2474	50	2429	54	98.17	1
10.1	0.449	0.157819	0.77	10,117	1.7	0.464987	1.5	0.88	2432	28	2462	62	101.19	1
11.1	0.396	0.165003	1.21	11,178	1.88	0.491307	1.43	0.76	2508	42	2576	60	102.73	2
12.1	0.398	0.167547	1.25	11,259	1.96	0.487415	1.51	0.77	2533	42	2559	64	101.03	2
13.1	0.486	0.156771	0.58	9,284	1.46	0.429519	1.33	0.91	2421	20	2304	52	95.14	2
14.1	0.592	0.15827	1.02	9,130	1.67	0.418364	1.32	0.78	2437	34	2253	50	92.43	2

Errors are 1-sigma; Pbc and Pb* indicate the common and radiogenic portions, respectively.

Error in Standard calibration was 0.15% (not included in above errors but required when comparing data from different mounts).

Common Pb corrected using measured 204Pb.

Discordance calculated as (1-(^{206}Pb/^{238}U age/^{207}Pb/^{206}Pb age))*100

1 -Analyses used for age calculations

2 - Data discarded due to high analytical error or discordance

TABELA B: Dados U-Pb da amostra AS-362 (LA-ICPMS)

					Ratios*					Ages (Ma)*							
Spot	f206(%)	Th	207Pb	err (%)	207Pb	err (%)	206Pb	err (%)	Rho	207Pb		207Pb		206Pb			Remarks
Name		U	206Pb	1sigma	235U	1sigma	238U	1sigma		206Pb	2s	235U	2s	238U	2s	Conc.(%)	
003-ZR1C	0.003	0.21	0.160735	0.48	9,594	0.93	0.432873	0.7	0.75	2463	16	2397	17	2319	28	94.12	1
004-ZR1R	0.043	0.409	0.150068	0.54	6,746	1.07	0.326024	0.85	0.79	2347	18	2079	19	1819	27	77.51	1
005-ZR2	0.129	0.346	0.143716	0.43	5,038	0.98	0.254265	0.8	0.81	2272	15	1826	17	1460	21	64.26	1
006-ZR3N	0.002	0.405	0.161615	0.35	10,078	0.79	0.45227	0.6	0.75	2473	12	2442	15	2405	24	97.27	1
007-ZR3B	0.072	0.186	0.157517	0.34	8,728	0.97	0.40188	0.83	0.85	2429	12	2310	18	2178	31	89.64	1
008-ZR4	0.001	0.3143	0.159548	0.46	9,559	1.41	0.43452	1.28	0.9	2451	16	2393	26	2326	50	94.9	1
009-ZR5	0.006	0.304	0.161931	0.49	10,336	1.01	0.46294	0.8	0.79	2476	17	2465	19	2453	33	99.05	1
010-ZR6	0.024	0.254	0.159641	0.49	9,570	0.87	0.434785	0.61	0.7	2452	17	2394	16	2327	24	94.91	1
011-ZR7	0.002	0.262	0.161177	0.69	10,341	1.02	0.465334	0.64	0.63	2468	23	2466	19	2463	26	99.79	1
012-ZR8	0.008	0.332	0.160427	0.67	10,597	1.21	0.47905	0.93	0.77	2460	23	2488	22	2523	39	102.55	2
013-ZR9	0.002	0.325	0.161964	0.66	10,084	1	0.451539	0.65	0.65	2476	22	2443	18	2402	26	97	1
016-ZR10	0.004	0.394	0.162359	0.56	10,399	0.92	0.464514	0.63	0.68	2480	19	2471	17	2459	26	99.15	1
017-ZR11N	0.011	0.207	0.163885	0.54	10,273	0.93	0.454595	0.67	0.71	2496	18	2460	17	2416	27	96.77	2
018-ZR11B	0.005	0.225	0.162422	0.48	10,644	0.85	0.475279	0.59	0.69	2481	16	2493	16	2507	25	101.03	1
019-ZR12	0.007	0.317	0.162161	0.44	10,620	0.81	0.474953	0.57	0.7	2478	15	2490	15	2505	24	101.08	1
020-ZR13	0.006	0.34	0.161654	0.46	10,346	0.87	0.464165	0.63	0.73	2473	16	2466	16	2458	26	99.38	1
021-ZR14	0.006	0.384	0.164206	0.51	11,465	0.87	0.506386	0.59	0.68	2499	17	2562	16	2641	26	105.67	1
022-ZR15	0.011	0.254	0.159617	0.5	9,076	1.07	0.412388	0.86	0.81	2452	17	2346	20	2226	33	90.79	1
023-ZR16N	0.005	0.463	0.162193	0.57	10,373	1.03	0.463835	0.78	0.75	2479	19	2469	19	2456	32	99.1	1
024-ZR16B	0.014	0.04	0.163553	0.66	9,170	1.07	0.40663	0.76	0.71	2493	22	2355	20	2199	29	88.23	2
025-ZR17N	0.01	0.404	0.164441	0.66	10,256	1.06	0.452308	0.74	0.7	2502	22	2458	20	2406	30	96.14	2
028-ZR17B	0.003	0.182	0.163247	0.53	10,456	0.84	0.46454	0.54	0.64	2490	18	2476	16	2460	22	98.79	1
029-ZR18	0.075	0.254	0.160262	0.56	9,345	1.31	0.42289	1.12	0.85	2458	19	2372	24	2274	43	92.48	1
031-ZR20	0.004	0.424	0.162222	0.55	10,293	0.95	0.460165	0.68	0.71	2479	19	2462	18	2440	28	98.43	1
032-ZR21	0.002	0.384	0.162857	0.47	10,533	0.79	0.469084	0.52	0.65	2486	16	2483	15	2480	21	99.75	1
033-ZR22N	0.001	0.444	0.162654	0.47	10,516	0.77	0.468897	0.48	0.62	2483	16	2481	14	2479	20	99.8	1
034-ZR22B	0.122	0.341	0.161185	0.48	10,219	1.48	0.459817	1.35	0.91	2468	16	2455	27	2439	55	98.8	1

TABELA B: Continuação

					Ratios*					Ages (Ma)*							
Spot	f206(%)	Th	207Pb	err (%)	207Pb	err (%)	206Pb	err (%)	Rho	207Pb		207Pb		206Pb			Remarks
Name		U	206Pb	1sigma	235U	1sigma	238U	1sigma		206Pb	2s	235U	2s	238U	2s	Conc.(%)	
035-ZR23N	0.019	0.398	0.159938	0.52	9,250	0.94	0.419459	0.69	0.73	2455	18	2363	17	2258	26	91.97	1
037-ZR24	0.019	0.568	0.155536	0.33	8,363	0.7	0.389951	0.5	0.71	2408	11	2271	13	2123	18	88.15	1
041-ZR26	0.001	0.334	0.169827	0.36	10,872	0.71	0.464277	0.49	0.69	2556	12	2512	13	2458	20	96.18	2
042-ZR27	0.006	0.57	0.153605	0.71	7,489	1.9	0.353586	1.72	0.9	2386	24	2172	34	1952	58	81.78	1
043-ZR28	0.009	0.335	0.162091	0.42	10,559	0.84	0.472453	0.62	0.74	2478	14	2485	16	2494	26	100.67	1
044-ZR29	0.003	0.475	0.160545	0.36	9,740	1.06	0.440014	0.92	0.86	2461	12	2411	19	2351	36	95.5	1

Data not corrected for common-Pb

Discordance calculated as (1-(^{206}Pb/^{238}U age/^{207}Pb/^{206}Pb age))*100

1 -Analyses used for age calculations

2 - Data discarded due to high analytical error or discordance

C-core; R-rim

TABELA C: Dados U-Pb da amostra AS-319 (LA-ICPMS)

					Ratios*							Ages (Ma)*					
Spot	f206(%)	Th	207Pb	err (%)	207Pb	err (%)	206Pb	err (%)	Rho	207Pb		207Pb		206Pb			Remarks
Name		U	206Pb	1sigma	235U	1sigma	238U	1sigma		206Pb	2s	235U	2s	238U	2s	Conc.(%)	
003-Z1	0.009	0.456	0.147359	0.16	9,098	0.99	0.447803	0.98	0.98	2316	3	2348	9	2385	20	101.60	2
004-Z2	0.01	0.265	0.145806	0.23	8,223	0.82	0.409033	0.79	0.95	2297	4	2256	7	2211	15	97.99	3
005-Z3	0.022	0.443	0.147142	0.25	8,503	0.76	0.419116	0.71	0.93	2313	4	2286	7	2256	14	98.70	3
006-Z04N	0.019	0.427	0.147228	0.41	8,996	1.17	0.443192	1.09	0.93	2314	7	2338	11	2365	22	101.17	3
011-Z05	0.019	0.34	0.145929	0.27	8,611	0.77	0.427973	0.72	0.92	2299	5	2298	7	2297	14	99.95	3
012-Z06	0.013	0.468	0.146716	0.22	8,214	0.93	0.40607	0.91	0.96	2308	4	2255	8	2197	17	97.43	3
013-Z07	0.04	0.639	0.149459	0.31	8,983	0.88	0.435934	0.82	0.92	2340	5	2336	8	2332	16	99.83	3
016-Z08	0.009	0.384	0.146297	0.2	8,655	0.69	0.429103	0.66	0.94	2303	3	2302	6	2302	13	99.97	1
017-Z09	0.017	0.366	0.147433	0.28	8,409	0.91	0.413687	0.87	0.94	2316	5	2276	8	2232	16	98.05	3
017-Z10	0.013	0.326	0.149445	0.55	8,807	4.32	0.427417	4.29	0.99	2340	9	2318	39	2294	82	98.96	3
018-Z11	0.012	0.379	0.146385	0.18	9,143	0.82	0.453033	0.8	0.97	2304	3	2353	8	2409	16	102.39	3
023-Z12	0.017	0.212	0.15078	0.61	8,806	1.78	0.423599	1.67	0.93	2355	10	2318	16	2277	32	98.22	3
024-Z13	0.033	0.251	0.14536	0.31	8,651	1.24	0.431676	1.2	0.96	2292	5	2302	11	2313	23	100.49	1
025-Z14	0.136	0.259	0.171151	0.35	11,044	1	0.46801	0.94	0.93	2569	6	2527	9	2475	19	97.94	2
029-Z16	0.007	0.35	0.146188	0.24	8,640	1.19	0.428695	1.16	0.97	2302	4	2301	11	2300	23	99.95	1
030-Z17	0.049	0.58	0.154671	0.93	9,518	1.35	0.446354	0.97	0.7	2398	16	2389	12	2379	19	99.57	2
031-Z18	0.012	0.225	0.145817	0.22	8,655	0.94	0.430524	0.91	0.96	2297	4	2302	9	2308	18	100.24	1
032-Z19	0.008	0.34	0.146526	0.2	8,849	0.67	0.43804	0.64	0.94	2306	3	2323	6	2342	13	100.83	3
033-Z20	0.178	0.197	0.164317	0.97	10,599	1.63	0.467842	1.31	0.79	2501	16	2489	15	2474	27	99.41	2
034-Z21.1	0.017	0.29	0.145607	0.26	8,591	0.81	0.427949	0.76	0.93	2295	5	2296	7	2296	15	100.03	1
035-Z21.2	1,334	0.227	0.145772	0.2	5,611	1.33	0.27918	1.31	0.98	2297	4	1918	11	1587	18	82.76	3
036-Z23	0.026	0.467	0.164819	0.21	10,929	0.81	0.480952	0.78	0.95	2506	4	2517	8	2531	16	100.57	2
040-Z24	0.007	0.278	0.146021	0.27	8,739	0.64	0.434081	0.58	0.87	2300	5	2311	6	2324	11	100.56	3
041-Z25	0.018	0.255	0.144791	0.21	7,948	0.66	0.398131	0.62	0.93	2285	4	2225	6	2160	11	97.09	3
042-Z26	0.018	0.302	0.146836	0.23	8,445	0.91	0.417151	0.88	0.96	2309	4	2280	8	2247	17	98.57	3

Not corrected for common-Pb

Concordance calculated as ($^{206}Pb/^{238}U$ age/$^{207}Pb/^{206}Pb$ age)*100

1 -Analyses used for age calculations

2 - Analyses interpreted as inheritance

3 - Data discarded due to high analytical error or discordance

TABELA D: Dados U-Pb da amostra AS-377A (LA-ICPMS)

					Ratios*					Ages (Ma)*							
Spot	**f206(%)**	**Th**	**207Pb**	**err (%)**	**207Pb**	**err (%)**	**206Pb**	**err (%)**	**Rho**	**207Pb**		**207Pb**		**206Pb**			**Remarks**
Name		**U**	**206Pb**	**1sigma**	**235U**	**1sigma**	**238U**	**1sigma**		**206Pb**	**2s**	**235U**	**2s**	**238U**	**2s**	**Conc.(%)**	
003-ZR1N	0.047	0.562	0.147379	0.8956517	8,533	1.28	0.419861	0.84	0.65	2316	31	2289	23	2260	32	97.58	1
004-ZR1B	0.004	0.486	0.146104	0.452187	8,443	0.89	0.419094	0.68	0.76	2301	15	2280	16	2256	26	98.06	1
005-ZR2	0.011	0.594	0.146133	0.4496269	7,756	0.87	0.384893	0.65	0.74	2301	15	2203	16	2099	24	91.21	1
006-ZR3	0.009	0.528	0.14649	0.418292	8,422	0.87	0.416953	0.67	0.77	2305	14	2278	16	2247	26	97.45	1
007-ZR4	0.01	0.614	0.143934	0.3928717	7,181	0.94	0.361802	0.77	0.82	2275	14	2134	17	1991	27	87.5	1
008-ZR5	0.098	0.611	0.146034	0.4028846	8,327	0.78	0.413535	0.56	0.72	2300	14	2267	14	2231	21	97	1
009-ZR6	0.351	0.543	0.141372	0.8836433	7,404	1.3	0.379821	0.88	0.67	2244	30	2161	23	2075	31	92.48	2
010-ZR7	0.012	0.611	0.146389	0.53499	8,259	0.93	0.409162	0.67	0.72	2304	18	2260	17	2211	25	95.96	1
011-ZR8	0.014	0.542	0.146785	0.6866449	8,816	1.01	0.435546	0.64	0.63	2309	23	2319	18	2331	25	100.94	1
012-ZR9	0.016	0.591	0.145858	0.6862085	8,688	1.02	0.431972	0.66	0.65	2298	23	2306	19	2315	26	100.72	1
015-ZR10	0.016	0.645	0.145823	0.5028311	8,562	0.85	0.425799	0.57	0.67	2298	17	2293	15	2287	22	99.53	1
016-ZR11N	0.006	0.401	0.145971	0.5040356	8,283	0.88	0.411525	0.62	0.7	2299	17	2262	16	2222	24	96.63	1
017-ZR11B	0.01	0.467	0.146992	0.5876848	8,585	0.96	0.423578	0.66	0.69	2311	20	2295	17	2277	26	98.5	1
018-ZR12	0.01	0.564	0.146248	0.3899755	8,218	0.85	0.407502	0.66	0.77	2303	13	2255	15	2203	25	95.69	1
019-ZR13	0.002	0.491	0.146251	0.382553	8,486	0.83	0.420798	0.64	0.77	2303	13	2284	15	2264	25	98.33	1
021-ZR14B	0.014	0.62	0.144775	0.8308777	8,249	1.06	0.413226	0.54	0.51	2285	28	2259	19	2230	21	97.57	1
022-ZR15	0.297	0.454	0.147427	0.4862574	8,172	0.87	0.401977	0.62	0.71	2316	17	2250	16	2178	23	94.03	1
023-ZR16	0.048	0.378	0.144567	0.5947714	8,296	1.08	0.41618	0.82	0.76	2283	20	2264	20	2243	31	98.26	1
024-ZR17	0.002	1,148	0.147205	0.5679566	8,454	1.03	0.4165	0.77	0.75	2314	19	2281	19	2245	30	97.01	1

TABELA D: Continuação

					Ratios*					Ages (Ma)*							
Spot	**f206(%)**	**Th**	**207Pb**	**err (%)**	**207Pb**	**err (%)**	**206Pb**	**err (%)**	**Rho**	**207Pb**		**207Pb**		**206Pb**			**Remarks**
Name		**U**	**206Pb**	**1sigma**	**235U**	**1sigma**	**238U**	**1sigma**		**206Pb**	**2s**	**235U**	**2s**	**238U**	**2s**	**Conc.(%)**	
027-ZR18	0.006	0.412	0.146017	0.495786	8,141	0.89	0.404309	0.64	0.72	2300	17	2247	16	2189	24	95.17	1
028-ZR19	0.007	0.534	0.146628	0.4545285	8,442	0.86	0.41752	0.64	0.73	2307	16	2280	16	2249	24	97.49	1
029-ZR20	0.399	0.808	0.14388	0.5002128	6,527	1.18	0.328968	1	0.85	2274	17	2049	21	1833	32	80.6	1
030-ZR21	0.007	0.669	0.146765	0.4653474	8,378	0.89	0.413976	0.67	0.74	2309	16	2273	16	2233	25	96.72	1
031-ZR22	0.003	0.665	0.1465	0.3926051	8,418	0.8	0.416734	0.59	0.74	2305	13	2277	15	2246	23	97.4	1
032-ZR23	0.005	0.414	0.145597	0.4103949	8,240	0.81	0.410452	0.59	0.73	2295	14	2258	15	2217	22	96.6	1
033-ZR24	0.005	0.665	0.145218	0.3835004	7,595	1.23	0.37931	1.11	0.9	2290	13	2184	22	2073	39	90.51	1
034-ZR25	0.007	0.639	0.147446	0.4735898	8,248	0.83	0.405666	0.58	0.69	2317	16	2259	15	2195	22	94.75	1
035-ZR26	0.009	0.401	0.145761	0.5260927	8,535	0.9	0.424625	0.62	0.69	2297	18	2290	16	2281	24	99.33	1
036-ZR27	0.008	0.443	0.146815	0.5408142	8,613	0.86	0.425452	0.57	0.65	2309	19	2298	16	2285	22	98.96	1
037-ZR28	0.004	0.566	0.146546	0.6073925	8,795	0.92	0.435227	0.59	0.64	2306	21	2317	17	2329	23	101	1
038-ZR29	0.005	0.606	0.146585	0.7923345	8,264	1.14	0.408859	0.73	0.64	2306	27	2260	21	2210	27	95.8	1
039-ZR30	0.007	0.538	0.14708	0.6516351	8,049	0.97	0.396891	0.62	0.63	2312	22	2237	17	2155	23	93.18	1

Not corrected for common-Pb

Discordance calculated as (1-(^{206}Pb/^{238}U age/^{207}Pb/^{206}Pb age))*100

1 -Analyses used for age calculations

2 - Data discarded due to high analytical error or discordance

TABELA E: Dados U-Pb da amostra AS-360 (LA-ICPMS)

				Ratios*					Ages (Ma)*							
Spot	**Th**	**207Pb**	**err (%)**	**207Pb**	**err (%)**	**206Pb**	**err (%)**	**Rho**	**207Pb**		**207Pb**		**206Pb**			**Remarks**
Name	**U**	**206Pb**	**1sigma**	**235U**	**1sigma**	**238U**	**1sigma**		**206Pb**	**2s**	**235U**	**2s**	**238U**	**2s**	**Conc.(%)**	
004-Zir01	0.312	0.146621	0.81	7,839	1.56	0.387744	1.28	0.82	2307	28	2213	28	2112	46	91.56	1
005-Zir02	0.321	0.145444	0.69	8,053	1.24	0.401552	0.96	0.77	2293	24	2237	22	2176	36	94.9	1
006-Zir03	0.365	0.146041	0.46	8,224	1.12	0.408435	0.95	0.84	2300	16	2256	20	2208	36	95.98	1
007-Zir04	0.333	0.145023	0.92	8,163	1.65	0.40823	1.32	0.79	2288	32	2249	30	2207	49	96.45	1
008-Zir05	0.673	0.146357	0.44	8,242	0.91	0.408434	0.69	0.76	2304	15	2258	16	2208	26	95.83	1
009-Zir06	0.842	0.146349	0.45	8,207	0.85	0.406698	0.62	0.72	2304	16	2254	16	2200	23	95.49	1
010-Zir07	0.644	0.145178	0.64	8,374	1.03	0.418346	0.72	0.69	2290	22	2272	19	2253	28	98.38	1
013-Zir08	0.499	0.146464	0.47	8,624	0.88	0.427016	0.64	0.73	2305	16	2299	16	2292	25	99.44	1
014-Zir09	0.442	0.145245	0.5	8,684	0.91	0.433641	0.67	0.73	2291	17	2305	17	2322	26	101.37	1
015-Zir10	0.303	0.145631	0.77	8,083	1.32	0.402554	1	0.76	2295	26	2240	24	2181	37	95.01	1
016-Zir11	0.292	0.153927	3.46	8,678	4.76	0.408888	3.25	0.68	2390	116	2305	85	2210	121	92.46	2
017-Zir12	0.24	0.14442	0.69	9,286	1.05	0.466331	0.71	0.67	2281	24	2367	19	2467	29	108.17	1
018-Zir13	0.43	0.147846	0.73	9,310	1.36	0.456673	1.09	0.79	2321	25	2369	25	2425	44	104.46	1
019-Zir14	0.298	0.146751	0.51	8,313	1.04	0.410844	0.83	0.79	2308	18	2266	19	2219	31	96.11	1
020-Zir15	0.32	0.14353	0.87	8,369	1.37	0.422898	0.99	0.72	2270	30	2272	25	2274	38	100.14	1
024-Zir16	0.394	0.14509	0.56	9,051	1.09	0.452408	0.85	0.78	2289	20	2343	20	2406	34	105.11	1
025-Zir17	0.419	0.145806	0.64	8,631	1.12	0.429317	0.84	0.75	2297	22	2300	20	2303	33	100.23	1
026-Zir18	0.26	0.146197	1.12	8,906	1.36	0.441808	0.67	0.49	2302	38	2328	25	2359	27	102.46	1
027-Zir19	0.202	0.146111	0.33	9,106	0.75	0.451996	0.56	0.74	2301	12	2349	14	2404	23	104.48	1
028-Zir20	0.389	0.14608	0.5	8,624	1.03	0.428169	0.82	0.79	2301	17	2299	19	2297	32	99.86	1

TABELA E: Continuação

				Ratios*							Ages (Ma)*					
Spot	**Th**	**207Pb**	**err (%)**	**207Pb**	**err (%)**	**206Pb**	**err (%)**	**Rho**	**207Pb**		**207Pb**		**206Pb**			**Remarks**
Name	**U**	**206Pb**	**1sigma**	**235U**	**1sigma**	**238U**	**1sigma**		**206Pb**	**2s**	**235U**	**2s**	**238U**	**2s**	**Conc.(%)**	
029-Zir21	0.365	0.145675	1.04	8,425	1.44	0.419465	0.93	0.64	2296	36	2278	26	2258	35	98.35	1
030-Zir22	0.302	0.145579	1	8,617	1.65	0.429306	1.25	0.76	2295	34	2298	30	2303	49	100.34	1
033-Zir23	0.468	0.145786	0.84	8,099	2	0.402887	1.78	0.88	2297	29	2242	36	2182	66	95	1
034-Zir24	0.452	0.146804	0.7	8,849	0.99	0.437149	0.59	0.59	2309	24	2323	18	2338	23	101.24	1
036-Zir26	0.46	0.14752	1.17	8,890	1.37	0.437053	0.6	0.43	2317	40	2327	25	2337	24	100.86	1
037-Zir27	0.392	0.145701	0.53	8,450	0.92	0.420624	0.65	0.7	2296	18	2281	17	2263	25	98.57	1
038-Zir28	0.374	0.146382	0.35	8,645	0.74	0.428332	0.54	0.72	2304	12	2301	14	2298	21	99.74	1
039-Zir29	0.24	0.145537	0.53	8,627	0.98	0.429898	0.73	0.74	2294	18	2299	18	2305	28	100.48	1

Data not corrected for common-Pb

Discordance calculated as (1-(^{206}Pb/^{238}U age/^{207}Pb/^{206}Pb age))*100

Decay constants of Jaffey et al 1971 used

1 -Analyses used for age calculations

2 - Data discarded due to high analytical error or discordance

TABELA F: Dados U-Pb da amostra AS-360D (LA-ICPMS)

					Ratios*					Ages (Ma)*							
Spot	**f(206)%**	**Th**	**207Pb**	**err (%)**	**207Pb**	**err (%)**	**206Pb**	**err (%)**	**Rho**	**207Pb**		**207Pb**		**206Pb**			**Remarks**
Name		**U**	**206Pb**	**1sigma**	**235U**	**1sigma**	**238U**	**1sigma**		**206Pb**	**2s**	**235U**	**2s**	**238U**	**2s**	**Conc.(%)**	
004-Zir01	0	0.678	0.147661	0.34	8,449	0.75	0.414961	0.56	0.74	2319	12	2280	14	2238	21	96.48	2
005-Zir02	0.01	0.2	0.159967	0.25	9,544	1.65	0.432712	1.58	0.96	2455	9	2392	30	2318	62	94.4	1
006-Zir03	0.01	0.338	0.159967	0.26	6,223	0.8	0.362975	0.6	0.75	2019	14	1996	21	2008	14	98.86	4
007-Zir04	0.07	0.23	0.156748	0.24	8,125	1.11	0.375923	1.02	0.91	2421	8	2245	20	2057	36	84.97	1
008-Zir05	0.01	0.477	0.145549	0.41	8,736	1.34	0.435325	1.22	0.9	2294	14	2311	24	2330	48	101.54	2
009-Zir06	0	0.68	0.163454	0.44	5,998	0.72	0.359221	0.51	0.71	1972	12	1978	17	1976	12	100.31	4
010-Zir07	0.01	0.571	0.145061	0.38	8,567	0.85	0.428294	0.66	0.77	2289	13	2293	15	2298	26	100.41	2
013-Zir08	0.01	0.554	0.14628	0.32	8,704	0.76	0.43154	0.58	0.76	2303	11	2308	14	2313	23	100.42	2
014-Zir09	0.02	0.491	0.147088	0.86	8,298	1.18	0.409162	0.71	0.6	2312	30	2264	21	2211	27	95.62	2
015-Zir10	0.02	0.255	0.124484	0.35	5,280	0.78	0.307626	0.59	0.75	2021	13	1866	13	1729	18	85.53	3
016-Zir11	0.04	0.326	0.163454	0.44	10,692	1.83	0.474392	1.73	0.94	2492	15	2497	34	2503	72	100.44	1
017-Zir12	0.04	0.666	0.146062	0.37	7,808	0.9	0.387709	0.73	0.81	2300	13	2209	16	2112	26	91.82	2
018-Zir13	0.01	0.825	0.146869	0.43	8,337	0.77	0.411699	0.51	0.66	2310	15	2268	14	2223	19	96.22	2
019-Zir14	0.01	0.402	0.161351	0.36	5,640	0.95	0.341047	0.58	0.61	1955	23	1892	19	1922	16	96.76	4
023-Zir16	0.01	0.174	0.183679	0.47	11.52	0.9	0.455173	0.67	0.74	2686	16	2567	17	2418	27	90.01	4
024-Zir17	0.01	0.534	0.146707	0.5	7.92	1.01	0.391993	0.8	0.78	2308	17	2223	18	2132	29	92.38	2
025-Zir18	0.01	0.516	0.125745	0.49	6.13	0.84	0.353649	0.58	0.68	2039	17	1995	15	1952	20	95.71	4
026-Zir19	1.85	0.414	0.135698	1.76	6.6	1.93	0.352908	0.69	0.36	2173	61	2060	34	1948	23	89.66	3

TABELA F: Continuação

					Ratios*					Ages (Ma)*							
Spot	**f(206)%**	**Th**	**207Pb**	**err (%)**	**207Pb**	**err (%)**	**206Pb**	**err (%)**	**Rho**	**207Pb**		**207Pb**		**206Pb**			**Remarks**
Name		**U**	**206Pb**	**1sigma**	**235U**	**1sigma**	**238U**	**1sigma**		**206Pb**	**2s**	**235U**	**2s**	**238U**	**2s**	**Conc.(%)**	
027-Zir20	0.01	0.675	0.146645	0.45	8.21	0.83	0.406165	0.58	0.7	2307	16	2255	15	2197	22	95.24	2
028-Zir21	0.03	0.597	0.141458	1.32	7.66	1.74	0.39319	1.07	0.61	2245	45	2193	31	2138	39	95.21	3
029-Zir22C	1.35	1,417	0.146432	1.09	5.25	2.43	0.260136	2.14	0.87	2305	37	1861	41	1491	57	64.67	4
030-Zir22R	0.15	0.049	0.137837	0.53	7,016	0.85	0.369156	0.54	0.64	2200	18	2114	15	2025	19	92.05	3
033-Zir23	0.02	0.437	0.14688	0.51	7,948	0.97	0.392473	0.74	0.75	2310	18	2225	18	2134	27	92.39	2
034-Zir24	0	0.667	0.146152	0.33	8,216	0.8	0.407717	0.63	0.78	2301	11	2255	15	2204	24	95.78	2
035-Zir25	0.01	0.608	0.146175	0.41	8.15	0.92	0.404367	0.73	0.79	2302	14	2248	17	2189	27	95.11	2
036-Zir26	0.01	0.204	0.161351	0.35	9.76	0.84	0.4387	0.66	0.79	2470	12	2412	15	2345	26	94.93	1

Data not corrected for common-Pb

Discordance calculated as (1-(^{206}Pb/^{238}U age/^{207}Pb/^{206}Pb age))*100

f(206)%: Percentage of ^{206}Pb which is common Pb

Decay constants of Jaffey et al 1971 used

1 -Data used in calculation of 2481 Ma

2 -Data used in calculation of 2302 Ma

3 -Data used in calculation of 2318 Ma

4 -Data not used in age calculation

C-core; R-rim

TABELA G: Sumário dos dados obtidos para o padrão de zircão 91500 nas sessões analíticas das amostras AS-319, AS-360D, AS-360, AS-362 e AS-377A.

SAMPLES	RESULT 91500					
	UPPER INTERCEPT CONCORDIA		WHEIGHTED AVERAGE			
			$^{207}Pb/^{206}Pb$		$^{206}Pb/^{238}U$	
	Age (Ma)	MSWD	Age (Ma)	MSWD	Age (Ma)	MSWD
AS-319	1064±14	0.65	1071±17	1.13	1050±28	6.5
AS-360 and AS-360D	1050±18	0.92	1051±17	1.02	1004±20	4.4
AS-362	1065±10	0.48	1070±4	0.84	1032±8	7.9
AS-377A	1064±22	0.09	1070±4	0.18	1022±5	3.7

TABELA H: Dados analíticos dos padrões primário (Temora zircon) e secundário (SL-13 zircon). Disponível em: https://doi.org/10.1016/j.precamres.2020.105901

TABELA I: Dados U-Pb (LA-ICPMS) da amostra AS-378 (256831; 8692693, coordenadas UTM). * Discordance calculated as (1-($^{206}Pb/^{238}U$ age/$^{207}Pb/^{206}Pb$ age))*100.

									Data for Wetherill plot[4]					Ages[4]						
Identifier	206* (%)	^{204}Pb cps	^{206}Pb mV[1]	Th/U	$^{206}Pb/^{204}Pb$	1σ%	$^{207}Pb/^{206}Pb$	1σ %	$^{207}Pb/^{235}U$	1σ %	$^{206}Pb/^{238}U$	1σ %	Rho	$^{207}Pb/^{206}Pb$	2σ abs	$^{206}Pb/^{238}U$	2σ abs	$^{207}Pb/^{235}U$	2σ abs	% U-Pb disc[5]
ZR1N	0.0092	18	0.0052	0.745	163508	20.47	0.14624	0.46	8.456	0.92	0.4194	0.71	0.77	2302	16	2258	27	2281	17	1.95
ZR2	00.132	20	0.0060	0.639	114044	27.36	0.14531	0.45	8.733	0.73	0.4358	0.45	0.61	2291	15	2332	17	2311	13	-1.77
ZR4N	00.078	16	0.0067	0.696	193035	19.37	0.14701	0.39	8.477	0.75	0.4182	0.52	0.69	2311	13	2252	20	2283	14	2.57
ZR5	0.0061	12	0.0073	0.620	244865	15.80	0.14660	0.49	8.994	0.84	0.4449	0.57	0.68	2307	17	2373	23	2337	15	-2.86
ZR6	0.0161	26	0.0070	0.774	93081	32.98	0.14515	0.51	8.649	1.03	0.4322	0.81	0.79	2290	17	2315	32	2302	19	-1.13
ZR8	0.0137	40	0.0075	0.689	110232	49.46	0.14517	0.98	8.343	1.19	0.4168	0.57	0.47	2290	34	2246	21	2269	22	1.92
ZR12	0.3367	456	0.0294	0.348	4538	8.67	0.14193	0.42	6.320	0.91	0.3229	0.72	0.79	2251	15	1804	23	2021	16	19.85
ZR14	0.0068	11	0.0053	0.465	221316	21.01	0.14399	0.81	8.375	1.06	0.4218	0.58	0.55	2276	28	2269	22	2273	19	0.31
ZR16	0.0091	6	0.0041	0.533	164762	12.96	0.14604	0.49	8.337	0.87	0.4140	0.61	0.70	2300	17	2233	23	2268	16	2.90
ZR17	0.0035	24	0.0320	0.345	427443	37.96	0.14499	0.84	8.258	1.07	0.4131	0.55	0.51	2288	29	2229	21	2260	19	2.57
ZR18	0.0141	22	0.0046	0.506	106481	24.99	0.14436	0.63	8.469	1.03	0.4255	0.72	0.70	2280	22	2285	28	2283	19	-0.22
ZR19	0.0062	31	0.0095	0.550	242462	23,93	0.14534	0.48	8.551	0.90	0.4267	0.67	0.74	2292	16	2291	26	2291	16	0.05
ZR23	0.0130	24	0.0048	0.618	116392	24.21	0.14518	0.45	8.188	0.85	0.4090	0.62	0.73	2290	16	2210	23	2252	15	3.47
ZR25	0.1289	214	0.0366	0.399	11809	6.45	0.14193	0.36	6.828	0.84	0.3489	0.66	0.79	2251	12	1929	22	2089	15	14.28
ZR28	0.0110	26	0.0067	0.448	137202	30.84	0.14537	0.49	8.161	0.97	0.4071	0.75	0.78	2292	17	2202	28	2249	17	3.94
Data not used in the calculation of Concordia age																				
ZR1B	0.0140	353	0.0098	0.649	106431	49.15	0.14851	1.13	9.640	1.39	0.4708	0.72	0.52	2329	38	2487	30	2401	25	-6.79
ZR3	0.0094	70	0.0287	0.913	159428	50.09	0.14774	0.34	8.608	0.76	0.4226	0.56	0.74	2320	12	2272	22	2297	14	2.06
ZR4B	0.0055	12	0.0068	0.540	271248	20.04	0.14788	0.42	8.634	0.72	0.4234	0.45	0.63	2322	14	2276	17	2300	13	1.97
ZR9	0.0069	49	0.0166	0.778	218032	67.33	0.14728	0.41	8.601	0.81	0.4235	0.60	0.74	2315	14	2276	23	2297	15	1.65
ZR11	0.0450	39	0.0024	0.812	33081	33.47	0.14572	0.84	9.521	1.45	0.4738	1.12	0.77	2296	29	2500	46	2390	26	-8.88
ZR15	0.0671	126	0.0433	0.378	22731	6.86	0.13923	0.40	6.380	0.83	0.3323	0.63	0.76	2218	14	1850	20	2030	15	16.59
ZR20	0.0116	99	0.0076	0.659	128504	37.70	0.14546	0.56	9.041	1.29	0.4507	1.10	0.85	2293	19	2399	44	2342	23	-4.59
ZR21	0.0259	68	0.0068	0.562	57883	58.75	0.14756	0.63	9.063	1.07	0.4454	0.78	0.73	2318	22	2375	31	2344	19	-2.46
ZR24	0.0368	61	0.0024	0.529	41046	47.96	0.14351	1.09	7.982	1.45	0.4034	0.89	0.61	2270	37	2185	33	2229	26	3.77
ZR26	0.0345	139	0.0078	0.769	43805	83.37	0.15156	1.06	8.211	1.27	0.3929	0.58	0.46	2364	36	2136	21	2255	23	9.62
ZR27	0.0041	15	0.0126	0.363	363932	22.31	0.14706	0.37	8.266	0.73	0.4076	0.51	0.70	2312	13	2204	19	2261	13	4.67

ZR29N	0.0062	22	0.0122	0.645	244583	23.06	0.14681	0.47	7.918	0.81	0.3911	0.54	0.67	2309	16	2128	20	2222	15	7.85
ZR29B	0.0087	18	0.0075	0.552	174312	27.03	0.14667	0.51	8.071	0.81	0.3991	0.51	0.63	2307	18	2165	19	2239	15	6.18
ZR30	0.0142	18	0.0033	0.420	107248	27.12	0.14074	0.94	6.459	1.69	0,3328	1.36	0.80	2236	32	1852	44	2040	29	17.18
Discarded data by the great analytical error																				
ZR7	0.2690	401	0.0368	0.321	5737	2.10	0.12949	3.24	4.178	3.29	0.2340	0.47	0.14	2091	112	1355	11	1670	53	35.19
ZR10	0.8522	335	0.0067	0.699	1779	22.75	0.14266	1.27	7.431	3.21	0.3778	2.93	0.91	2260	43	2066	103	2165	57	8.59
ZR22	0.4198	1090	0.0237	1.011	3606	20.02	0.13712	2.14	7.293	2.25	0.3857	0.61	0.27	2191	73	2103	22	2148	40	4.02
Discarded data by the great 204Pb																				
ZR13	1.5242	257	0.0037	0.603	978	8.07	0.16029	1.21	10.234	1.57	0.4630	0.93	0.59	2459	41	2453	38	2456	29	0.24

TABELA J: Dados U-Pb (LA-ICPMS) da amostra AS-205 (225847; 8692171, coordenadas UTM). * Discordance calculated as (1-(^{206}Pb/^{238}U age/^{207}Pb/^{206}Pb age))*100.

									Data for Wetherill plot[4]					Ages[5]						
Identifier	206* (%)	^{204}Pb cps	^{206}Pb mV[1]	Th/U	^{206}Pb/^{204}Pb	1σ%	^{207}Pb/^{206}Pb	1σ %	^{207}Pb/^{235}U	1σ %	^{206}Pb/^{238}U	1σ %	Rho	^{207}Pb/^{206}Pb	2σ abs	^{206}Pb/^{238}U	2σ abs	^{207}Pb/^{235}U	2σ abs	% U-Pb disc[4]
ZR1	0.0085	15	0.0061	0.496	176585	19.84	0.14318	0.52	8.406	0.88	0.4258	0.60	0.69	2266	18	2287	23	2276	16	-0.91
ZR2	0.0215	33	0.0063	0.407	69934	33.42	0.14400	0.51	8.356	0.93	0.4208	0.69	0.74	2276	17	2264	26	2270	17	0.51
ZR3	0.0071	16	0.0059	0.484	212644	19.08	0.14314	0.49	8.318	0.97	0.4215	0.75	0.77	2266	17	2267	29	2266	17	-0.07
ZR4	0.5063	576	0.0099	0.492	2978	24.35	0.14165	1.02	7.991	1.56	0.4091	1.11	0.72	2247	35	2211	42	2230	28	1.63
ZR5N	0.0145	17	0.0038	0.590	104131	22.95	0.14198	0.46	8.154	0.87	0.4165	0.65	0.74	2251	16	2245	24	2248	16	0.31
ZR5B	0.0089	20	0.0084	0.211	168556	22.66	0.14324	0.74	8.217	1.00	0.4160	0.55	0.55	2267	25	2242	21	2255	18	1.08
ZR6N	0.0055	16	0.0103	0.406	277551	20.00	0.13954	0.42	6.985	0.85	0.3630	0.64	0.75	2222	15	1996	22	2110	15	10.13
ZR6B	0.0170	27	0.0093	0.407	89415	30.16	0.14034	0.45	7.215	0.84	0.3729	0.61	0.73	2231	15	2043	21	2138	15	8.45
ZR7	0.0013	23	0.0090	0.410	1125665	84.89	0.14022	0.47	7.404	0.86	0.3829	0.62	0.72	2230	16	2090	22	2161	15	6.28
ZR8N	0.0107	13	0.0040	0.523	140411	17.60	0.14332	0.58	8.031	0.95	0.4064	0.65	0.69	2268	20	2198	24	2235	17	3.05
ZR8B	0.0111	16	0.0041	0.401	136031	16.44	0.14463	0.51	8.107	0.97	0.4065	0.74	0.76	2283	17	2199	28	2243	18	3.70
ZR9	0.0143	25	0.0049	0.484	105230	34.19	0.14546	0.44	8.140	0.84	0.4058	0.62	0.73	2293	15	2196	23	2247	15	4.25
ZR10	0.0078	11	0.0052	0.503	194380	20.33	0.14528	0.45	8.254	0.94	0.4120	0.73	0.78	2291	15	2224	28	2259	17	2.92
ZR11	0.8799	285	0.0070	0.788	1731	10.76	0.14105	1.28	6.771	1.70	0.3481	1.05	0.62	2240	44	1926	35	2082	30	14.05
ZR12	0.0048	13	0.0096	0.423	315210	15.72	0.14358	0.38	8.152	0.90	0.4118	0.73	0.81	2271	13	2223	27	2248	16	2.10
ZR13N	0.0086	16	0.0094	0.588	177402	26.35	0.13969	0.50	6.708	1.29	0.3483	1.13	0.87	2223	17	1926	37	2074	23	13.36
ZR13B	0.0165	70	0.0082	0.528	92305	30.79	0.14186	0.44	6.940	1.03	0.3548	0.85	0.83	2250	15	1958	29	2104	18	13.00
ZR14N	0.0172	11	0.0024	0.611	87536	21.15	0.14361	0.73	8.241	1.19	0.4161	0.87	0.73	2271	25	2243	33	2258	22	1.24
ZR14B	0.0235	11	0.0019	0.424	64297	14.63	0.14441	0.86	7.986	1.22	0.4011	0.78	0.64	2281	29	2174	29	2229	22	4.68
ZR15N	0.0054	25	0.0124	0.492	280993	22.47	0.14049	0.61	6.879	1.27	0.3551	1.05	0.83	2233	21	1959	36	2096	22	12.28
ZR16	0.0143	17	0.0055	0.411	105401	21.80	0.14386	0.50	7.818	0.94	0.3941	0.71	0.75	2274	17	2142	26	2210	17	5.82
ZR18N	0.0246	59	0.0088	0.452	61427	51.42	0.14391	0.49	7.779	1.02	0.3920	0.81	0.80	2275	17	2132	29	2206	18	6.27
ZR18B	0.1177	58	0.0090	0.439	12804	13.53	0.14420	1.10	8.185	1.43	0.4116	0.84	0.59	2278	38	2222	32	2252	26	2.46
ZR19	0.0123	37	0.0110	0.653	123449	36.92	0.14133	0.98	6.802	1.59	0.3490	1.20	0.75	2244	34	1930	40	2086	28	13.98
ZR20N	0.0109	14	0.0047	0.416	138383	18.74	0.14379	0.51	7.859	0.88	0.3964	0.62	0.70	2273	18	2152	23	2215	16	5.33
ZR20B	0.0063	17	0.0072	0.307	240015	26.73	0.14291	0.58	7.655	0.97	0.3884	0.68	0.70	2263	20	2116	25	2191	17	6.51
ZR21	0.0192	15	0.0033	0.555	78650	21.18	0.14319	0.69	7.932	1.07	0.4017	0.73	0.68	2266	24	2177	27	2223	19	3.93

ZR22	0.0060	15	0.0045	0.536	253288	42.14	0.14304	0.68	7.872	1.07	0.3991	0.74	0.69	2264	23	2165	27	2216	19	4.38
ZR23	0.0057	13	0.0047	0.560	262763	51.68	0.14379	0.58	7.974	0.92	0.4021	0.61	0.66	2273	20	2179	23	2228	17	4.16
ZR24	0.0303	63	0.0086	0.542	49808	72.54	0.14284	0.51	7.936	1.02	0.4029	0.81	0.79	2262	18	2183	30	2224	18	3.51
ZR25N	0.0111	22	0.0057	0.550	136221	22.52	0.14395	0.50	7.885	0.88	0.3972	0.62	0.71	2275	17	2156	23	2218	16	5.23
ZR26	0.0265	24	0.0029	0.624	57168	27.83	0.14436	0.70	7.792	1.10	0.3914	0.77	0.69	2280	24	2129	28	2207	20	6.61
ZR27	0.0098	24	0.0077	0.380	155125	26.13	0.13958	0.41	6.719	1.11	0.3491	0.96	0.87	2222	14	1930	32	2075	20	13.12
ZR28	0.0165	12	0.0031	0.455	91178	17.13	0.14274	0.53	8.119	0.99	0.4125	0.75	0.75	2261	18	2226	28	2244	18	1.52
ZR29	0.0111	18	0.0059	0.239	135504	21.47	0.14409	0.57	8.293	1.03	0.4174	0.78	0.75	2277	20	2249	29	2264	19	1.24
ZR30N	0.0330	47	0.0079	0.717	46089	48.12	0.14116	0.84	6.880	1.37	0.3535	1.01	0.74	2241	29	1951	34	2096	24	12.96
ZR30B	0.0166	30	0.0086	0.272	91237	41.30	0.14134	0.67	7.239	1.27	0.3715	1.01	0.80	2244	23	2036	35	2141	22	9.24
Data not used in the calculation of Concordia age																				
ZR17	0.5229	355	0.0130	0.449	2934	8.73	0.14213	0.97	5.716	1.46	0.2917	1.03	0.70	2253	33	1650	30	1934	25	26.78
ZR15B	0.0120	92	0.0125	0.484	127056	34.90	0.14242	0.56	6.357	1.31	0.3237	1.13	0.86	2257	19	1808	35	2026	23	19.90
ZR25B	0.0210	28	0.0035	0.455	71204	23.28	0.14380	0.54	8.745	1.08	0.4410	0.85	0.79	2273	19	2355	34	2312	19	-3.60

TABELA L: Dados U-Pb (LA-ICPMS) da amostra AS-217 (249919; 8736872, coordenadas UTM). * Discordance calculated as (1-(^{206}Pb/^{238}U age/^{207}Pb/^{206}Pb age))*100.

											Apparent Ages							
Grain.spot	f206(%)	Th U	206Pb 204Pb	207Pb 206Pb	err (%) 1sigma	207Pb 235U	err (%) 1sigma	206Pb 238U	err (%) 1sigma	Rho	207Pb 206Pb	(Ma)	207Pb 235U	(Ma)	206Pb 238U	(Ma)	Conc.(%) 6/8-7/6	Conc.(%) 6/8-7/5
Sample AS-R-217																		
03-Z01	0.01	0.09	101249	0.137462	0.99	7.493	1.38	0.395319	0.97	0.68	2195	17	2172	12	2147	18	97.81	98.87
05-Z03	0.33	0.16	4680	0.138277	1.25	6.614	1.65	0.346881	1.08	0.64	2206	22	2061	14	1920	18	87.03	93.14
07-Z05	0.09	0.18	16212	0.133861	0.78	6.552	0.92	0.355003	0.49	0.44	2149	13	2053	8	1958	8	91.12	95.40
08-Z06	0.40	0.24	3701	0.138443	0.89	7.336	1.05	0.384299	0.55	0.46	2208	15	2153	9	2096	10	94.95	97.36
13-Z08B	0.02	0.11	100131	0.132329	0.95	5.551	1.14	0.304231	0.63	0.50	2129	16	1909	10	1712	9	80.42	89.72
18-Z13	0.01	0.15	117062	0.136810	1.39	6.580	1.56	0.348819	0.71	0.42	2187	24	2057	14	1929	12	88.19	93.79
19-Z14	0.12	0.17	13242	0.134111	1.47	5.462	1.97	0.295365	1.32	0.66	2152	25	1895	17	1668	19	77.51	88.06
25-Z17	0.08	0.19	20343	0.134348	1.31	4.967	1.47	0.268135	0.66	0.40	2156	23	1814	12	1531	9	71.04	84.43
27-Z19	1.15	0.16	1405	0.127180	1.80	4.413	2.12	0.251635	1.12	0.54	2059	31	1715	17	1447	14	70.26	84.38
29-Z21	0.00	0.10	317723	0.137218	1.00	6.611	1.32	0.349440	0.86	0.63	2192	17	2061	12	1932	14	88.12	93.74
33-Z23	0.02	0.11	98486	0.135940	0.92	5.992	1.15	0.319709	0.69	0.56	2176	16	1975	10	1788	11	82.18	90.56
34-Z24	0.45	0.23	3536	0.130755	1.26	4.905	1.97	0.272061	1.52	0.77	2108	22	1803	17	1551	21	73.58	86.03
heritage																		
09-Z07	0.01	0.34	96400	0.163963	1.82	10.089	1.97	0.446252	0.76	0.36	2497	30	2443	18	2379	15	95.26	97.37
10-Z08N	0.38	0.60	3700	0.161887	1.76	10.482	2.47	0.469588	1.73	0.70	2475	29	2478	23	2482	36	100.25	100.14
Discarded data by the great analytical error																		
04-Z02	0.59	0.09	2682	0.133444	2.23	5.624	2.32	0.305687	0.64	0.25	2144	38	1920	20	1719	10	80.21	89.56
06-Z04	0.03	0.13	53804	0.133278	2.39	4.393	5.34	0.239030	4.77	0.89	2142	41	1711	43	1382	59	64.51	80.75
14-Z09	1.50	0.14	1081	0.134744	9.38	4.736	9.65	0.254932	2.29	0.25	2161	155	1774	78	1464	30	67.75	82.53
15-Z10	6.25	0.33	260	0.154516	42.66	5.078	42.67	0.238351	1.08	0.03	2397	587	1832	310	1378	13	57.51	75.21
16-Z11B	2.20	0.08	685	0.153864	17.87	7.721	18.03	0.363945	2.40	0.15	2389	276	2199	150	2001	41	83.74	90.99
17-Z12	0.28	0.22	5380	0.128574	5.48	6.546	5.73	0.369234	1.66	0.29	2079	93	2052	49	2026	29	97.46	98.72
20-Z15	0.24	0.18	6338	0.1402102	2.19	6.687	2.26	0.345891	0.57	0.2	2230	37	2071	20	1915	9	85.88	92.47
24-Z16	1.76	0.23	956	0.117625	6.48	3.092	6.52	0.190655	0.71	0.11	1920	112	1431	49	1125	7	58.58	78.63
26-Z18	0.17	0.15	8838	0.137584	1.06	6.565	1.19	0.346058	0.53	0.38	2197	18	2055	10	1916	9	87.20	93.24
28-Z20	0.12	0.17	12532	0.134961	1.22	5.960	1.54	0.320272	0.94	0.59	2164	21	1970	13	1791	15	82.78	90.92
30-Z22	4.34	0.21	392	0.182390	45.47	4.171	46.74	0.165874	10.84	0.29	2675	604	1668	325	989	99	36.99	59.30
35-Z25	4.27	0.12	377	0.124936	5.37	4.426	5.69	0.256957	1.86	0.39	2028	92	1717	46	1474	25	72.70	85.85

TABELA M: Dados U-Pb (LA-ICPMS) da amostra AS-302 (300057; 8716673, coordenadas UTM). * Discordance calculated as (1-(^{206}Pb/^{238}U age/^{207}Pb/^{206}Pb age))*100.

											Apparent Ages							
Grain.spot	f206(%)	Th U	206Pb 204Pb	207Pb 206Pb	err (%) 1sigma	207Pb 235U	err (%) 1sigma	206Pb 238U	err (%) 1sigma	Rho	207Pb 206Pb	(Ma)	207Pb 235U	(Ma)	206Pb 238U	(Ma)	Conc.(%) 6/8-7/6	Conc.(%) 6/8-7/5
Sample AS-R-302																		
003-Z01	0.01	0.26	190402	0.134689	0.89	6.423	1.66	0.345849	1.40	0.84	2160	15	2035	14	1915	23	88.65	94.07
004-Z02	0.00	0.28	326412	0.138887	0.98	7.529	1.19	0.393184	0.67	0.52	2213	17	2176	11	2138	12	96.58	98.21
005-Z03	0.00	0.22	731163	0.138626	1.17	7.519	1.30	0.393399	0.56	0.37	2210	20	2175	12	2139	10	96.76	98.31
006-Z04	0.01	0.32	172173	0.138203	1.20	7.549	1.32	0.396175	0.56	0.36	2205	21	2179	12	2151	10	97.58	98.74
009-Z05	0.00	0.31	348780	0.139052	1.25	7.788	1.40	0.406232	0.63	0.40	2215	21	2207	12	2198	12	99.20	99.58
010-Z06N	0.00	0.22	420923	0.137931	0.97	7.502	1.14	0.394467	0.59	0.46	2201	17	2173	10	2144	11	97.37	98.63
011-Z06B	0.02	0.23	90428	0.135151	1.15	6.287	1.43	0.337392	0.84	0.56	2166	20	2017	12	1874	14	86.53	92.93
012-Z07	0.00	0.26	469771	0.138501	1.04	7.744	1.17	0.405527	0.52	0.37	2209	18	2202	10	2194	10	99.36	99.67
016-Z09	0.00	0.30	522949	0.136925	1.41	6.772	2.33	0.358721	1.86	0.79	2189	24	2082	20	1976	32	90.29	94.91
024-Z13N	0.00	0.37	395180	0.139916	1.17	7.860	1.34	0.407449	0.64	0.43	2226	20	2215	12	2203	12	98.97	99.46
025-Z13B	0.0063	0.2327	236038	0.1431152	2.8706	7.834	2.9286	0.397001	0.5797	0.2	2265	48.7	2212	26	2155	10.6	95.14281	97.4279
34-Z15	0.01	0.27	247633	0.136888	1.39	7.487	1.48	0.396664	0.49	0.26	2188	24	2171	13	2154	9	98.42	99.18
35-Z16	0.00	0.21	337077	0.133757	1.36	5.398	1.55	0.292669	0.75	0.45	2148	24	1884	13	1655	11	77.05	87.82
36-Z17	0.01	0.21	200346	0.138522	1.01	7.368	1.16	0.385756	0.57	0.43	2209	17	2157	10	2103	10	95.21	97.50
37-Z18	0.01	0.23	261677	0.133268	1.21	5.390	1.74	0.293342	1.24	0.70	2141	21	1883	15	1658	18	77.43	88.05
38-Z19	0.00	0.20	578104	0.138087	0.96	7.223	1.14	0.379363	0.61	0.48	2203	17	2139	10	2073	11	94.10	96.91
39-Z20	0.01	0.26	261532	0.135203	1.15	6.096	1.49	0.326987	0.95	0.61	2167	20	1990	13	1824	15	84.17	91.66
40-Z21	0.00	0.22	305623	0.137989	0.97	7.396	1.13	0.388707	0.58	0.45	2202	17	2160	10	2117	10	96.13	97.98
44-Z22N	0.00	0.29	960396	0.138444	0.80	7.398	1.00	0.387538	0.61	0.54	2208	14	2161	9	2111	11	95.63	97.72
45-Z22B	0.00	0.20	447733	0.136895	0.84	6.278	1.10	0.332617	0.71	0.60	2188	14	2015	10	1851	11	84.59	91.84
46-Z23	0.01	0.22	274593	0.137834	1.54	7.215	1.73	0.379664	0.79	0.42	2200	27	2138	15	2075	14	94.30	97.02
z11b	0.00	0.22	434518	0.138839	1.22	8.323	1.38	0.434775	0.65	0.42	2213	21	2267	12	2327	13	105.17	102.66
Discarded data by the great analytical error																		
023-Z12	3.44	0.32	439	0.228176	54.35	11.270	54.39	0.358226	2.16	0.05	3039	677	2546	411	1974	37	64.94	77.53
017-Z10	0.01	0.30	181092	0.146964	7.65	8.548	7.69	0.421832	0.79	0.09	2311	126	2291	68	2269	15	98.18	99.03
018-Z11	0.01	0.30	190539	0.138687	4.69	7.318	4.86	0.382713	1.27	0.25	2211	79	2151	43	2089	23	94.48	97.11
015-Z08	0.02	0.31	98139	0.137672	7.01	7.536	7.10	0.396999	1.14	0.15	2198	117	2177	62	2155	21	98.05	98.99

TABELA N: Dados U-Pb (LA-ICPMS) da amostra AS-34 (295888; 8711760, coordenadas UTM). * Discordance calculated as (1-(^{206}Pb/^{238}U age/^{207}Pb/^{206}Pb age))*100.

Grain. spot	U (ppm)	Th (ppm)	Th/U	F^{206}	^{207}Pb /^{235}U	error	^{206}Pb /^{238}U	error	^{207}Pb /^{206}Pb	error	^{206}Pb /^{238}U Age	error	^{207}Pb /^{206}Pb Age	erro	Disc.
Sample AS-R-34															
8.1	259	71	0.28	0.25	7.51	1.5	0.3999	1.3	0.1362	0.7	2168.6	23.0	2179	13	0
2.1	248	63	0.26	0.14	7.55	1.4	0.4013	1.3	0.1365	0.7	2174.9	23.2	2183	12	0
6.1	168	39	0.24	0.51	7.64	1.7	0.4077	1.3	0.1358	1.1	2204.2	24.1	2175	19	-1
11.1	479	145	0.31	0.05	7.68	1.5	0.4086	1.4	0.1363	0.4	2208.3	26.9	2181	7	-1
7.1	258	53	0.21	0.00	7.87	2.0	0.4171	1.9	0.1368	0.6	2247.3	35.8	2188	11	-3
Data not used in the calculation of concordia age															
1.1	468	115	0.25	0.44	6.35	1.5	0.3435	1.2	0.1340	0.8	1903.2	20.2	2151	14	13
heritage															
3.1	271	119	0.45	1.10	9.50	1.9	0.4244	1.3	0.1623	1.3	2280.5	24.5	2480	23	9
9.1	275	52	0.20	0.20	10.42	1.7	0.4712	1.4	0.1604	0.9	2488.8	28.8	2460	16	-1
Data with high common Pb content															
12.1	314	85	0.28	3.02	6.49	3.7	0.3334	1.3	0.1409	3.1	1854.7	21.5	2241	59	21
10.1	636	126	0.20	2.25	2.83	5.1	0.1971	1.4	0.1039	4.8	1159.6	14.5	1696	91	46
4.1	796	150	0.19	6.64	3.83	8.4	0.2179	1.5	0.1270	7.8	1271.0	17.1	2062	145	62
5.1	413	47	0.12	5.29	6.29	8.7	0.3303	1.7	0.1379	8.2	1839.9	25.8	2205	149	20
13.1	262	48	0.19	20.96	5.22	64.2	0.2522	8.7	0.1478	61.6	1449.9	99.5	2347	1087	62
3.2	1196	397	0.34	80.39			0.0864	40.0	0.4822	90.7	534.0	200.9	4463	1385	736